CR-102570

FINAL REPORT

MCR-69-405 Copy No.

Development of Advanced Materials for Integrated Tank Insulation System for the Long Term Storage of Cryogens in Space

SEPTEMBER 1969

MARTIN MARIETTA DENVER DIVISION

MCR-69-405

FINAL REPORT

DEVELOPMENT OF ADVANCED MATERIALS FOR INTEGRATED TANK INSULATION SYSTEM FOR THE LONG TERM STORAGE OF CRYOGENS IN SPACE

September 1969

By

John P. Gille

Prepared under Contract NAS8-21330

By

Martin Marietta Corporation
Denver, Colorado, 80201

for

National Aeronautics and Space Administration
George C. Marshall Space Flight Center
Huntsville, Alabama

FOREWORD

This report was prepared by Martin Marietta Corporation under Contract NAS8-21330, Development of Advanced Materials for Integrated Tank Insulation System for the Long Term Storage of Cryogens in Space, for the George C. Marshall Space Flight Center of the National Aeronautics and Space Administration. The NASA contract monitor was Dr. James M. Stuckey of the MSFC Astronautics Laboratory.

Significant contributions to this report were made by the following Martin Marietta personnel:

Dr. Thomas E. Bowman
Dr. Ralph E. Hise
Ron L. Kirlin
Ernest G. Littler
Jack S. Marino
Arlen I. Reichert
Lawrence J. Rose

CONTENTS

Figure

Table

SUMMARY

The objectives of this study have been to evaluate, analytically and experimentally, certain concepts for improving the long term space storability of liquid hydrogen in large scale tankage systems. In particular, concepts were evaluated for the reduction of total boiloff by use of the vented hydrogen to intercept a part of the heat leak to the tank.

All analyses are compared to predicted performance of a reference vehicle. The reference vehicle consists of a tank, roughly equivalent to the combined fuel and oxidizer tanks in an SIV-B stage, supported within a load-carrying shroud. The tank is supported by a tubular titanium truss system, and insulated with multilayer insulation. Thermal conductivity and density of the insulation are treated parametrically.

The cooling of piping connections to the tank was evaluated and optimized for a typical case. A heat flux reduction of up to 60% is calculated for the case where the vent gas used to cool the pipe equals the boiloff resulting from the pipe heat flux. In this case, the heat exchanger is installed over most of the pipe length, depending on the entrance temperature. Local cooling of a short section of the pipe was also evaluated for the case of several heat exchangers connected in series. The cooling of the tank support structure was generally found to be unfeasible because of the complexity of the required heat exchanger circuit and the relatively small heat flux due to the support system.

The interception of heat within the tank insulation system was evaluated in detail. A concept that appears attractive is the division of the tank insulation into two parts -- a shroud- and a tank-mounted blanket. A heat exchanger is installed between the two and is coupled by radiation, rather than physical attachment, to the blankets. A reduction of heat flux through the insulation is calculated to be 50% or more, with predicted net increases in remaining liquid hydrogen of up to 1500 lb (out of 50 to 60,000 lb), depending on insulation properties. A small scale test (4-ft diameter tank) was conducted which demonstrated the insulation heat interception concept using a radiatively coupled heat exchanger.

The use of nonmetallic composite materials in the tank support structure, was considered as a means of reducing heat input to the tank. Thermal conductivity tests were conducted for S-glass epoxy, boron epoxy, and graphite epoxy composites. Thermal conductances were also measured for a self-aligning spherical bearing and a stacked washer assembly. A concept for applying tension and compression loads to nonmetallic fibers, particularly boron, was developed and evaluated in preliminary feasibility tests. The use of S-glass and/or boron epoxy composite materials for tank supports results in an improvement in heat leak of 60% or more over the reference vehicle configuration.

A concept for interposing a layer of hydrogen vapor between the liquid and tank wall in the vicinity of concentrated heat input, such as the feed line penetration, was considered. The feasibility of a capillary internal insulation concept using nonmetallic honeycomb to position gas adjacent to the tank wall was demonstrated. When this internal insulation concept was analytically evaluated, it was found to lack promise for long-term hydrogen storage applications.

I. INTRODUCTION

With the first steps of manned exploration of the lunar system an accomplished fact, attention will be focused on more advanced space missions including manned exploration of the planets. The nature of these advanced missions will result in larger vehicles, longer missions, and more extensive use of cryogens for upper stages. The objective of this study has been the investigation of techniques for improving the long term storability of liquid hydrogen in large scale space tankage systems. Particular emphasis has been placed on the use of the refrigeration capability of vent gas to reduce overall boiloff.

Of utmost importance to the problem of long term storage of liquid hydrogen and other cryogens is the development of high performance insulation systems. Promising work has been done in this area in recent years, leading to the possibility that heat leakage from a liquid cryogen tank can be reduced to the point that venting will be totally eliminated for storage periods of several months, if not years. However, some question remains as to whether the laboratory performance of insulation systems can be achieved when applied to large scale tankage. The present study has been largely divorced from the question of insulation performance; rather, conservative insulation characteristics, resulting in a vented tankage system, have been assumed. The results will be applicable for more promising insulation materials, but mission durations of interest may be correspondingly longer.

For vented storage systems, opportunity exists for using the cold vent gas as a heat sink. By transferring heat from major conduction paths to this vent gas, a portion of the incoming heat flow will be intercepted, resulting in a lower heat flux to the cryogen tank and, consequently, a lower boiloff rate. For the typical shroud-mounted storage tank, heat will reach the tank through three major paths; tank support structure, connecting pipes, and tank insulation system. Therefore, concepts for effecting the interception of heat in these conduction paths by use of vent gas have been evaluated in significant detail.

To reduce heat transfer through structural support members, the use of nonmetallic composite materials was considered. The materials that were evaluated were glass-epoxy and boron-epoxy. The predicted performance of tubular struts of these composites

was compared with a reference titanium strut system. An experimental program was conducted to determine the thermal conductivity of these materials down to near liquid hydrogen temperature. Thermal conductivity was also determined for graphite-epoxy specimens. Limited thermal conduction tests were made for a multiple stacked washer linkage and a commercially available spherical bearing with applied force as a parameter.

Analytical predictions were quite favorable toward the use of an insulation heat exchanger, placed between shroud and tank-mounted insulation blankets to intercept a portion of the insulation heat leakage. Therefore, a system demonstration test of this concept was performed, using radiation coupling between the heat exchanger and the insulation blanket surfaces.

Computer techniques for solving analytical problems have been used liberally throughout this study. The use of efficient iterative numerical routines frequently permits solution of problems in their most basic form, without extensive algebraic manipulation and simplification. In this case, the bulk of the programing effort is concerned with numerical techniques, iteration schemes, convergence criteria and other details not directly bearing on the physics of the problem being solved. For this reason, results are in many instances presented with only a minimum explanation of the method of solution.

II. TECHNICAL DISCUSSION OF TECHNIQUES FOR REDUCING BOILOFF LOSSES

A. STUDY REQUIREMENTS AND GROUND RULES

In order to permit direct comparison of results of the various analyses, a single vehicle configuration was considered. A tankage system of SIV-B scale with a mission duration of 120 days was selected. A single liquid hydrogen tank with hemispherical ends, equivalent to the combined SIV-B fuel and oxidizer tanks, was assumed to be supported within a load carrying shroud. The tank diameter was constrained to a fixed value of 260 inches, while the shroud diameter and tank barrel length were allowed to vary as necessary.

An arbitrary mission was considered. Therefore, a thermal space environment was not specified, but rather a fixed shroud temperature of 400°R was assumed. For structural considerations, boost acceleration values of 5 g aft, 2 g forward, and 2.5 g lateral, with a safety factor of 1.4 were assumed. Tank ullage volume was taken as 5% and a tank operating pressure of 2 to 40 psig was assumed. The tank pressurant was assumed to be gaseous hydrogen. The tank piping was functionally equivalent to that connected to the SIV-B hydrogen tank.

An optimization criterion was adopted that permits comparison of all system alternatives directly in terms of the quantity of liquid hydrogen remaining after 120 days in space. For each system to be evaluated, the total weight of the following items is constrained to a fixed value: loaded hydrogen, tank and tank support structure, insulation, shroud, heat exchanger system, if any, and piping. This is accomplished by adjusting the tank barrel length, and consequently the shroud length, for each configuration. Thus, if the thickness or density of the tank insulation is increased, for example, the tank barrel length is decreased so that the decrease of tank, shroud, and hydrogen weight balances the increase in insulation weight.

The use of subcooled or partially solidified hydrogen to increase the heat sink capability of the propellant was not considered. In keeping with the arbitrary shroud temperature definition, thermal coatings, sun shields, and other means of reducing shroud temperature were not considered.

B. REFERENCE VEHICLE

In order to evaluate improvements in system performance attained by incorporating heat interception devices, a reference vehicle was defined. This reference vehicle is based on conservative, current design practice. It is designed in sufficient detail to define its thermal characteristics and weight, but is not intended as the mainstream effort of the study. All thermal improvement studies that were subsequently performed are, in effect, modifications to this reference vehicle.

The tank and support system are shown in Figure II-1. A monocoque shell with hemispherical domes was selected as the lightest tank concept, since the tank is to be supported within a load carrying shroud. 2014-aluminum was selected as the best candidate material because of its high strength, low weight, compatibility with liquid hydrogen, excellent weldability, and reliable mechanical and physical properties at cryogenic temperatures. The shell is a rolled 2014-aluminum sheet welded longitudinally to form the barrel section with chemically milled land areas for welding. The domes are formed 2014-aluminum sections with chemically milled land areas for welding the sections together and the finished dome to the barrel.

At the fore and aft dome-barrel junction, frames were designed to facilitate ground handling and to implement the airborne load path for the support system. Rolled ring forgings of 2014-aluminum were selected for the tank frames. Forgings were selected instead of extrusions because of the higher design allowables, capability of machining integral lugs and gussets for the support system tie-in, and a higher predictable accuracy in overall dimensions. Integral lugs are used because of better design allowables and dimensional control than those of welded-on lugs. A tension truss consisting of 36 tubular titanium bi-pods was chosen to support the tank, insulation, and hydrogen weight. A series of 24 tension supports at 12 points on the upper barrel-dome intersection provide lateral stabilization.

For sizing the tank, the static load factors used were 5 g aft, 2 g forward, 2.5 g lateral, and a 1.4 safety factor. It should be noted that these loads are arbitrary and do not necessarily correspond to any mission configuration. Actual design load calculations would require more information than has been specified. A temperature of 30°R to 620°R was assumed. A minimum pressure of 2 psi was assumed to be available to stabilize the unloaded tank. The maximum operating pressure was 40 psig.

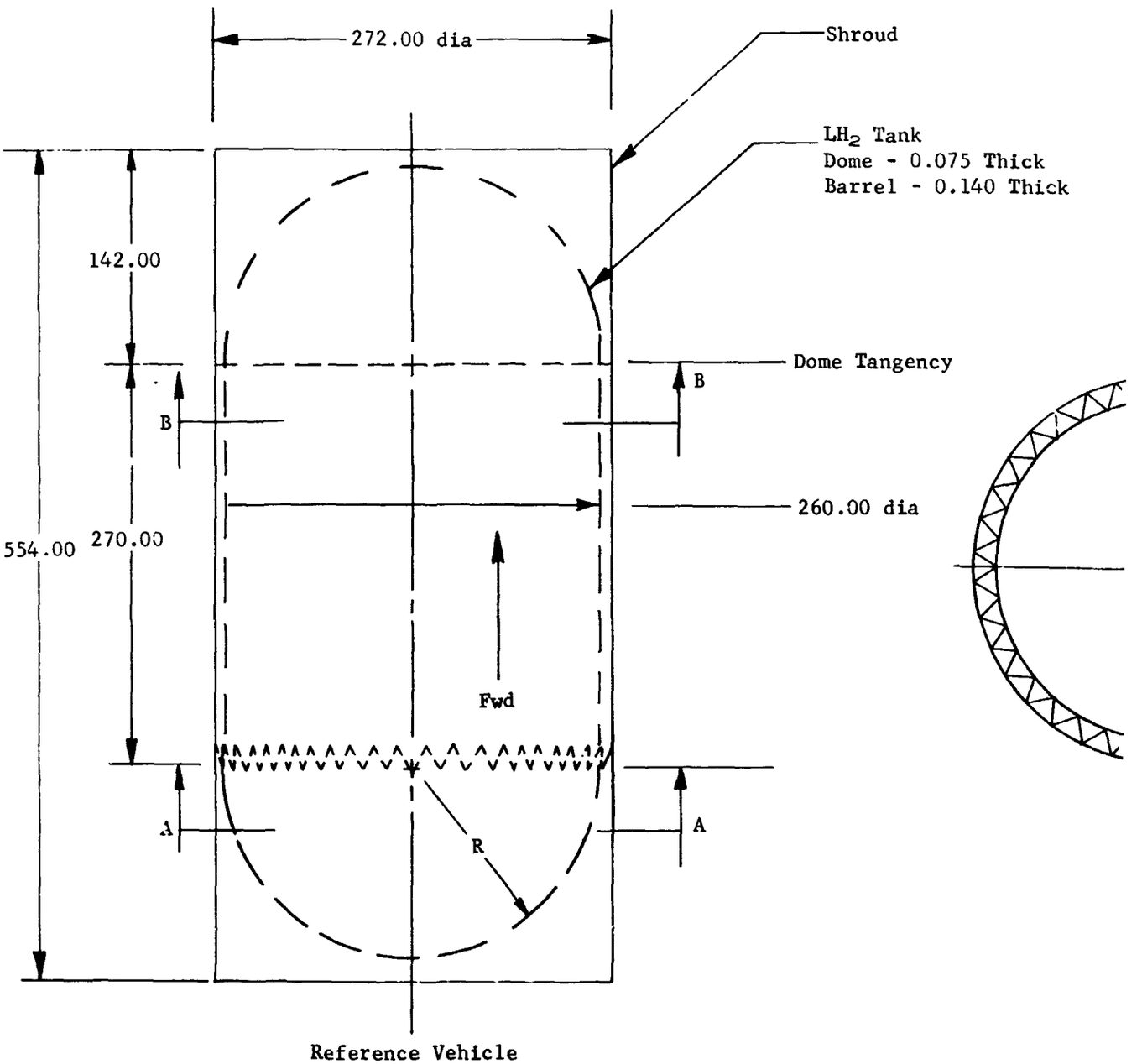

FOLDOUT FRAME 1

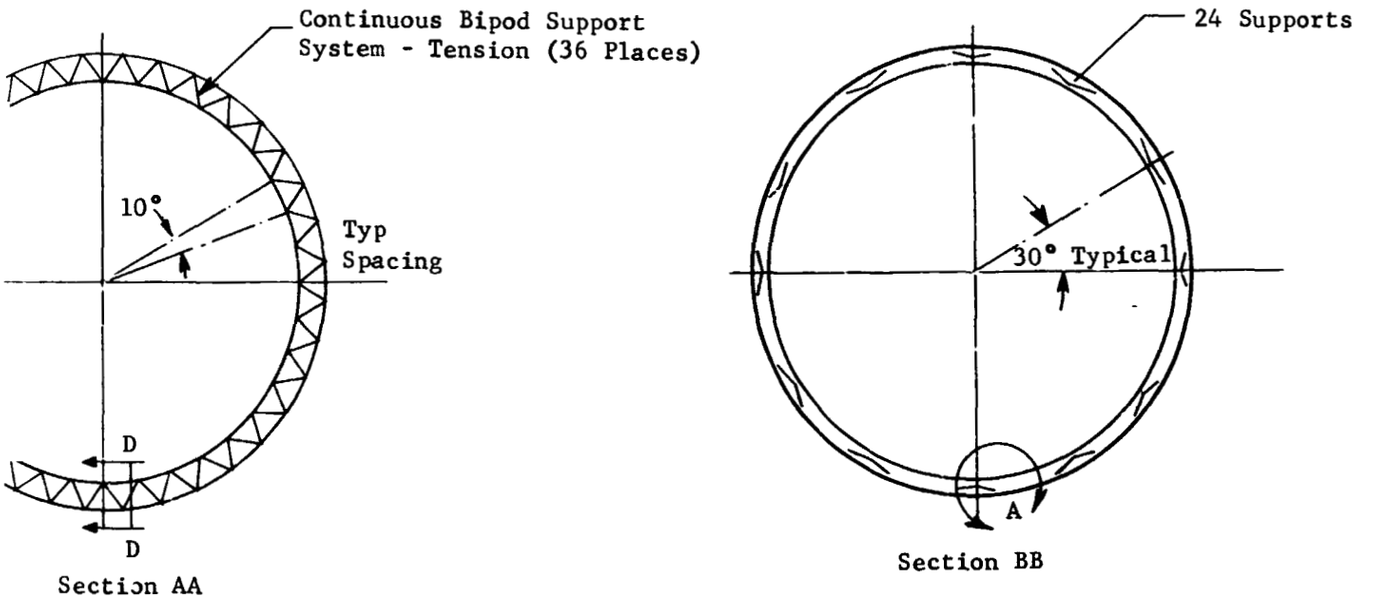

Figure II-1 Reference Vehicle - Structural Configuration

FOLDOUT FRAME 2

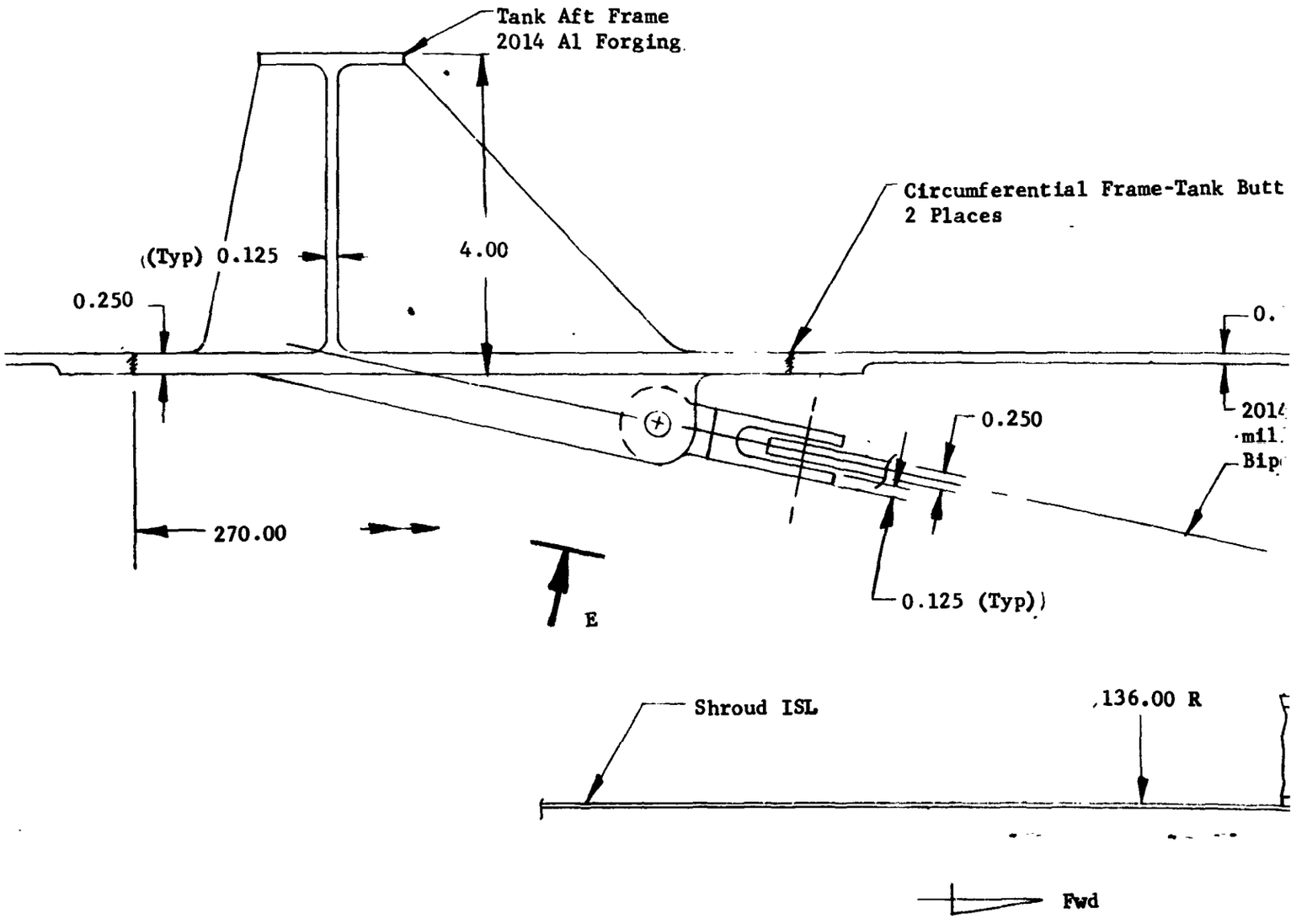

Section DD

FOLDOUT FRAME

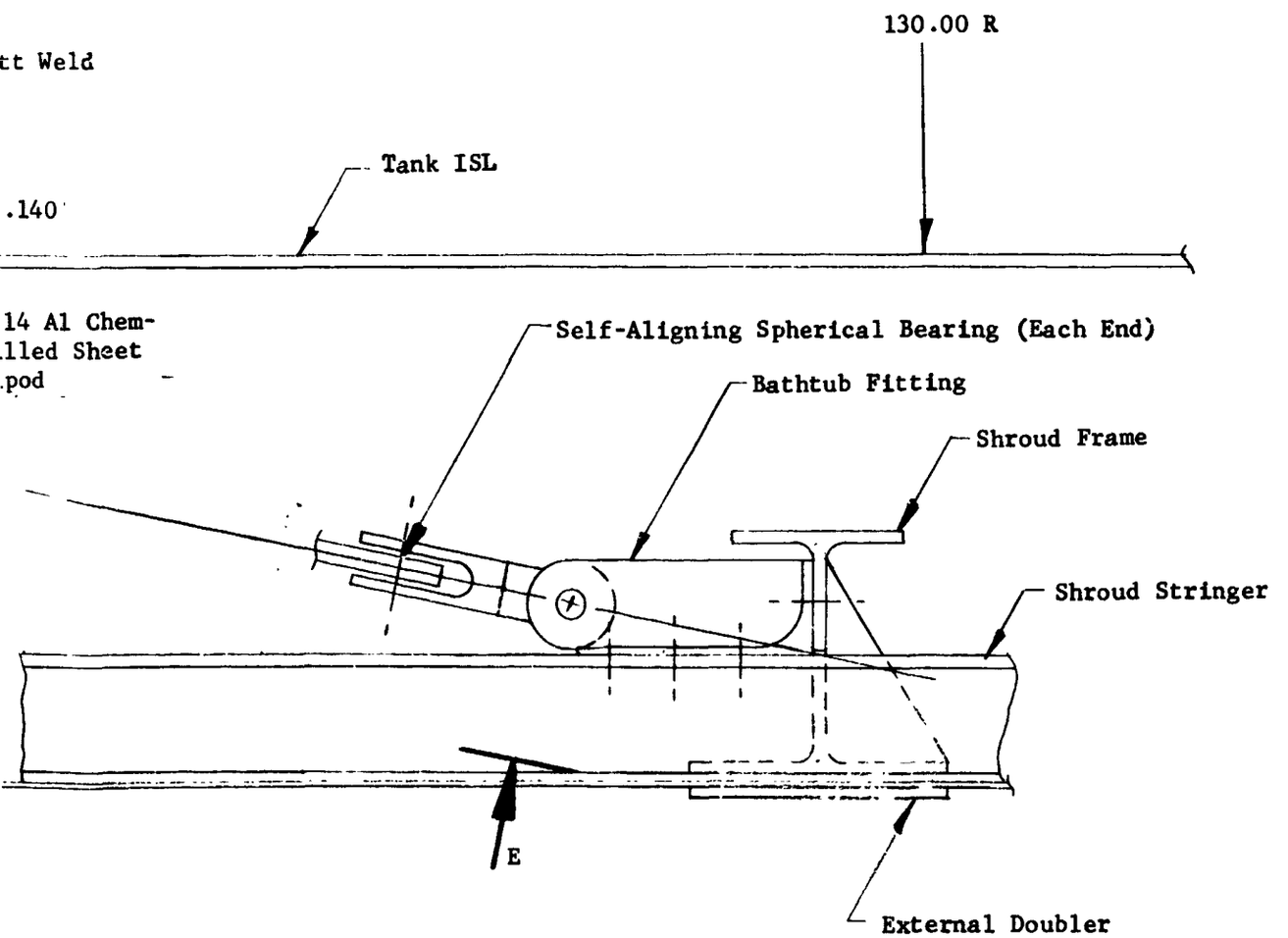

FOLDOUT FRAME 2

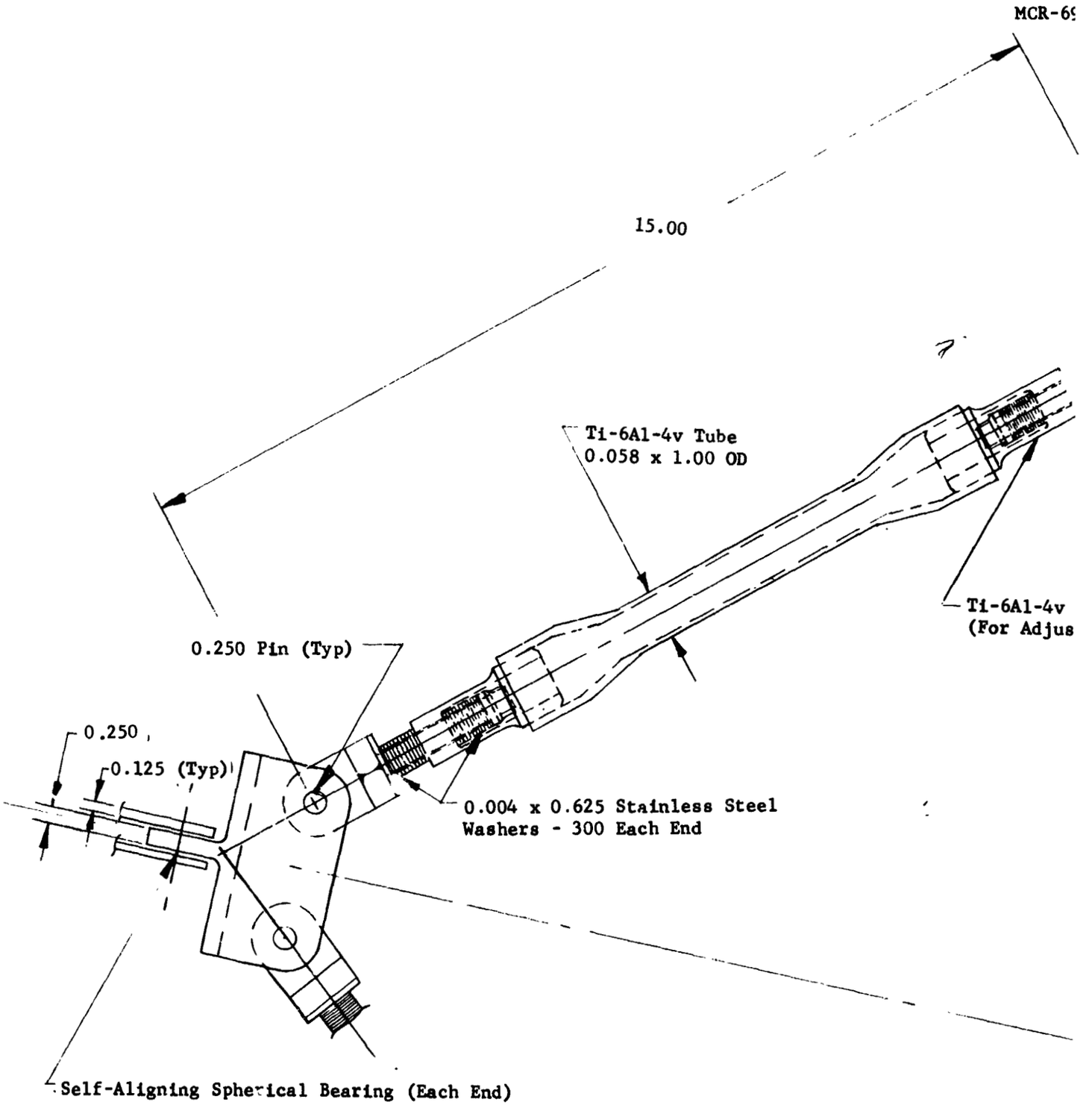

View EE

FOLDOUT FRAME 3

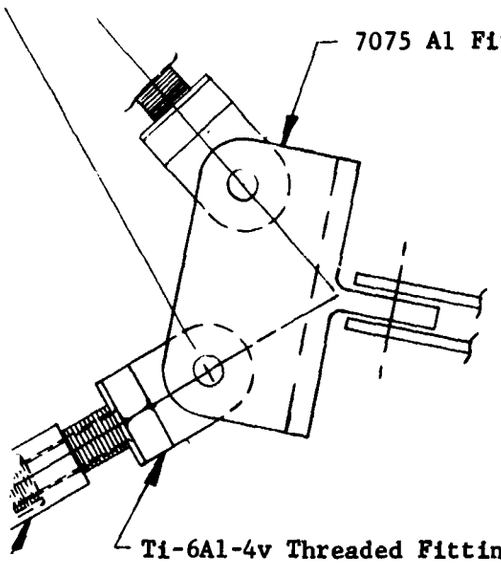

1-4v Threaded Fitting (Each End)
Adjusting Bipod Tube on Instl)

℄ Sym About

Figure II-1 (cont)

FOLDOUT FRAME 2

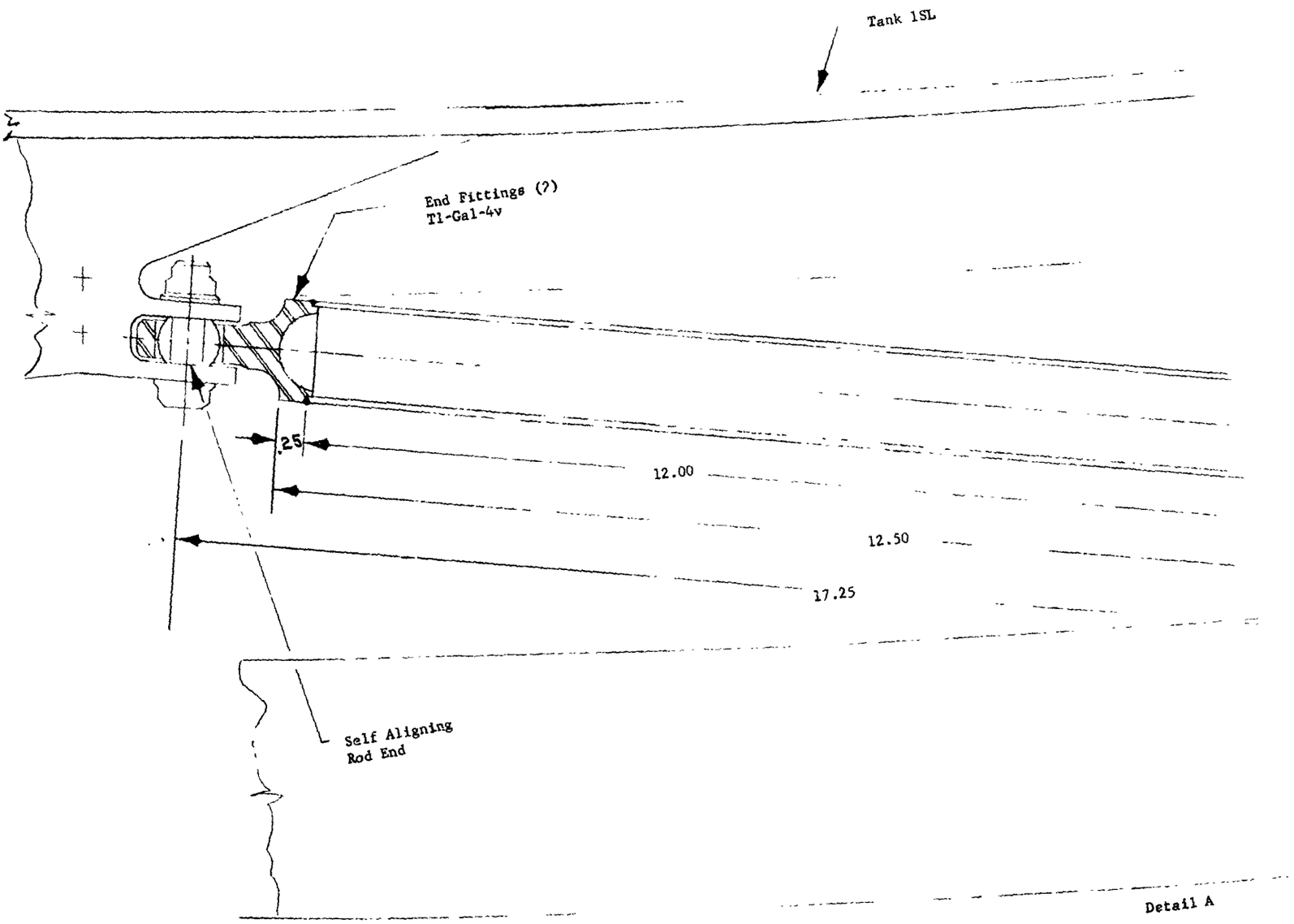

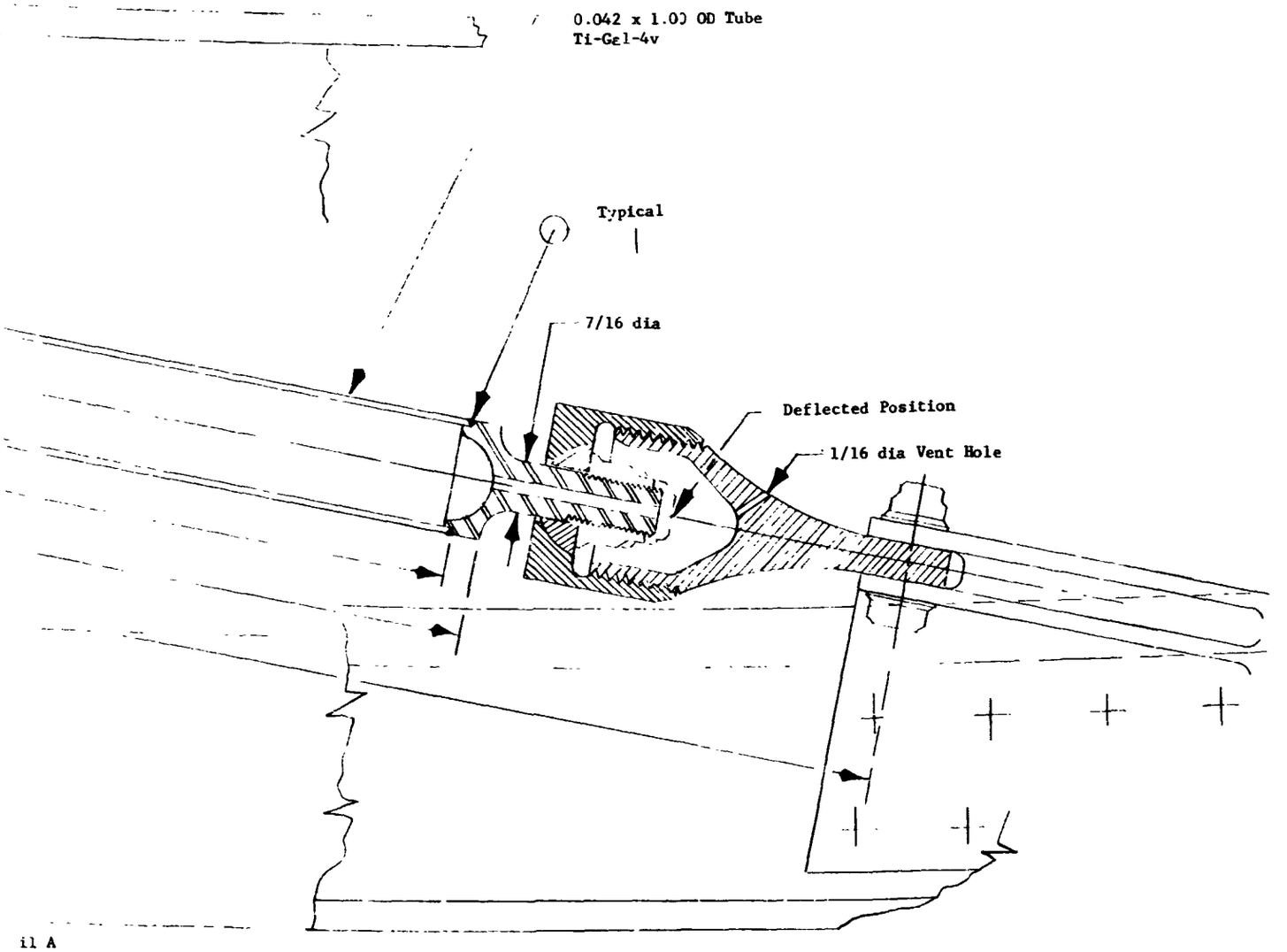

il A

FOLDOUT FRAME 2

Figure II-1 (concl)

Using the above assumptions and data, a total 1 g loaded and insulated tank weight of 65,000 lb was estimated. From this, an axial load of 455,000 lb, a springback load of 183,000 lb, and lateral loads of 105,000 and 124,000 lb at the forward and aft dome barrel junctions, a tank barrel thickness of 0.140 inches and a dome thickness of 0.075 were determined from these data and assumptions. On the basis of conservative, simple beam assumptions and lateral support at 12 places, the maximum moment on the forward tank frame was calculated to be 242,000 in.-lb. A standard I-shape 4.0 x 4.0 x 0.25 in. thick was selected to provide the required section modulus of 4.02 $in.^3$. Similarly, a maximum moment of 63,000 in.-lb and a required section modulus of 1.04 $in.^3$ was estimated for the lower tank frame. This requirement is met by a standard I-shape 4.0 x 2.0 x 0.125 in.

Because of the large differential expansion and contraction caused by pressurization and temperature changes, a tubular support system was chosen. A series of tangential tension supports provides lateral and torsional stabilization of the upper tank without restricting the vertical motion. A tension bi-pod truss at the lower dome-barrel intersection supports the weight of the loaded tank plus lateral and torsional loadings. In addition, the lower support system must act in compression to react the springback loads occurring at thrust termination.

The aft bi-pod support system is made of titanium tabular supports, each with a series of stacked stainless steel washers at each end to increase thermal resistance. On the basis of the above load figures and the assumption that one-half the bi-pods react the loads, a required area of 0.165 $in.^2$ was calculated, based on a 44,000 psi column allowable for Ti-6Al-4V. The cross-section selected was 1.0 in. O.D. x 0.058 in. wall, giving an area of 0.1716 $in.^2$ and a radius of gyration of 0.3337 in. Tension, column and crushing allowables were determined to be adequate. Lug thickness on the tube ends is based on Ti tension allowable applied across the net lug area after subtracting hole area for a press-fit, self-aligning spherical bearing. The pin for the lug was designed using a double shear allowable for a 160,000 psi heat treated alloy steel.

The upper support system was designed to react lateral and torsional loads only. A release fitting was incorporated to assure that the tubes were loaded in tension only, permitting longer tube lengths with higher thermal resistance. The mounting points for the supports extended into the annular space so as to minimize interference with tank- and shroud-mounted insulation blankets. The

adjustable nut, housing the self-aligning spherical rod end, was pre-tensioned on installation to allow a slight relaxation due to tank shrinkage and pressurization. Assuming that the lateral loads will be reacted by the six supports most nearly aligned with the load vector, the maximum ultimate support load for any one member is 18,500 lb, with a maximum tank displacement of 0.1 in.

The pipes connected to the tank were assumed to be:

Main Feedline
10 in. O.D. x 0.188 in. wall, stainless steel
Case 1 - 36 in. long
Case 2 - 60 in. long

Vent Line
6 in. O.D. x 0.078 in. wall, stainless steel
170 in. long

Pressurization Lines (2)
3/8 in. O.D. x 0.035 in. wall, stainless steel
160 in. long, each

1. Weight Estimate for Reference Vehicle

The following weight estimate is based on a tank insulation thickness of 3 in. with a density of 3 lb/ft^3 and a nominal tank barrel length of 270 in.

	Weight (lb)
Tank	5,084
Tank supports	148
Shroud & support structure	13,076
Insulation	2,320
Insulation installation	225
Plumbing	130
Liquid hydrogen	56,850
Total weight	77,833

2. Optimization of Insulation Thickness

A parametric evaluation was made of the optimum tank-mounted insulation thickness. For the reference vehicle, the liquid and vapor were assumed to be separated, and the tank directly vented from the vapor region. Actual accomplishment of this venting scheme is a formidable problem, requiring some active or passive

means for locating the vapor at a known position in the tank. However, it was assumed in the reference vehicle evaluation that this requirement can be met with no weight or performance penalty. The previously described optimization criterion used maximizes the hydrogen remaining after 120 days when the initial weight of loaded hydrogen plus tankage is held constant. As the thickness and density of the insulation are varied, the tank length is varied to constrain the total weight of tank, shroud, liquid, and insulation to a fixed value of 77,330 lb. It is noted that this criterion gives the maximum quantity of available hydrogen after 120 days, but would not result in the greatest ΔV capability for a propulsion stage. For this case, optimum ΔV would occur with less insulation, depending on the magnitude of the fixed mass or payload versus the weight of tank, propellant, and insulation. As the payload increases, the optimum insulation thickness approaches the same value for both cases.

For this analysis, the following data were used:

Total weight of liquid hydrogen, insulation, tank and shroud	= 77,330 lb
Heat leak caused by pipes and supports (initial estimate)	= 30 Btu/hr
Liquid (and tank wall) temperature	= 40°R
Shroud temperature	= 400°R
Shroud weight (assumed)	= 25 lb/ft radius/ft length
Tank barrel weight	= 137.2 lb/ft length

A k value was assumed to represent the average effective thermal conductivity of the applied insulation, and the value for insulation density represents the average density of the applied insulation system. If the decrease in weight of the loaded propellant were a linear function of the product of insulation thickness and density, it could readily be shown that the maximum remaining propellant is a function of the product of the effective thermal conductivity and the average insulation density, ρ. Since this is not the case, a numerical survey was made for insulation thickness from 1 to 6 in. for various values of k and ρ. Results of this survey indicate that the nonlinear effect is negligible, and that the remaining hydrogen after 120 days is directly dependent on the parameter $k\rho$. Figure II-2 shows this relationship.

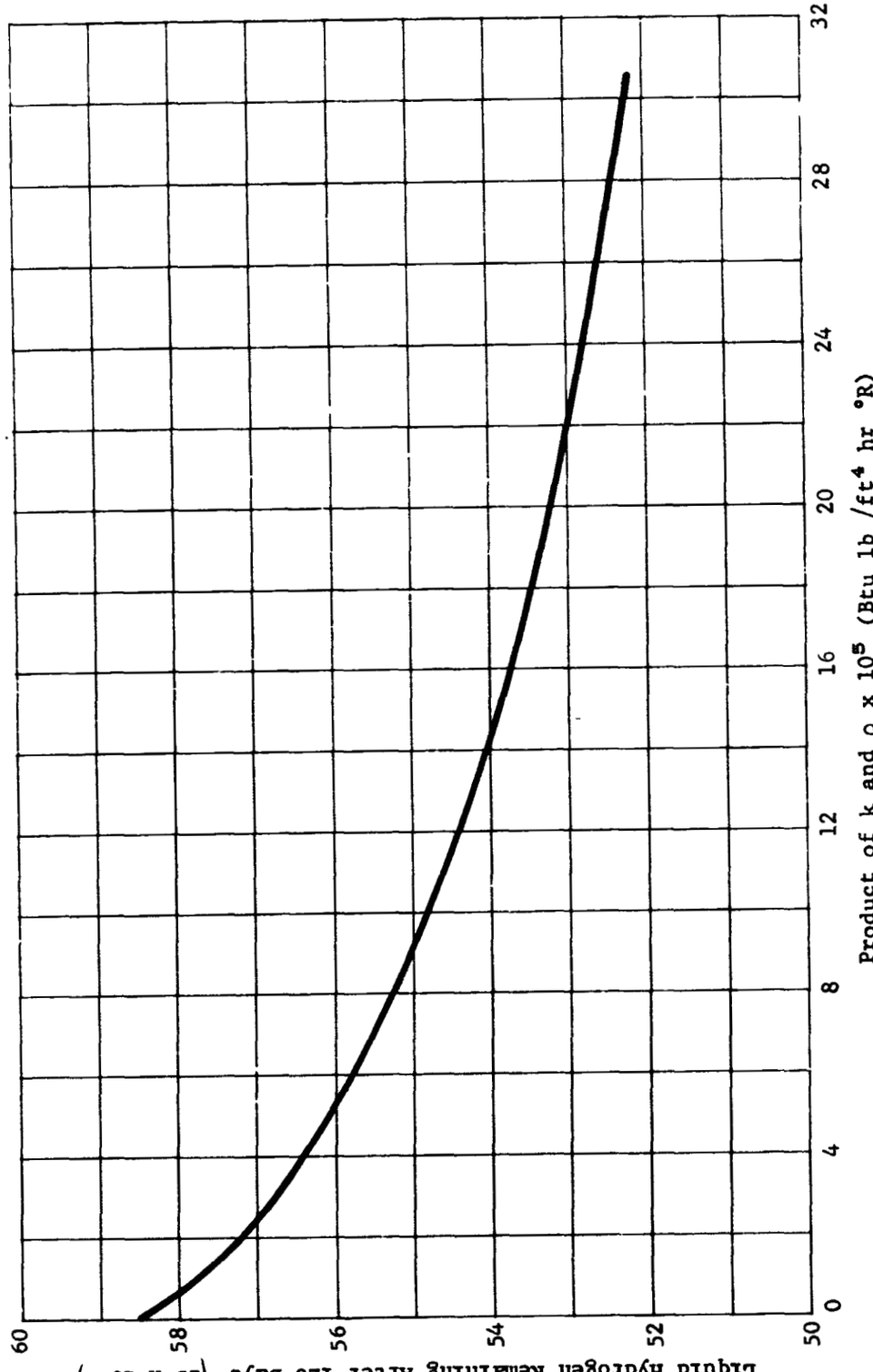

Figure II-2 Propellant Remaining Versus kρ for Optimized Insulation Thickness

Figure II-3 shows the effect of insulation blanket thickness, density, and thermal conductivity on the quantity of liquid hydrogen remaining after 120 days for a fixed value of 8×10^{-5} Btu lb_m/ft^4 hr °R, as a typical example, for the parameter, $k\rho$. Optimum thickness of the insulation versus thermal conductivity is plotted in Figure II-4 for several values of density.

For the above analysis, a simplifying assumption was made that the tank would be vented at 25 psig and that the tank contents would be at 40°R during the entire coast period. The heat input required to raise the liquid temperature from its initial saturation temperature of about 36 to 40°R was assumed to be roughly that caused by ground and boost heating. The assumption was made for the purpose of simplifying subsequent analyses and permitting direct comparison of the results.

For many vehicle, mission, and insulation combinations, the tank venting requirement can be eliminated by permitting a rise in the temperature of the liquid and an increase in tank pressure. In this case, all the heat reaching the tank is absorbed by the tank and its contents. In order to evaluate the applicability of the unvented mode to the reference vehicle and mission considered here, a numerical survey was conducted. This analysis was similar to that for the direct vent case. By digital computer iteration, the tank size and insulation thickness were found that would simultaneously result in a fixed total weight of tank, fluid, shroud, and insulation of 77,330 lb, and an increase in energy to the system resulting in the specified final temperature and pressure. In this analysis, changes in internal energy of the liquid and enthalpy of the gas, plus phase transition energy of the evaporating liquid were accounted for. Because of the low specific heat of aluminum, the change in energy of the tank was neglected. The effective thermal conductivity of the tank-mounted insulation was assumed to be constant over the range of the cold side temperature from initial to final conditions. Tank weight was based on a simple proportionality to the tank design pressure that was taken at 15 psi above operating pressure. Shroud diameter was adjusted to provide a 4-in. gap between insulation and shroud skin for all cases.

Two assumptions in the analysis of the unvented configuration bias the results in its favor: (1) the ground and boost heating are neglected and all heat gain occurs during coast; (2) the requirement for mixing, and its associated energy inputs, is neglected. In the near absence of gravity forces, natural mixing of the tank contents will be negligible, and forced mixing is required to limit thermal stratification and consequent over-pressurization of the tank. This subject is fully treated in Reference 1.

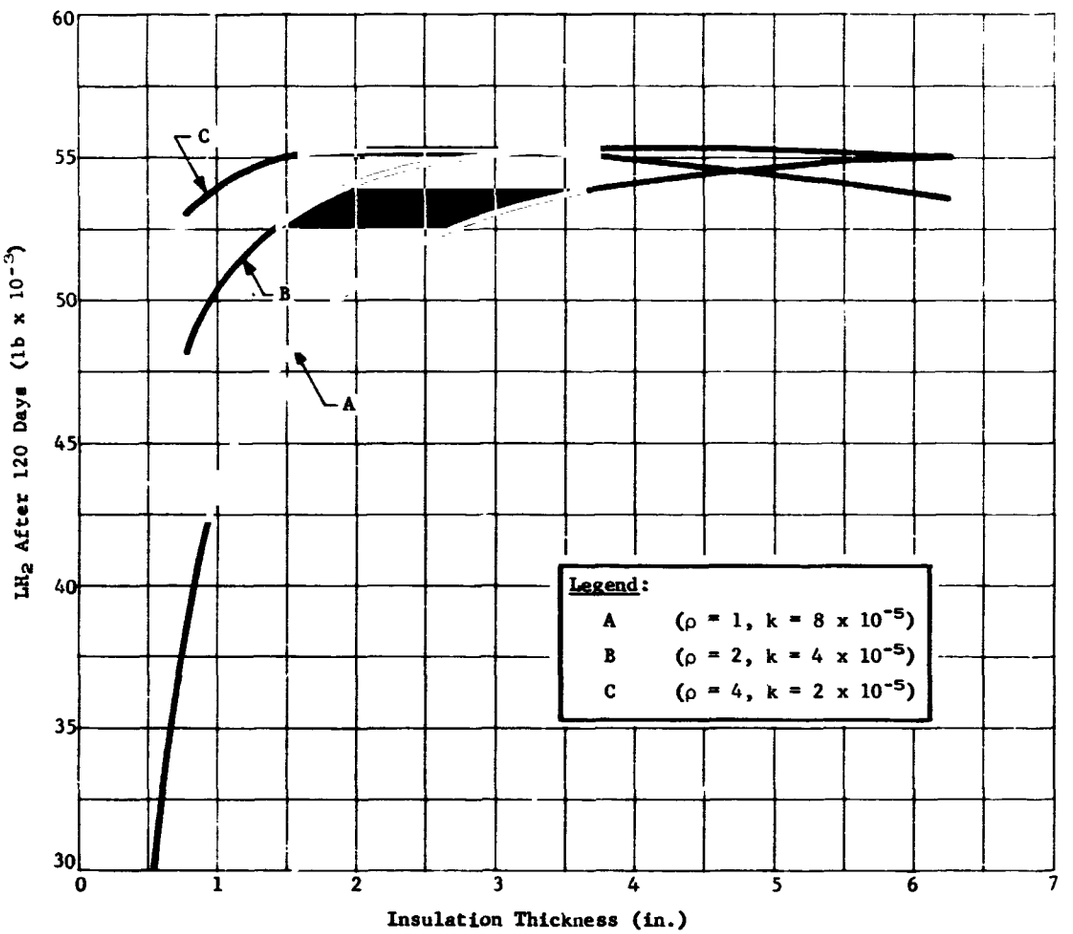

Figure II-3 Propellant Remaining Versus Insulation Thickness for $k\rho = 8 \times 10^{-5}$ Btu lb_m/ft^4 hr °R

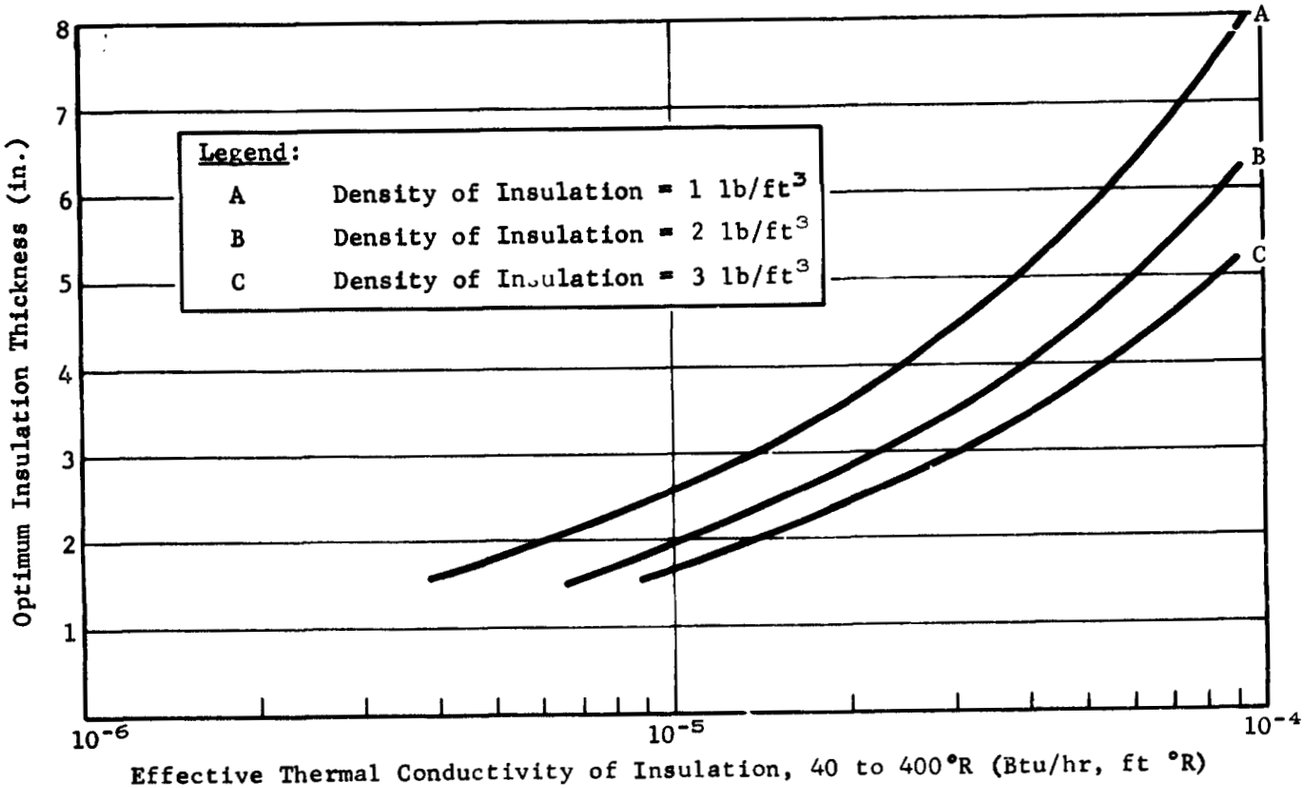

Figure II-4 Optimum Reference Vehicle Insulation Thickness Versus Thermal Conductivity

Results of the unvented survey are presented in Figure II-5 in terms of available propellant. The curve of Figure II-2 is included for comparison with the direct vent configuration. The slight scattering of the data points is due to the effect of the thermal conductivity of the tank insulation. This parameter was varied from 5×10^{-6} to 8×10^{-5} Btu/hr ft °R, the higher points representing the lower value. No safety factor was applied for either of the cases being compared. For very low values of the parameter $k\rho$, a disadvantage results because the increase in tank weight is greater than the decrease in insulation weight which becomes diminishingly small. In view of the assumptions that tend to favor the unvented system, it would appear that an improvement of up to 3% might be realized. The actual optimization procedure would result in choice of the most favorable tank pressure for the insulation system to be used. Figure II-6 gives the minimum insulation thickness required as a function of thermal conductivity. Insulation density has a negligible effect on this requirement.

C. THERMODYNAMIC VENT SYSTEM

In a vehicle coasting in space, the familiar effect of gravity acting to attract matter toward a particular direction relative to the vehicle is essentially absent. This is because the vehicle is essentially free of external forces, and is accelerating or free falling, along with its contents, in accordance with the local gravitational field. The small forces that actually exist, including aerodynamic drag and solar winds plus gravity gradient effects, may amount to 10^{-6} g or less.

In a zero-g or weightless environment, the static liquid-gas configuration is determined by the tendency for the liquid to wet solid materials (for most liquids including liquid hydrogen), and the effect of surface tension that causes liquid gas interfacial surfaces to act as stretched membranes. For the tank configuration considered here with a 5% ullage volume in a zero-g environment, the gas can be predicted to be contained in one or more spherical bubbles located randomly within the tank. In theory, the small acceleration effect caused by forces acting on the vehicle, if acting in an axial direction, is sufficient to relocate the ullage gas to the end of the tank. Under such an acceleration field (less than 10^{-6} g), however, the energy required to produce large scale liquid motion is extremely small. Such energy can result from attitude changes or pulsing of attitude control thrusters. It is, therefore, most difficult to predict the position of the ullage gas.

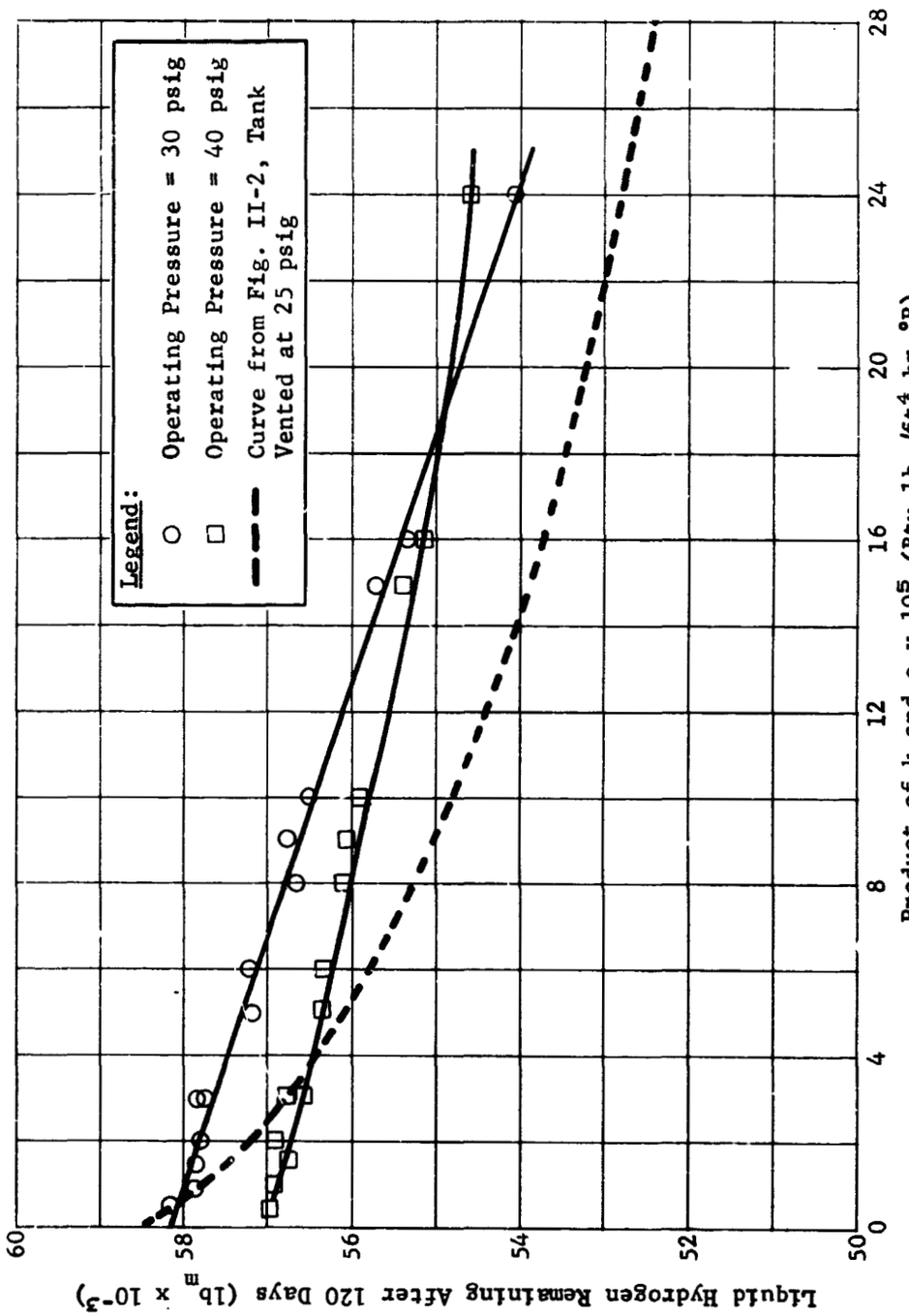

Figure II-5 Maximum Available Propellant for Unvented Reference Vehicle, 120-Day Mission

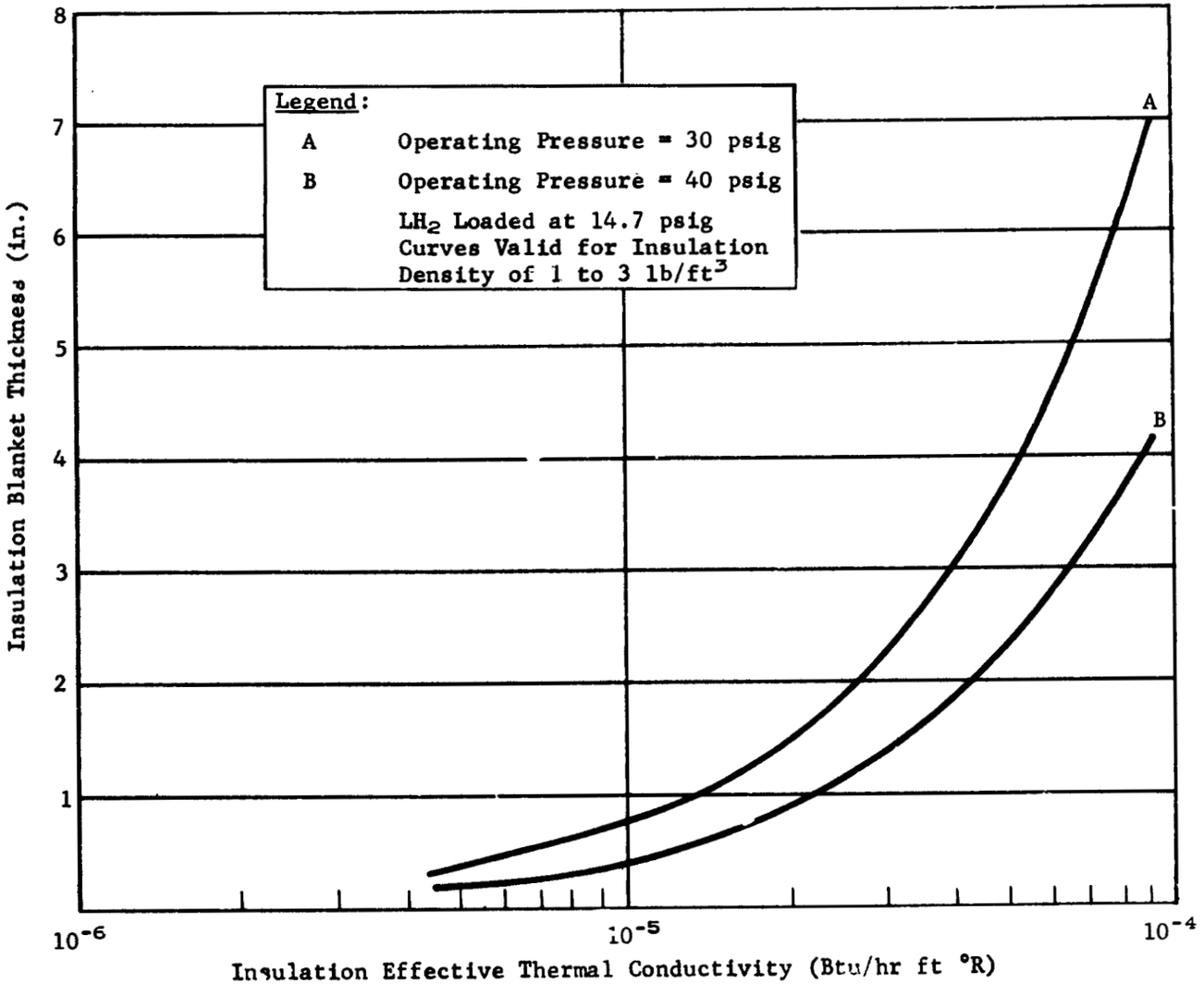

Figure II-6 Minimum Tank Insulation Thickness for Unvented Reference Vehicle, 120-Day Mission

The requirement for admitting only gas to the tank vent system can be circumvented by use of the thermodynamic vent system (References 2, 3, and 4). In this concept, liquid may be admitted to the vent system. On entry, it passes through a pressure reducing device such as an orifice. Beyond the pressure reducer is a heat exchanger located within the tank and/or on the tank wall. When the liquid vent fluid enters the heat exchanger at a pressure significantly below that of the tank, its boiling temperature is reduced. Thus, boiling heat transfer from the tank and its contained fluid takes place until the liquid is fully vaporized. The heat exchanger is sized to allow the vaporized fluid to reach essentially the temperature of the tank contents. The vent fluid thereby leaves the tank with approximately the same heat content as if it had been vented directly.

While the control of the gas position in a tank is difficult, it is relatively easy to position liquid to a vent inlet. This can be done with a capillary device working on the familiar principle of the blotter. However, in a very low gravity environment, closely separated plates of sheet metal spaced one inch or less apart, act effectively as a blotter or capillary sump. Some care must be taken to prevent this sump from receiving excessive heat that might block its action by evaporation. In addition to thermal isolation from the vicinity of the tank wall, use can be made of the heat exchanger to assure that the sump does not overheat.

Other problems to be concerned with in the use of the thermodynamic vent system include prevention of freezing of the liquid hydrogen on entry due to too low a reduced pressure, and design of the heat exchanger to limit thermal stratification in the tank to an acceptable value. The use of a powered mixer to accomplish the latter may be necessary, but this approach becomes decreasingly attractive as the mission duration increases.

D. INSULATION COOLING

1. Heat Leak Reduction by Cooling within Tank Insulation System

Results of the evaluation of the direct-vented and unvented reference vehicle configurations for typical insulation characteristics indicate that the most significant path for heat flow to the tank is through the tank insulation system. A promising means for reducing this heat input is to intercept part of it with the boiloff gas. Several approaches can be visualized for accomplishing this improvement.

It can be shown that the maximum reduction of heat flux should be obtained when the vent gas is used to cool all layers of the insulation blanket from inside out. Because the vent gas must be contained so as to prevent gas conduction within the insulation, this approach can be dismissed for the present time as being of questionable practicality. A second approach would be to install a conductive layer (such as light gage sheet aluminum), with heat exchanger attached, within the insulation blanket.

Since the tank being considered is mounted within a load carrying shroud, a more practical approach would be to divide the insulation into two blankets, tank- and shroud-mounted, with the heat exchanger between the two. For this insulation configuration, the heat exchanger can be physically and thermally attached to either the outer surface of the tank-mounted blanket or the inner surface of the shroud-mounted blanket. An alternative concept is to install the heat exchanger between the two, with a minimum of physical contact. Radiant heat transfer is the means, in this case, by which heat is intercepted by the heat exchanger. This approach appears to offer sufficient producibility advantages to justify its further consideration. Therefore, a detailed analysis of this concept was undertaken.

As with most analyses, simplifying assumptions were required to render the problem tractable to a reasonably manageable approach. The heat transfer along the foils of the insulation blankets is expected to be quite high compared to the flux through the blanket. Therefore, the assumption was made that this conduction was infinite, making each of the insulation surfaces isothermal. This reduces the problem to a single dimension. An alternative approach was to assume no conduction whatever along the annulus. A comparison of preliminary analyses based on these assumptions led to the conclusion that the one-dimensional case was slightly conservative. This conclusion was confirmed by a more detailed analysis that was later made on the basis of zero conduction for a single example.

Ideally, multilayer insulation is a series of radiation shields. The transfer of heat through such an ideal arrangement of reflective layers depends on the fourth powers of the layer temperatures. Hence, the effective thermal conductivity is strongly dependent on the operating temperature of the insulation. In practice, the assembly of such insulation introduces additional conduction between adjacent layers caused by contact with each other or with spacer material. This conduction is more nearly proportional to temperature difference, although the conductivity of the spacer may also increase as temperature increases. The effective conductivity of the combined system is highly dependent on temperature.

When heat is removed from an intermediate layer, reducing its temperature, the steady-state temperatures of all the layers, except the fixed temperature hot and cold sides, are reduced. Thus, in addition to diverting part of the heat out of the insulation system, the performance of the insulation is also improved. It is therefore clear that the model used to represent the insulation thermal conductivity is of considerable importance to this analysis. A simple model of a multilayer insulation, based on the properties of aluminized mylar and a nylon spacer material was used. This insulation thermal conductivity model is described in Appendix A, and is given by the equation:

$$k(T_2,T_1) = \frac{1}{T_2 - T_1}\left[\alpha\eta\left(T_2 - T_1 + \frac{e^{-\delta T_2} - e^{-\delta T_1}}{\delta}\right) + \frac{\sigma}{N}\left\{\left(\frac{\beta}{2} + \frac{\beta^2}{4}\right)(T_2^4 - T_1^4) + 0.4\gamma\,(1+\beta)\,(T_2^5 - T_1^5)\right\}\right] \qquad [1]$$

where

$k(T_2,T_1)$ = effective blanket thermal conductivity for surface temperatures of T_2, T_1, Btu/hr ft °R

α = apparent fraction of total area occupied by spacer material if assumed to be solid and in perfect contact with radiation shields, and includes the effect of contact resistance

σ = Stefan Boltzmann constant

β and γ = coefficients in the equation $\epsilon(T) = \beta + \gamma T$

$\epsilon(T)$ = emissivity of foil material at temperature T

δ and η = coefficients defining the spacer material thermal conductivity in the expression $k_{spacer} = \eta \left(1 - e^{-\delta T}\right)$, Btu/hr ft °R

N = number of reflective shields per ft

2. The Radiation Problem in the Region between the Two Insulation Blankets

At the heart of the insulation cooling problem is a three-body radiation situation involving the exposed surfaces of the two insulation blankets and the heat exchanger tubes in the region between the blankets, each of which will, in general, be at different temperatures. By assuming that each of these three surfaces is isothermal, the radiation analysis becomes tractable. For the sake of this analysis, conduction links between the heat exchanger and the insulation surfaces that might be added in an actual system are not considered, because their effect would be to improve the performance of the heat exchanger and complicate the analysis.

Consider two infinite parallel planes, at temperatures T_1 and T_2, and between them heat exchanger tubes of diameter d and temperature T_e, at a spacing L, as in Figure II-7. Since nothing is lost (and much gained) by making the heat exchanger tubes as black as possible, their emissivity and absorptivity will be taken as unity. The insulation surfaces, on the other hand, should have emissivities as low as possible to minimize the overall heat transfer. The emissivity and absorptivity of each plane will hence be taken to be ϵ, arbitrary in magnitude (and assumed independent of both wavelength and temperature).

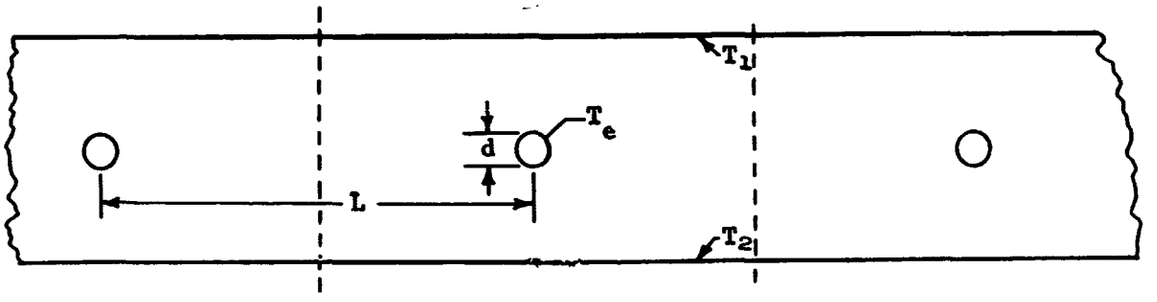

Figure II-7 The Annulus Radiation Problem

Because of the assumptions of uniform temperatures and grayness, the analysis can be carried out in a very straightforward manner using Poljak's method. By symmetry, we can consider only the segment between the two dashed lines in Figure II-7. Since the energy crossing each dashed line from left to right is in every respect the same as the energy crossing from right to left, there is no loss of rigor entailed in postulating that the tube "sees" only the two plane segments between the two dashed lines (as if the dashed lines were perfect reflectors), and that they in turn "see" only each other and the tube. That is, the radiation balances are the same as they would be if all the energy leaving the tube went directly to one or the other of the plane segments (half to each, since the tube radiates uniformly in all directions), and $\frac{\pi d}{2L}$ of the energy leaving each plane went first to the tube and the rest directly to the other plane segment.

Let R_1, R_2 and R_e be the total radiation leaving the surfaces at T_1, T_2 and T_e, respectively, per unit time. Since the tube is black, R_e consists entirely of emitted radiation:

$$R_e = \pi d \, \sigma \, T_e^4 \qquad [2]$$

The radiation leaving each plane segment consists of emitted radiation and a reflection of the radiation reaching the plane segment from the tube and the other plane segment. On the basis of the discussion of the preceding paragraph, the resulting equations are:

$$R_2 = L\epsilon\sigma \, T_2^4 + (1 - \epsilon)\left[\frac{1}{2} R_e + \left(1 - \frac{\pi d}{2L}\right) R_1\right] \qquad [3]$$

$$R_1 = L\epsilon\sigma \, T_1^4 + (1 - \epsilon)\left[\frac{1}{2} R_e + \left(1 - \frac{\pi d}{2L}\right) R_2\right] \qquad [4]$$

We wish to find the <u>net</u> radiation arriving at the heat exchanger tube and the cooler of the two plane segments. If these net radiation fluxes are called Q_e and Q_1, respectively, then

$$Q_e = \frac{\pi d}{2L} (R_1 + R_2) - R_e \qquad [5]$$

$$Q_1 = \left(1 - \frac{\pi d}{2L}\right) R_2 + \frac{1}{2} R_e - R_1 \qquad [6]$$

Solving [2], [3], and [4] simultaneously for R_1, R_2, and R_e, and substituting in [5] and [6] yields

$$Q_e = \frac{\sigma \pi d}{1 + \frac{\pi d}{2L}\left(\frac{1}{\epsilon} - 1\right)} \left(\frac{T_1^4 + T_2^4}{2} - T_e^4\right)$$

$$Q_1 = \frac{\sigma L}{1 + \frac{\pi d}{2L}\left(\frac{1}{\epsilon} - 1\right)} \left[\frac{T_2^4 - T_1^4}{\frac{1}{\epsilon}\left(\frac{2 - \pi d/2L}{1 - \pi d/2L}\right) - 1} + \frac{\pi d}{2L}\left(T_e^4 - T_1^4\right)\right]$$

or, expressing both per unit area of either <u>plane</u> surface:

$$q_e = \frac{\sigma\left(T_1^4 + T_2^4 - 2\,T_e\right)}{\frac{1}{F} + \frac{1}{\epsilon} - 1} \qquad \text{where } F \equiv \frac{\pi d}{2L} \qquad [7]$$

$$q_1 = \frac{\sigma}{1 + F\left(\frac{1}{\epsilon} - 1\right)} \left[\frac{T_2^4 - T_1^4}{\frac{1}{\epsilon}\left(\frac{2 - F}{1 - F}\right) - 1} + F\left(T_e^4 - T_1^4\right)\right] \qquad [8]$$

The above analysis considers the tubes only as radiators (or radiation absorbers). A greater radiative area per unit weight can be achieved by attaching a fin to the heat exchanger tube. In order to conserve the small available clearance between the heat exchanger and the insulation surfaces, the fin should be flat and mounted parallel to the insulation blankets. An analysis was conducted to determine the view factor of such a fin design.

The case analyzed considered a 4-in. wide fin attached lengthwise to the spiral heat exchanger tube with 30-in. vertical spacing between convolutions. The tube was assumed to be shadowed by the fin and its area was neglected. This fin was located midway between the insulation blanket surfaces that were separated by four inches. This spacing was chosen as a probable lower limit for practical assembly of the tank and heat exchanger within a shroud for an S-IVB scale system. A fin width of twice the separation distance between it and the surfaces viewed is assumed to be great enough to approach the point of diminishing returns.

Separate computer programs were used to determine black and gray body view factors for this fin arrangement. The emissivity of the fin was taken as 0.95, and the emissivity of the surfaces of the insulation blankets was varied as a parameter, both surface emissivities being equal for a given case. Diffuse reflectivity was assumed in all cases Figure II-8 gives the results of this analysis, where the view factor $\mathcal{F}$ is defined by the equation:

$$Q_{1,2} = \mathcal{F} A_1 \sigma (T_2^4 - T_1^4),$$

with

$Q_{1,2}$ = heat flow between fin and tank- or shroud-mounted insulation surface,

A_1 = area of fin, one side only,

T_2, T_1 = temperatures of insulation surface and fin.

The assumption of diffuse reflectivity strongly influences the result given in Figure II-8. As the infrared reflectivity becomes more specular, the heat exchanger will see more of the insulation, and for small ratios of heat exchanger to insulation area, the factor $\mathcal{F}$ will approach the emissivity of the fin, regardless of the insulation emissivity. On the other hand, as the fin area is increased, the radiative coupling can never exceed that of infinite parallel plates, because of the increasing tendency of the heat exchanger to view itself, that is, for the limiting case:

$$Q_{1,2} \leq \frac{A_2 \sigma (T_2^4 - T_1^4)}{\frac{1}{\epsilon_1} + \frac{1}{\epsilon_2} - 1}$$

where

A_2 = insulation blanket surface area,

ϵ_1 = fin emissivity,

ϵ_2 = insulation blanket surface emissivity.

However, as this limiting case is approached, the two insulation surfaces cease to see each other, and all heat is transferred via the heat exchanger. In general, as the heat exchanger coupling to the blanket surfaces increases, the coupling between the blankets decreases, resulting in further improvement of the heat exchanger effectiveness. The optimization of the heat exchanger design will require test data on the actual surface material combinations to be used. The analyses that have been performed indicate that the optimum pitch for a spiral-wound heat exchanger could be 3 ft or more, and is very unlikely to be less than 1 ft for any material combination.

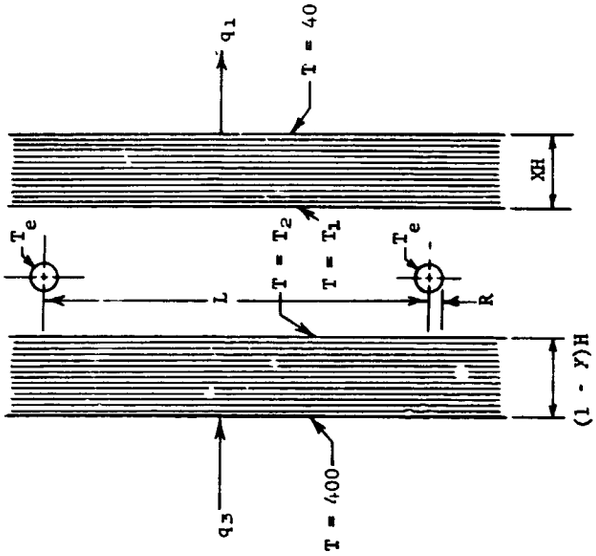

Figure II-9 The Complete One-Dimensional Model

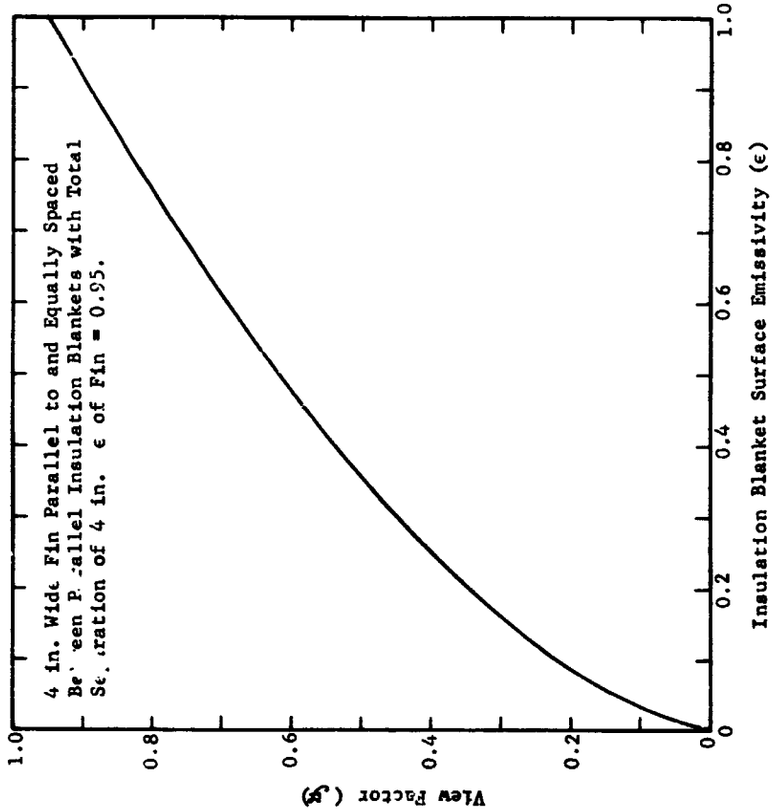

Figure II-8 View Factor for Heat Exchanger Fin as Function of Insulation Blanket Surface Emissivity

It is desirable to keep the emissivity of the blanket surfaces as low as possible because these surfaces represent reflective layers within the overall insulation system with almost perfect separation. A minimum emissivity would perhaps be achieved by using a very open net for the structural cover layer of the insulation blanket, permitting as much visibility of the reflective foil as possible. For the resulting composite surface, the effective emissivity can probably be determined only by experiment.

The analysis described below refers to the radiation coupling analysis for the circular tubes. In the computer solution of the problem, however, both configurations have been considered.

3. The Complete Analysis

The heat removed by the heat exchanger is equal to the enthalpy gain of the vent gas. Thus,

$$q_e = \alpha \dot{m} \left[h \left(T_e \right) - h(40) \right] \qquad [9]$$

where $\dot{m}$ is the total rate of boiloff from the vessel, α is the fraction of the total boiloff passing through the heat exchanger, h(T) is the gas enthalpy as a function of temperature (at the appropriate pressure), T_e is the heat exchanger tube temperature, and 40 is the vessel temperature. The overall situation being analyzed is diagramed in Figure II-9.

The total boiloff rate is, in turn, given by

$$\dot{m} = \frac{q_1 A + Q}{\lambda} \qquad [10]$$

where q_1 is the heat flow rate into the vessel per unit area, A is the total vessel surface area, Q is the total heat flux entering the vessel other than through insulation (assumed above), and λ is the enthalpy change per unit mass between the stored liquid and the vented gas.

The heat flux per unit mass into the vessel and from the shroud, respectively, are

$$q_1 = \frac{1}{xH} \left(T_1 - 40 \right) k \left(T_1, 40 \right) \qquad [11]$$

and

$$q_3 = \frac{1}{(1 - x)H} (400 - T_2)\ k\ (400, T_2) \qquad [12]$$

where H is the total insulation thickness, x is the fraction of the insulation on the vessel surface, and $k\left(T_{hot}, T_{cold}\right)$ is the insulation conductivity as given by Equation [1] (or some modification of Equation [1]). Finally, conservation of energy requires that

$$q_e = q_3 - q_1 \qquad [13]$$

Thus, we now have seven equations, [7] through [13], for the seven unknowns q_1, q_3, q_e, T_1, T_2, T_e, and $\dot{m}$ in terms of known x, H, α, R, L, ϵ, and insulation and gas properties.

The equations are solved by an iterative procedure. We begin by picking a T_e, and guessing a T_1 and T_2. With these values, and with h(T) given by Reference 5 and $k\left(T_{hot}, T_{cold}\right)$ given by Equation [1], Equations [9] through [13] can be solved exactly as before for x, q_1, q_3, q_e, and $\dot{m}$ (for some given H, R, L, and ϵ). The calculated values of q_1 and q_e allow new values of T_1 and T_2 to be calculated from Equations [7] and [8], and these values can then be used to arrive at a new solution to the equations of this section. This iteration process is continued until a satisfactory solution is obtained. By repeating the entire procedure for several values of T_e, the proper insulation distribution (x) for this set of values H, R, L, ϵ can be found (that is, the value of x that leads to minimum q_1). Results of these calculations are given in a later section.

4. Catalytic Conversion of Para- to Orthohydrogen

As a part of the analysis of insulation cooling, the use of catalytic reactors was considered. By conversion of the vapor in the heat exchanger from its original parahydrogen state to equilibrium conditions, the heat sink capacity of the vented fluid is increased. The incorporation of para-ortho converters influence only Equations [9] and [10] involving the enthalpy gain of the vent gas. By appropriate modification of these equations, the effects of one or two discrete reactors and that for a continuous reactor in the insulation heat exchanger were obtained. Results

that are given later indicate a significant advantage to be gained from each of these alternatives. No significant change in the optimum insulation blanket thicknesses resulted from the incorporation of para- to orthohydrogen conversion.

5. Expansion Engines

The use of an efficient energy conversion device to improve the performance of the vent system was also considered. This would be accomplished by reducing the pressure of the gas through a turbine or other suitable engine, extracting power in the form of electrical energy, and transmitting that energy outside the system boundary. In this process, the gas temperature is reduced, increasing the refrigeration capacity of the downstream heat exchanger. In evaluating such expanders, it was assumed that a 100% efficient expander would effect an isentropic enthalpy reduction, and a less efficient expander would reduce the gas enthalpy by a proportionately smaller amount. The total enthalpy change in Equation [9], then, was the parahydrogen enthalpy at final equilibrium temperature and near-zero pressure, minus the vessel discharge enthalpy, plus the enthalpy reduction in the expander.

Expanders were investigated in terms of both expander efficiency and the degree of closeness to thermal equilibrium (with the heat exchanger tubes) of the entering gas. It was found that, to be of very much value, an expander would have to be extremely efficient and even then would not be as effective as a para-ortho converter. A 20% efficient expander, for example, did not measurably decrease the amount of boiloff from the tank. In fact, in most cases the boiloff increased. (If the gas is not brought out of the vessel at the lowest possible pressure, it will not have achieved the maximum amount of direct cooling of the stored liquid. The difference can be significant because of the dependence of enthalpy on pressure at low temperatures.) A 50% efficient expander provided a slight gross improvement if it received the gas at thermal equilibrium: approximately 50 pounds of hydrogen over 120 days, perhaps not enough to justify the extra weight and complication introduced by the expander itself. A 90% efficient expander would save over 100 pounds gross if it received gas at thermal equilibrium, or about 60 pounds if the gas had only been heated to a midpoint between the vessel temperature and the heat exchanger equilibrium temperature.

It was therefore concluded that for typical efficiencies of expansion engines, no significant net gain could be realized. This conclusion would not necessarily be valid for systems in which, for other reasons, the hydrogen is stored at much higher pressures.

6. System Optimization

An optimization analysis was conducted to determine the improvement that could be obtained for a system utilizing the vent gas to reduce heat leakage through the insulation. A comparison was made with a system utilizing a single insulation blanket of optimum thickness applied to the tank. The effective overall thermal conductivity and installed insulation density were varied as independent parameters.

The following assumptions and ground rules were used:

a) Initial temperature of liquid hydrogen was 40°R;

b) Tank pressure controlled throughout mission to maintain 40°R liquid temperature;

c) A fixed weight of 77,330 lb was assumed for each case to include tank, liquid hydrogen, insulation, heat exchanger system, and shroud;

d) The fixed total weight is obtained by adjustment of the tank barrel section and shroud lengths, with attendant changes in tank, shroud, insulation, and liquid weights. The tank barrel section weight is taken as 137.2 lb/ft length.

e) The shroud was assumed to extend 1 ft beyond the tank at top and bottom and its weight was adjusted to account for changes in length and diameter, assuming shroud weight = 25 x length x radius (lb). A fixed annular gap of 4 in. between insulation blankets was assumed, the shroud diameter being adjusted accordingly;

f) The heat exchanger weight was assumed to be 443.5 lb and discrete para-ortho converters were taken to weigh 20 lb each, but the continuous converter weight was neglected;

g) Heat leakage into the tank in addition to that through the insulation was taken to be 30 Btu/hr;

h) Shroud temperature was 400°R;

i) Mission duration was 120 days.

The results of this optimization analysis are presented in Tables II-1 and II-2. For the cases presented, shroud and tank-mounted insulation surface temperatures ranged from 183 to 154°R for the heat exchanger only case and from 167 to 122°R for the cases with para-to-ortho conversion. Vent gas discharge temperatures ranged from 178 to 144°R without and from 158 to 122°R with conversion. In general, these temperatures decreased as the insulation thermal conductivity increased.

It is interesting to note that a gain is indicated for all of the cases considered, including that for an insulation density of 1 lb/ft^3 and an effective insulation thermal conductivity of 4.5×10^{-6} Btu/ft hr °R. It is well to note, however, that this result is strictly dependent on the assumption that the temperature of the liquid hydrogen remains constant throughout the mission with venting required from the beginning. For the higher performance insulation systems, allowing only a few degrees temperature rise of the hydrogen would postpone the requirement for venting for a large part, if not all, of the mission. It can be concluded from this study that the use of boiloff gas to intercept and reduce heat leakage offers definite advantages for long term space storage of hydrogen, but that "long term" is dependent on the performance of the tank insulation systems, and may be in excess of 120 days for the more favorable insulation materials available.

Table II-1 Optimum Insulation Thickness

Effective Thermal Conductivity of Insulation (Btu/ft-hr-°R)	Installed Insulation Density (lb/ft^3)	Uncooled Tank-Mounted (in.)	Tank Mounted (in.)	Cooled Insulation Shroud-Mounted (in.)	Total Insulation Thickness (in.)
4.5×10^{-6}	1	1.7	0.25	0.65	0.90
1×10^{-5}	1	2.6	0.90	0.90	1.80
1×10^{-5}	2	2	0.65	0.75	1.40
1×10^{-5}	3	1.7	0.55	0.65	1.20
3×10^{-5}	1	4.5	1.72	1.68	3.40
3×10^{-5}	2	3.5	1.30	1.30	2.60
3×10^{-5}	3	3.0	1.10	1.10	2.20
8×10^{-5}	1	7.4	2.76	2.74	5.5
8×10^{-5}	2	5.8	2.11	2.19	4.30
8×10^{-5}	3	4.9	1.90	1.80	3.70

Table II-2 Total Propellant Remaining After 120 Days for Optimized Systems

Insulation Effectiveness Thermal Conductivity (Btu/ft-hr-°R)	Insulation Installed Density (lb/ft^3)	Tank-Mounted Blanket Only - Uncooled (lb_m)	Insulation Heat Exchanger (lb_m)	Heat Exchanger + One Para-Ortho Converter (lb_m)	Heat Exchanger + Two Para-Ortho Converters (lb_m)	Heat Exchanger + Continuous Para-Ortho Conversions (lb_m)
4.5×10^{-6}	1	58,120	58,388 (268)*	58,410 (290)*	58,410 (290)*	58,440 (320)*
1×10^{-5}	1	57,660	57,890 (230)	57,927 (267)	57,932 (272)	57,970 (310)
1×10^{-5}	2	57,162	57,578 (416)	57,626 (464)	57,636 (474)	57,676 (514)
1×10^{-5}	3	56,789	57,326 (537)	57,376 (587)	57,387 (598)	57,433 (644)
3×10^{-5}	1	56,640	57,032 (392)	57,111 (471)	57,126 (486)	57,174 (534)
3×10^{-5}	2	55,745	56,460 (715)	56,553 (808)	56,573 (828)	56,628 (883)
3×10^{-5}	3	55,010	56,003 (993)	56,123 (1113)	56,151 (1141)	56,206 (1196)
8×10^{-5}	1	55,126	55,800 (674)	55,930 (804)	55,962 (836)	56,007 (881)
8×10^{-5}	2	55,690	54,867 (1177)	55,037 (1347)	55,075 (1385)	55,136 (1446)
8×10^{-5}	3	52,718	54,087 (1369)	54,311 (1593)	54,356 (1638)	54,422 (1704)

*Values in parentheses indicate net increase of liquid hydrogen.

E. STRUCTURAL HEAT LEAK

Analyses were conducted to d termine the heat leak to the hydrogen tank contributed by the structural support members. This analysis, as well as that for the tank piping connections, was accomplished largely through the use of a steady-state thermal network computer program. This program uses conventional finite difference techniques for driving node temperatures to values that result in no heat gain or loss by the node. An input routine is incorporated to set up arbitrary networks from descriptive node names designating conductor connections. Any number of nodes can be assigned fixed temperatures, and nodes can be biased with fixed external heat fluxes. Provision is made to gain access to several points in the program for auxiliary subroutines that can be used for solving special problems, such as the computation of external fluxes for simulation of heat exchanger operation. Thermal conductivity data for a number of materials, including all considered in this study, are incorporated into the program. Conductor values are calculated on the basis of the effective thermal conductivity of the material, which is obtained by integration of a thermal conductivity versus temperature c rve fit polynomial between the end point temperatures. Therm l conductivity data was obtained from several sources, including est results on composite materials and structural components obtained in this program and reported in Chapter IV of this report.

In order to predict heat flux caused by the tank support structure for the reference vehicle, it is necessary to assume a load on the individual members. This is because the thermal conductance of the stacked washer assembly and the spherical bearings are dependent on applied rce as well as temperature. In a zero gravity environment, the fully loaded tank imposes no load on the support structure. However, it is well to question whether this no-load condition results in very low loads on the individual members. Because the tubular struts, in the case of the lower tank support, are connected to form a truss, they may act to load each other. Unless the adjustment of the length of each member can be made so as to result in precisely the correct length after thermal contraction has occurred, such loading will be induced. It can readily be shown that each 0.001 in. of discrepancy in length of a strut over and above any free motion in the system, can result in a loading on the order of 100 lb. In view of the very large thermal contraction that does occur after installation of these members, it appears very doubtful that forces on the order of a few pounds can be realized. Therefore, for this analysis, loadings

of 100- and 1000-lb force have been considered. Results of the analysis for the titanium reference vehicle support system are as follows:

Lower Strut (72 struts) -

100-lb force	0.36 Btu/hr each	25.9 Btu/hr total
1000-lb force	0.71 Btu/hr each	51.1 Btu/hr total

Upper Stabilizer Supports (24 supports) -

100-lb force	0.32 Btu/hr each	7.7 Btu/hr total
1000-lb force	0.74 Btu/hr each	17.8 Btu/hr total

Total Structural Heat Leak -

100-lb force	33.6 Btu/hr
1000-lb force	68.9 Btu/hr

It has been assumed that all of the support members are well insulated. The effect of a heat flux over the area of the tube of 0.1 Btu/hr ft^2, to represent the heat gain through the insulation, has been evaluated and found to result in a negligible effect. However, the absence of insulation on the strut may increase the heat flux by a factor of 2 or more, depending on the area of the strut not protected by the tank insulation. It is of interest to note that the spherical bearings are more effective in reducing heat flux through the titanium lower support members than are the stacked washers. This results directly from the nature of the test data obtained for these components as presented in Chapter IV.

Nonmetallic composite structural materials, such as glass epoxy and boron epoxy, display significantly lower ratios of thermal conductivity to strength than metals such as titanium or stainless steel. They also have favorable strength-to-weight ratios. The use of these materials was therefore evaluated as a means of reducing structural heat leak. This was accomplished by considering the same basic support system, with composite tubular supports replacing the titanium supports. The preliminary design of these members is discussed in Chapter III of this report.

Thermal analyses of the glass and boron composite struts were accomplished in the same manner as for the titanium supports. Spherical bearings are included, and the thermal performance is dependent on load. Loadings of 100- and 1000-lb force were assumed. The following results were obtained:

Lower Strut (72 struts) -

S-Glass Epoxy Support Tube, 1.157 in. O.D., 1.049 in. I.D., 12.75 in. tube length (including inserts) -

100-lb force	0.120 Btu/hr each	8.64 Btu/hr total
1000-lb force	0.147 Btu/hr each	10.58 Btu/hr total

Boron Epoxy Support Tube, 0.810 in. O.D., 0.750 in. I.D. plus a single layer of S-glass epoxy overwrap, 12.75 in. tube length (including inserts) -

100-lb force	0.149 Btu/hr each	10.73 Btu/hr total
1000-lb force	0.189 Btu/hr each	13.61 Btu/hr total

Upper Stabilizer Support (24 supports) -

S-Glass Epoxy Support Tube, 0.820 in. O.D., 0.750 in. I.D., 12.5 in. tube length (including inserts) -

100-lb force	0.064 Btu/hr each	1.54 Btu/hr total
1000-lb force	0.072 Btu/hr each	1.73 Btu/hr total

Total Structural Heat Leak -

S-Glass Epoxy, Upper and Lower Supports -

100-lb force	10.2 Btu/hr
1000-lb force	12.3 Btu/hr

Boron Epoxy Lower and S-Glass Epoxy Upper Supports -

100-lb force	12.3 Btu/hr
1000-lb force	15.3 Btu/hr

Because the upper stabilizer support is designed for tension loading only, boron epoxy was not considered for this application. The above results indicate that S-glass epoxy offers a slight improvement over the boron epoxy for this application. However, the support members considered are designed primarily for tension loading. If the tube loading is primarily in compression, boron epoxy may give the best results. A very significant reduction in heat leak can be achieved with either of these materials. It is noted that the graphite epoxy composites, which are structurally very attractive, have much higher thermal conductivity characteristics and would not be suitable for this application.

The use of glass epoxy structural elements in the tank support system is recommended for long term hydrogen storage as a means of reducing boiloff losses. The possible further reduction of boiloff by using the vent gas to intercept heat entering through the support members was considered. The physical connection of a heat exchanger system to 72 lower struts and/or 24 upper stabilizers is a formidable design problem. It would be further complicated by the problem of attaching the heat exchanger at the optimum location on the support This would vary with vent gas temperature around the tank, assuming the support tubes to be cooled in series.

The design configuration in which the tank insulation is divided into two blankets, tank- and shroud-mounted, with a heat exchanger between, offers a possible alternative approach. By leaving the central part of the support tube uninsulated, it will view the annular region and heat will be transferred by radiation from the support to the heat exchanger and insulation blanket surfaces. An evaluation of this mode of support cooling for glass and boron tube designs indicates that heat flux reaching the tank through the support members can be reduced by 25 to 40%, depending on the emissivity of the tube surface. However, this process does not result in optimum interception of the heat flow. Therefore, for each Btu intercepted, 2.5 or more Btu are added to the annular region, and consequently to the insulation heat exchanger load. It is therefore concluded that interception of support heat leak by use of vent gas is not feasible.

F. PIPE HEAT LEAK AND COOLING

A major source of heat leak to the propellant tank is the combination of pipes which are assumed to connect the tank to the 400°R shroud. The pipes considered in this analysis are intended to approximate those incorporated on the SIV-B stage hydrogen tank. A pair of 0.078-in. wall, stainless steel pipes, 6 in. in outside diameter and 164 in. in total length, were assumed as the fill and drain and vent lines. A 90° bend was assumed at 32 in. from each end of each pipe. The other pipe considered is the feed pipe located at the tank bottom. This pipe was assumed to be fabricated of 0.188-in. thick stainless steel tubing, 10 in. in outside diameter. Two lengths, 36 in. and 60 in. were analyzed as probable limits. A 0.375 x 0.035 x 160-in. stainless instrumentation line was found to contribute a negligible heat leak.

The internal pipe radiation, thermal conductivity of the pipe, and heat added through the pipe insulation were considered in the determination of the temperature distribution and heat flux along the various pipes. Internal pipe radiation effects were treated parametrically for a range of emissivities from 0.15 to 1.0, where 0.6 was assumed as a representative value for stainless steel. Thermal conductivity of the stainless steel pipe was treated as a function of temperature, based on data presented in Reference 6, and is represented by the following expression:

$$k = 4.422 \times 10^{-4} + 0.027942\ T^{1.8} - 0.29233\ T^{1.9} + 0.00767345\ T^{2}\ \text{Btu/hr ft °R}$$

A heat input of 0.1 Btu/hr ft^2 was applied over the total pipe area to represent heat gained through the pipe insulation. This would be achieved physically by varying the number of layers of multilayer insulation as a function of the pipe temperature profile so as to minimize temperature gradients along the insulation layers.

The analysis of the heat flux to the tank and the corresponding pipe temperature profile was accomplished by using two digital computer programs. The first determined the black body and grey body view factors, $\mathcal{F}A$, associated with internal radiation heat transfer characteristics of the pipes. This program considers diffuse grey or black body radiation only. The 6-in. diameter x 164-in. long pipes were separated into two 32-in. long sections, one at each end of a 100-in. long section. The ends were considered to be discs having an emissivity of 1 for all cases.

Each 32-in. long section was considered to be at 90° to the 100-in. section. Each bend was considered to be simulated, from an internal radiation point of view, by a disc having an emissivity of 1. Each disc was divided into 4 nodes with the 32-in. long sections having 5 equal area nodes and the 100-in. long section having 10 equal area nodes. The 10-in. diameter pipes contained 14 equal area nodes in the pipe and 4 nodes in each end disc. The output ($\overline{GA}$ factors) were appropriately summed for each node and pipe end and used as input to the second computer program. This program simultaneously considered the internal radiation, pipe conduction, and external flux simulating insulation heat leak.

The heat added to the tank by the two 6 x 0.078 x 164-in. lines was found to be 2.5 Btu/hr each, and was independent of internal emissivity over the range of 0.15 to 1. Figure II-10 shows the dependence of heat flux to the tank on internal surface emissivity for the 10-in. O.D. x 0.188 wall stainless steel pipes for 36 and 60-in. lengths. For the nominal emissivity of 0.6, values of heat flux were 29 and 19.6 Btu/hr, respectively. Figures II-11, II-12, and II-13 give temperature profiles of the three pipes considered for the uncooled case. No effect of emissivity can be noted for the 6 x 164-in. pipe, and little effect of emissivity was found for the 10-in. pipes.

The use of vent gas to reduce the heat leak through the 10-in. feed line was investigated in detail for the 36-in. long case. Emissivity of the internal pipe surface was taken as 0.6. A heat exchanger was assumed in all cases to be made of stainless steel tubing welded or brazed to the tank wall. In view of the light weight of this tubing, assumed to be no larger than 0.375 in. in diameter, the heat exchanger was assumed to be adequately sized to operate with no more than 5°R temperature difference between the coolant gas and the pipe.

Two cases were considered. First, local cooling of a small region of the pipe was evaluated for the case where several heat exchangers are connected in series. For this case, maximum heat reduction to the tank with a minimum increase in vent gas temperature is sought. The second case assumes parallel connection of heat exchangers, with the vent gas arriving at the heat exchanger at near tank temperature. Here the vent gas is allowed to heat to whatever temperature results in maximum cooling. For this case, the heat exchanger starts at an optimum point on the pipe and continues outward to near the hot end. This analysis is also valid for the last of several series-connected heat exchangers, for which the entering coolant temperature may be significantly greater than the tank temperature.

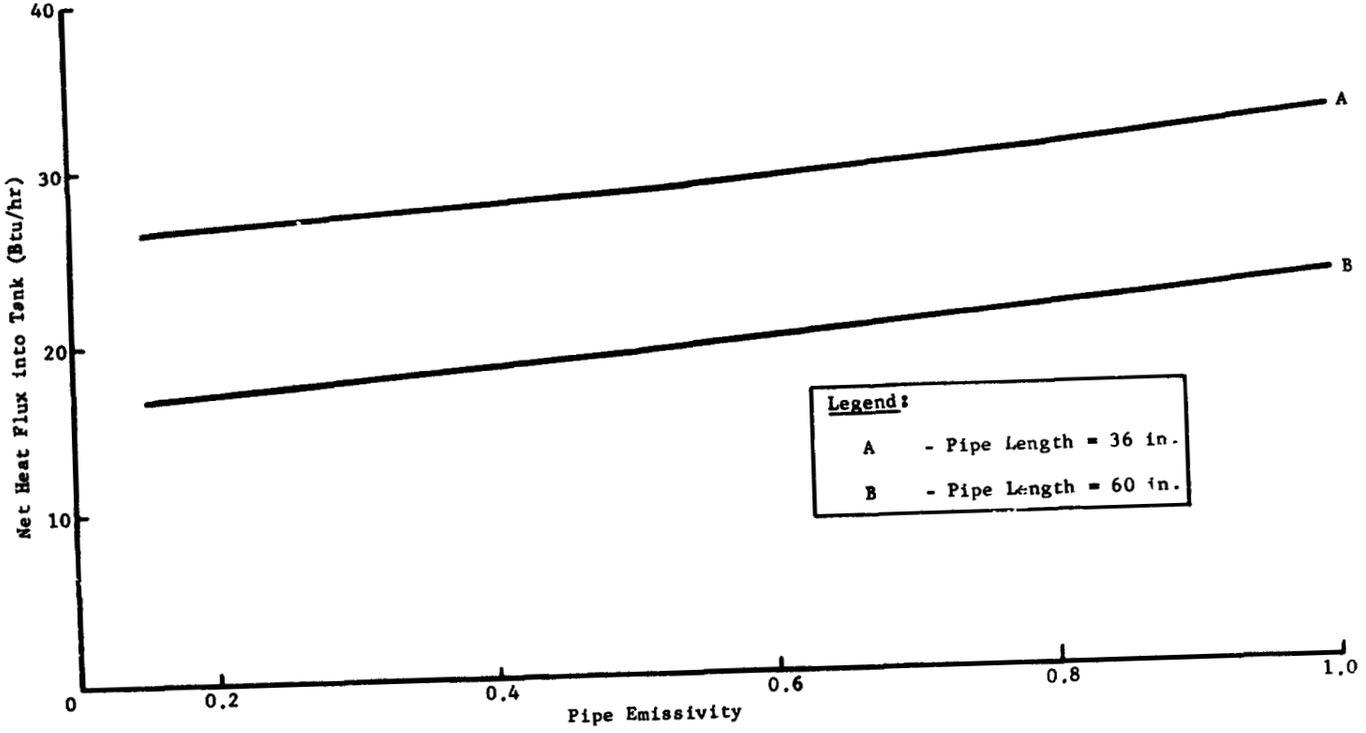

Figure II-10 Heat Flux as a Function of Internal Surface Emissivity for 10-in. O.D. x 0.188-in. Wall Stainless Steel Feed Line

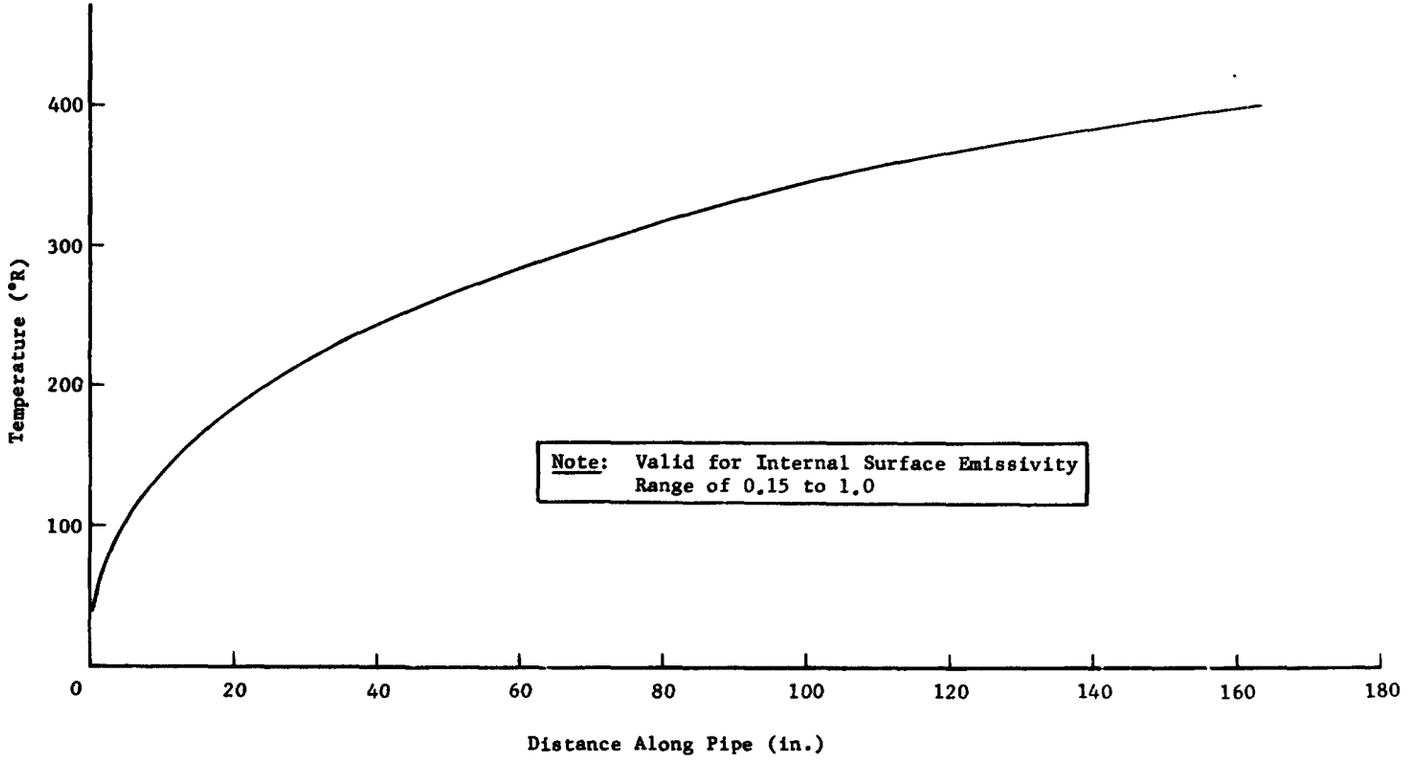

Figure II-11 Temperature Profile on 6-in. O.D. x 0.078-in. Wall x 164-in. Stainless Steel Pipe

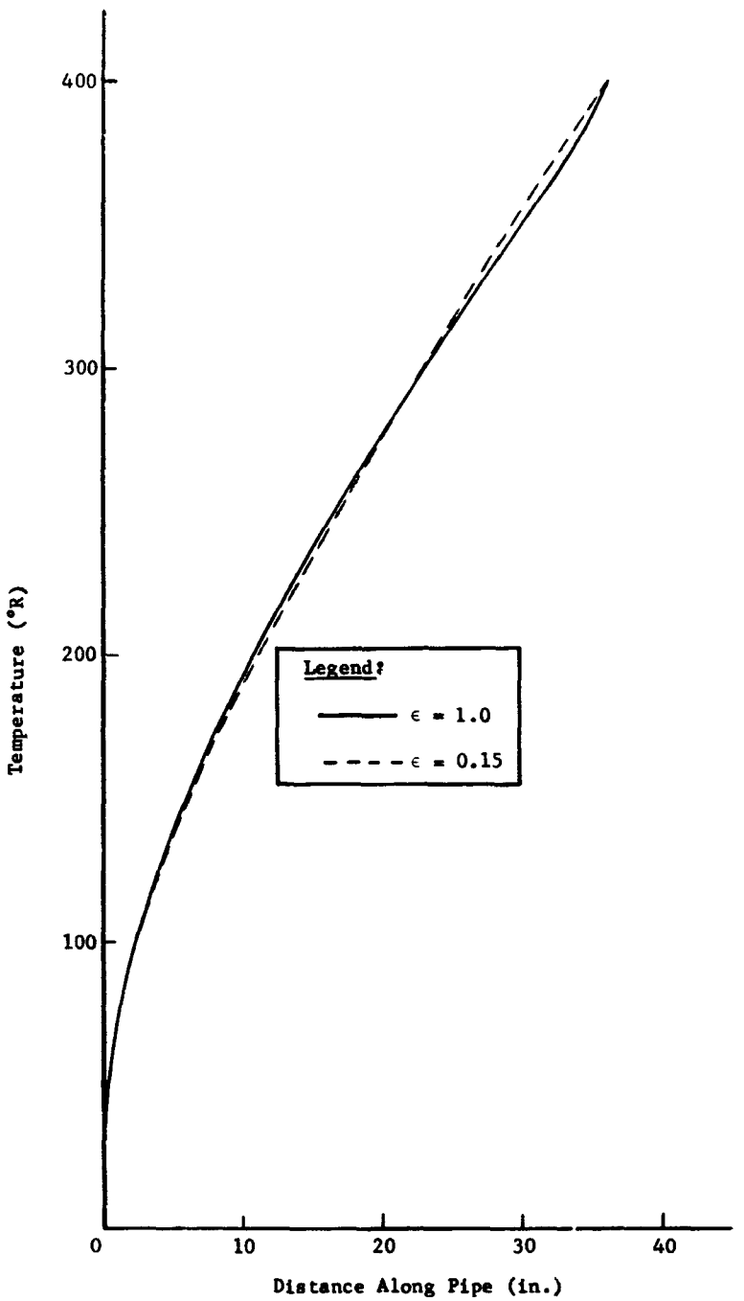

Figure II-12 Temperature Profile of 10-in. O.D. x 0.188-in. Wall x 36-in. Stainless Steel Pipe

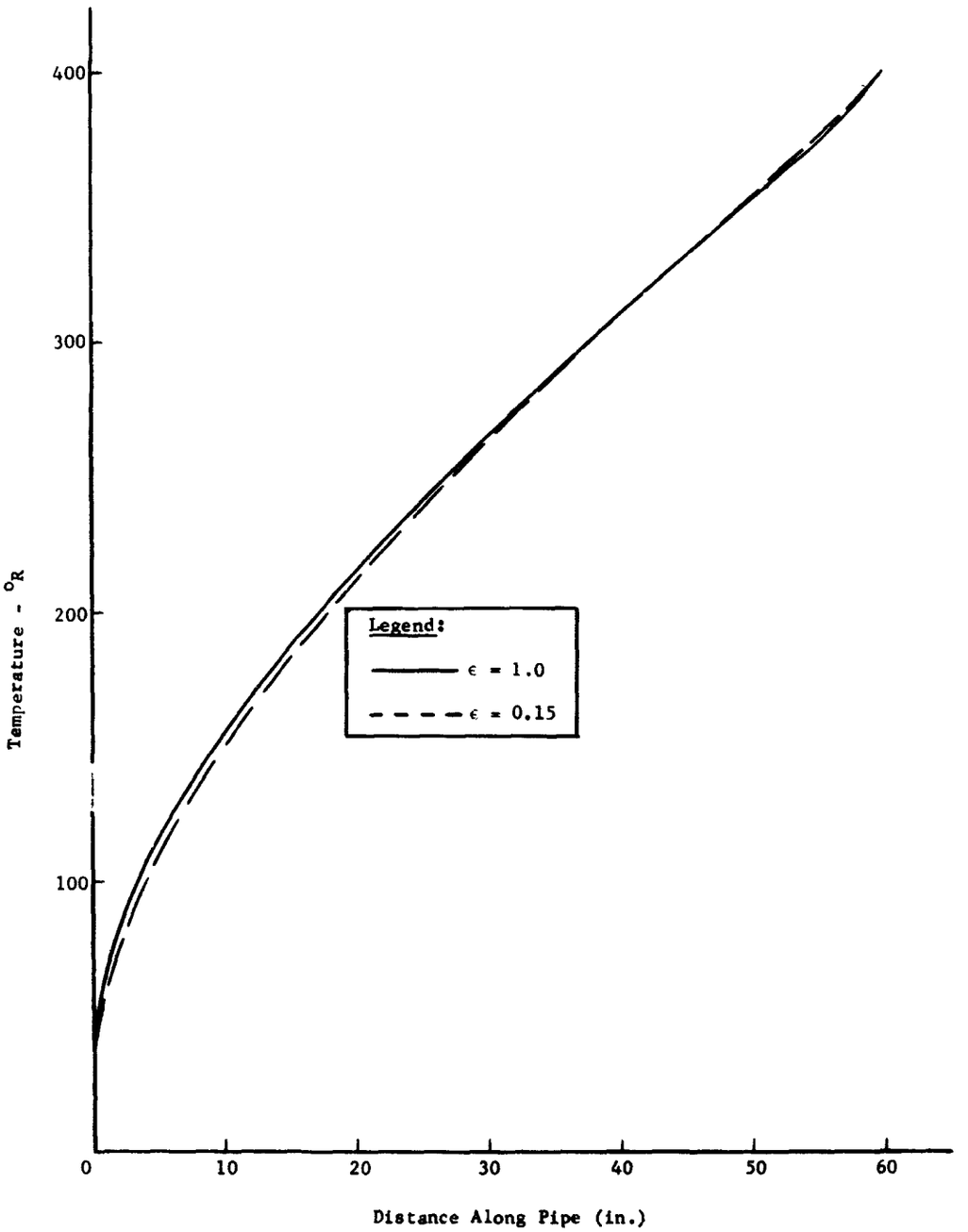

Figure II-13 Temperature Profile of 10-in. x 0.188-in. Wall x 60-in. Stainless Steel Pipe

The pipe cooling analyses were accomplished by solution of the steady-state network analysis with heat exchanger operation simulated by external heat fluxes out of the pipe at appropriate points. Gaseous para-hydrogen properties were incorporated into the computer program, and these cooling fluxes were continuously calculated through the iteration procedure on the basis of pipe temperature and gas flow rate.

Figure II-14 presents the effect of placement of the local, or series, heat exchanger. For 120°R entering gas temperature, it is noted that minimum heat flux to the tank occurs when the heat exchanger is located at approximately 55 to 60% of the distance from the cold end for hydrogen coolant flow rates of 0.05 to 0.15 lb/hr. This indicates that optimum placement of a spot, or local, heat exchanger is a function of entering gas temperature only. The relationship between coolant temperature and optimum placement is given in Figure II-15. Results of a survey to determine the optimum heat flux to the tank for the 36-in. feed line for various gas temperatures and flow rates are given in Figure II-16. These results are for optimum placement of the heat exchanger as given in Figure II-15.

For the second case of the optimum length heat exchanger, the significant problem is to determine the proper location for the cold end of the heat exchanger. If the gas temperature is warmer than the uncooled pipe temperature at the entrance of the heat exchanger, the heat flux through the pipe may be increased. Beginning the heat exchanger too near the hot end will result in a loss of efficiency. Unlike the locally cooled pipe case, the optimum placement of the cold end of the heat exchanger is dependent on both the gas inlet temperature and the flow rate. This relationship for the 10 x 36-in. feed line is shown in Figure II-17. The minimum heat flux to the tank is shown in Figure II-18 for various inlet temperatures and flow rates. Finally, Figure II-19 presents a comparison between local and optimum length cooling for a typical inlet temperature to the heat exchanger of 120°R.

This analysis has assumed that the pipes were evacuated. The presence of gaseous hydrogen would result in an additional heat flux on the order of 5 Btu/hr for the 10 x 36-in. pipe and less than 0.5 Btu for the 164-in. pipes, assuming only gas conduction in a weightless environment. If a pipe is open to the tank interior, it will be filled with vapor during the long term coast period. This is true regardless of the liquid position in the tank, because the pipe temperature will be greater than the boiling temperature of liquid hydrogen. For large diameter, short pipes, the installation of a valve at or near the tank interface and the evacuation of the line should be considered as a means for reducing boiloff.

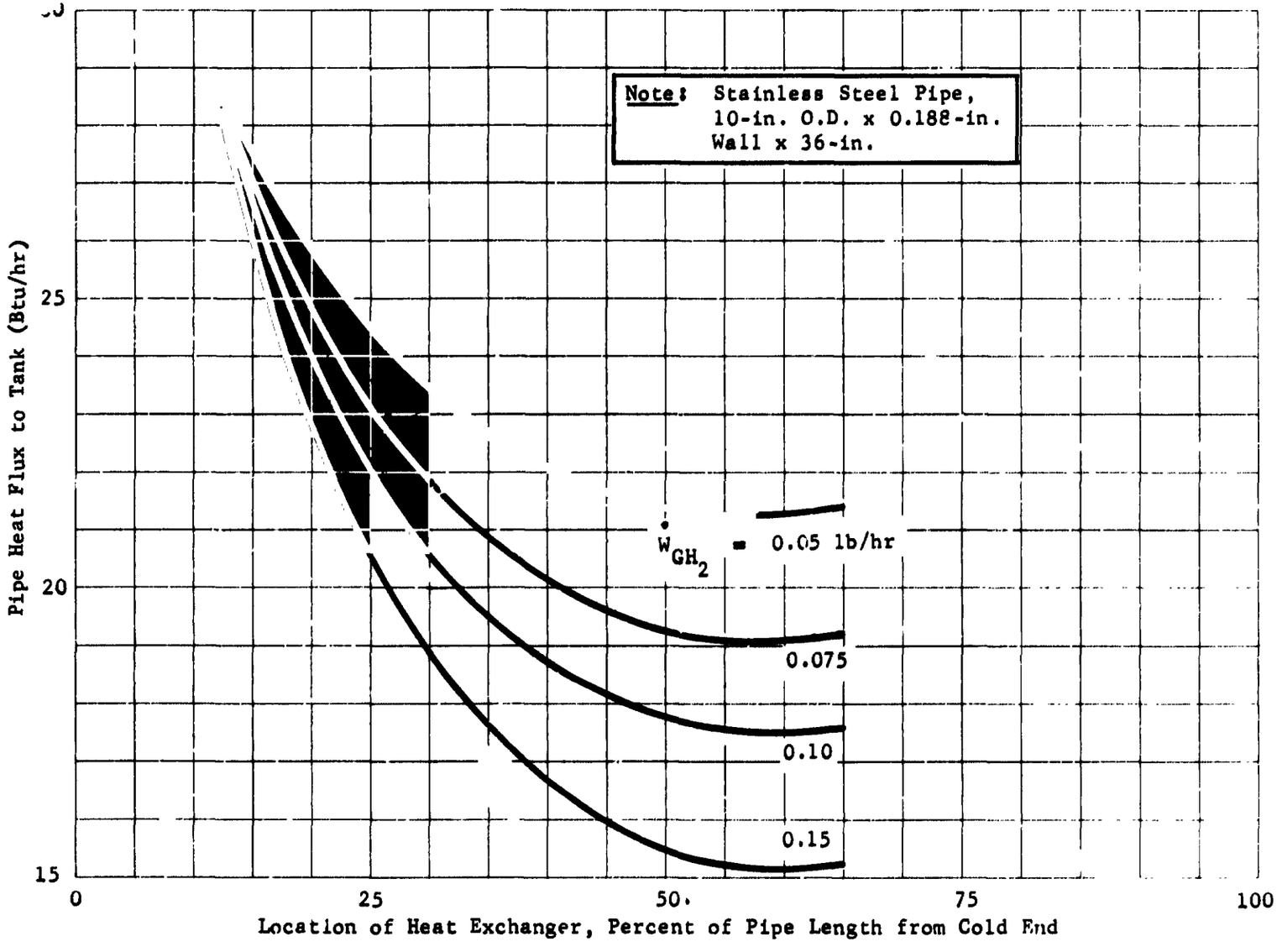

Figure II-14 Reduced Heat Flux as a Function of Local Heat Exchanger Placement for Entering Coolant Temperature of 120°R

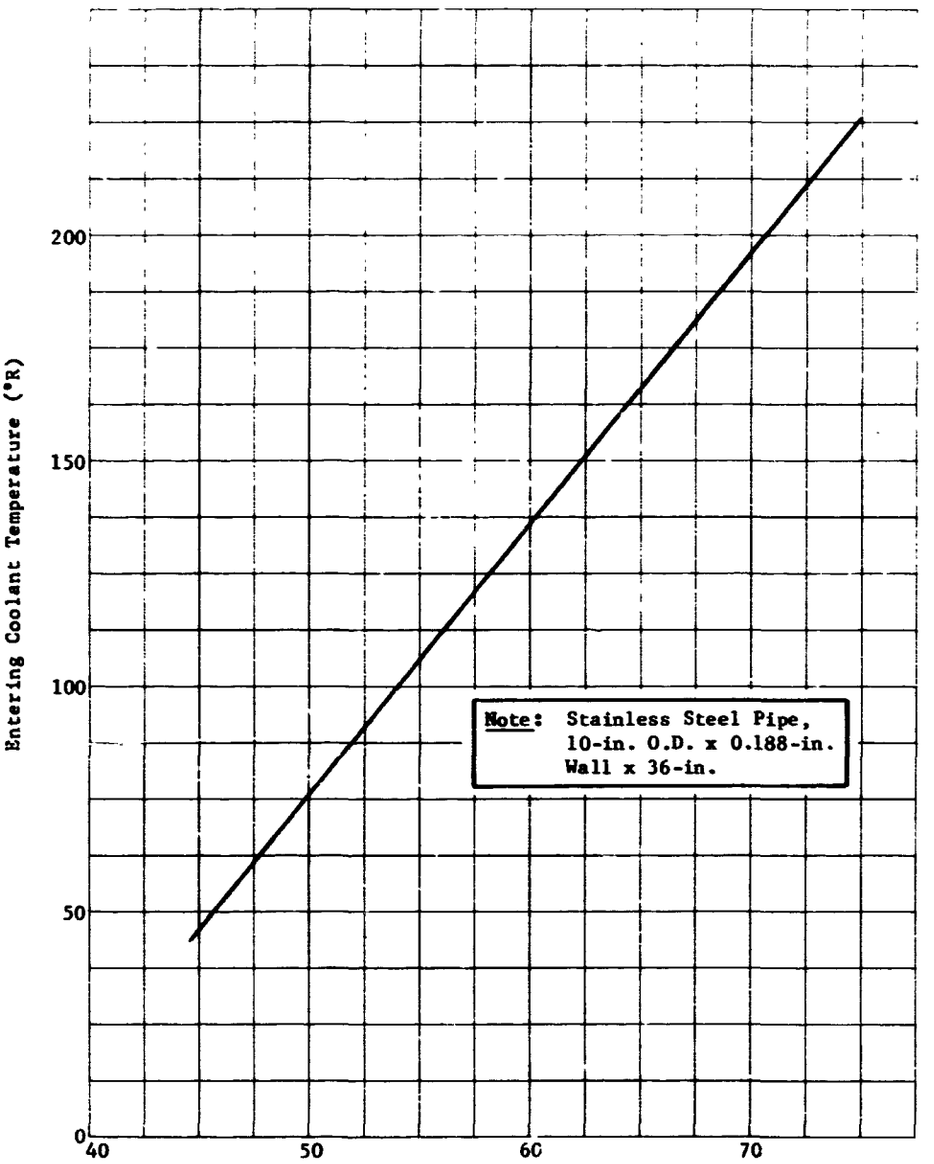

Figure II-15 Optimum Location of Local Heat Exchanger as a Function of Entering Gas Temperature

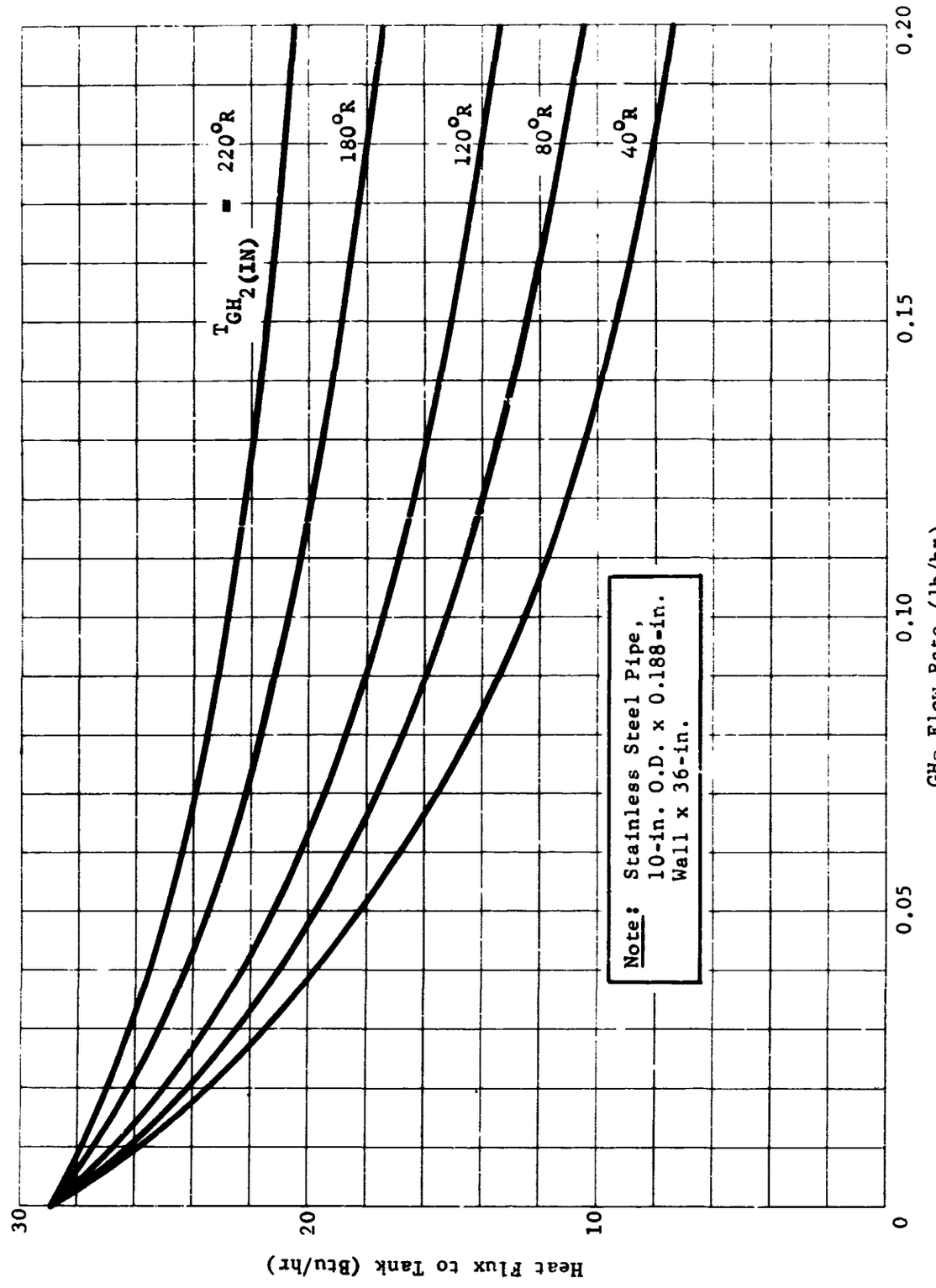

Figure II-16 Optimized Heat Flux to Hydrogen Tank for Locally Cooled Pipe for Various Inlet Temperatures and Flow Rates

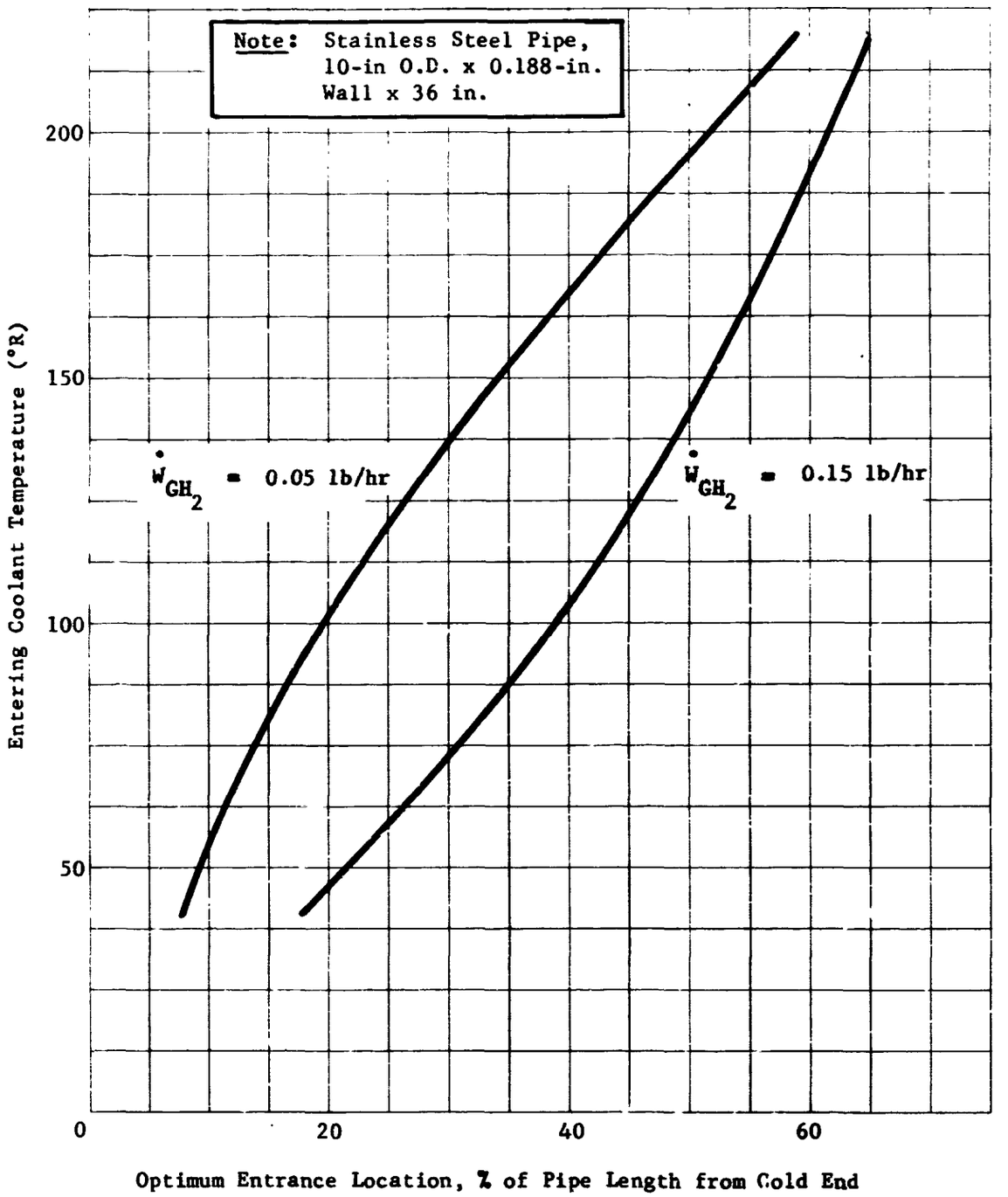

Figure II-17 Optimum Placement of Heat Exchanger Inlet as a Function of Coolant Temperature and Flow Rate for Optimum Length Cooling

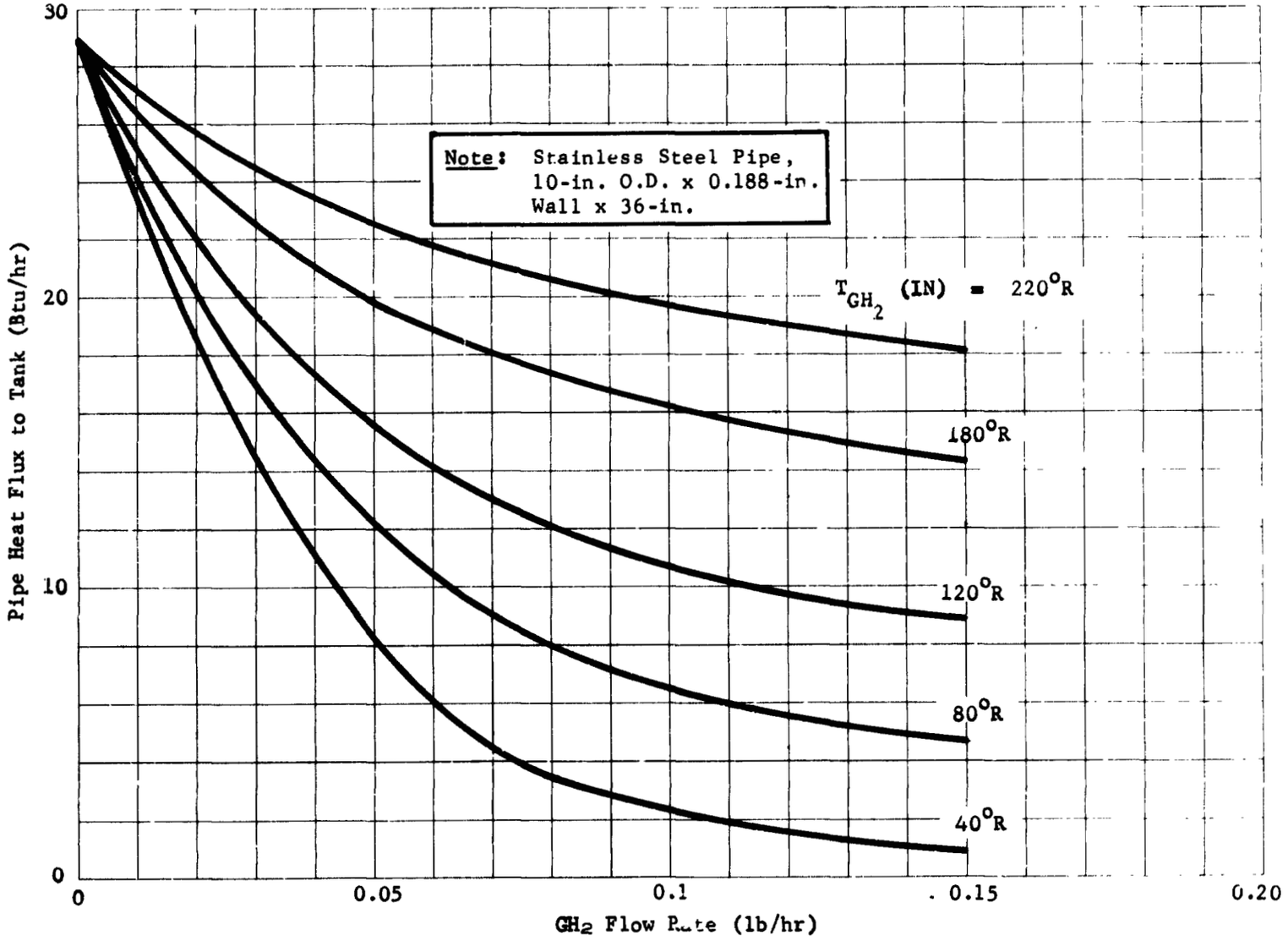

Figure II-18 Minimum Pipe Heat Flux for Optimum Length Heat Exchanger as a Function of Coolant Flow Rate and Temperature

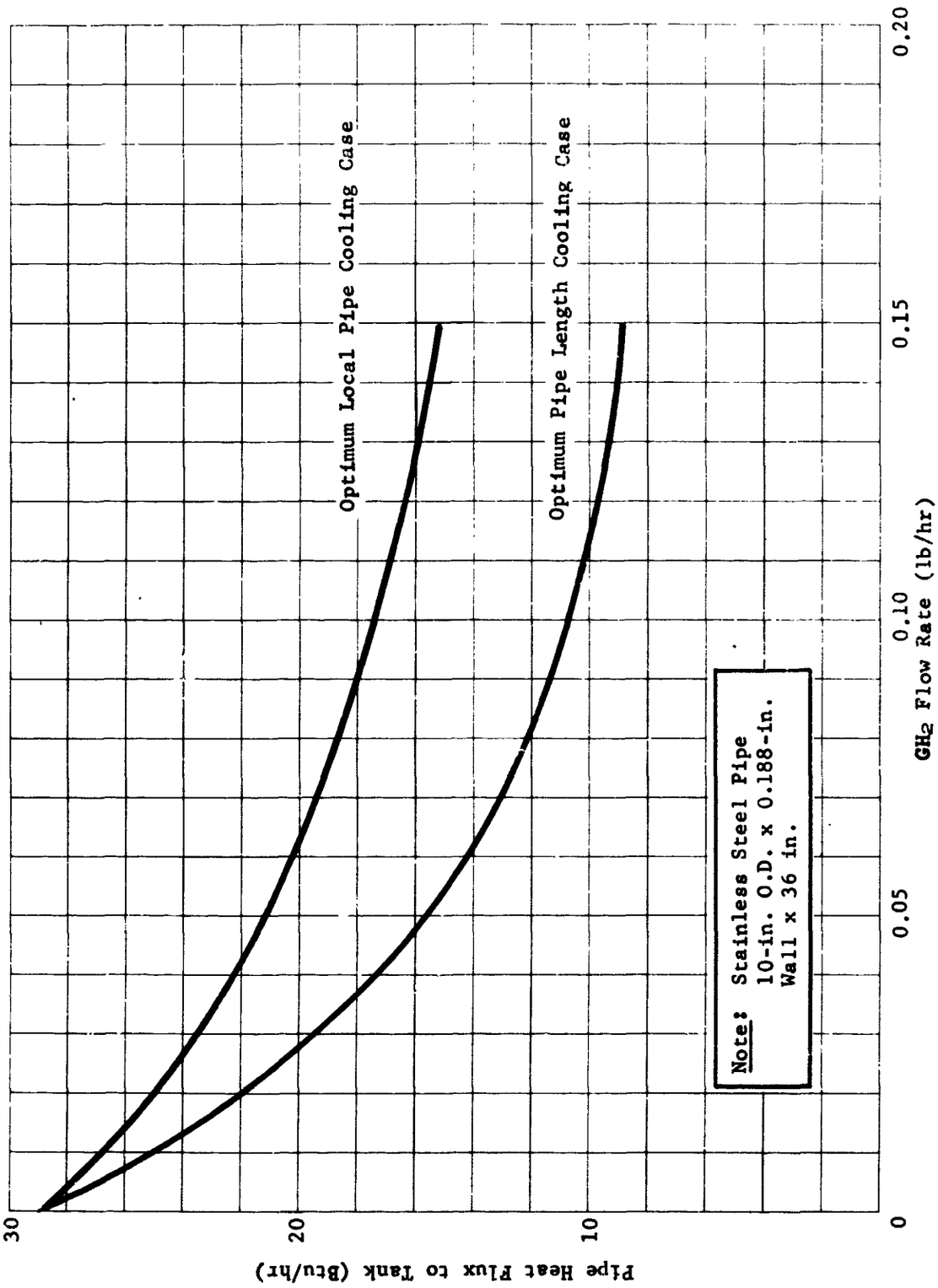

Figure II-19 Comparison of Local Pipe Cooling and Optimum Pipe Length Cooling for Inlet Coolant Temperature of 120°R

G. INTERNAL CAPILLARY INSULATION

1. Concept Description

Methods for interposing a layer of hydrogen gas between the liquid hydrogen and the tank wall to reduce boiloff losses were investigated. This internal insulation would not be for the purpose of supplementing the high performance multilayer insulation applied to the tank; rather, it would be used in areas of high heat leakage, such as a tank discharge pipe, to increase the resistance between the heat leak and the liquid hydrogen. Without such supplemental insulation, the temperature at the juncture of the pipe and tank wall would be close to liquid hydrogen temperature because of high heat transfer coefficients.

Two concepts were investigated, both depending on capillary (surface tension) effects. In the first concept, a layer of honeycomb bonded to the tank wall was used to position the gas. A capillary barrier, such as a woven screen, was used to prevent interchange of liquid and gas in the second concept.

The principle of the honeycomb concept is illustrated in Figure II-20a. A layer of honeycomb, bonded to the tank wall, is assumed to be initially filled with liquid. As heating of the wall occurs, the liquid will reach saturation temperature and then begin to evaporate. The liquid in the cells will be displaced by vapor or will be evaporated. If the liquid-solid contact angle is in the vicinity of 90° or above, the liquid-vapor interface will be stabilized by capillary forces and the vapor will be positioned so as to form a thermal resistance between the tank wall and the liquid.

If the cells of the honeycomb were circular, this explanation would be valid for liquids with zero or any contact angle. However, by the nature of its construction, honeycomb material has sharp corners. A liquid with a very small contact angle will tend to wet the corner, drawing liquid along the edges, and the liquid-gas interface will not be stable. Capillary stability in a round tube can be demonstrated by the familiar soda straw experiment in which liquid can be positioned above gas in a small tube closed at the upper end. The lack of stability in a tube with sharp corners has been demonstrated by a similar experiment, using a tube of diamond cross-section fabricated from two pieces of clear plastic. The major dimension of this cross-section was made very small (approximately 0.05 in.) to assure that the result obtained was not merely due to the tube being greater than its critical dimension.

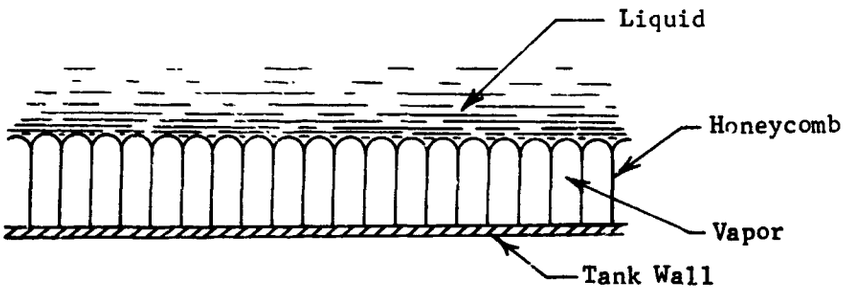

a

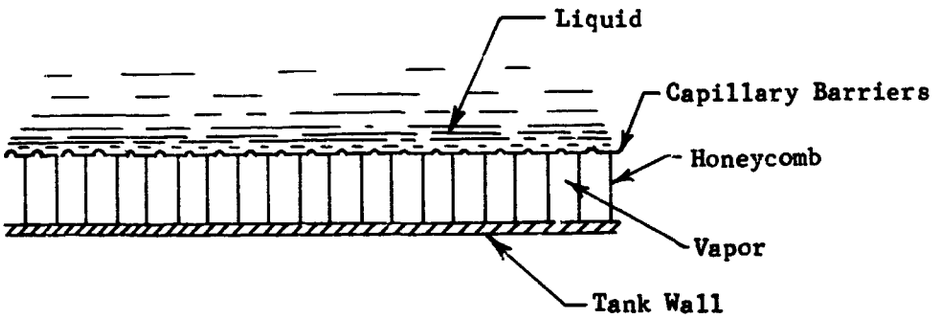

b

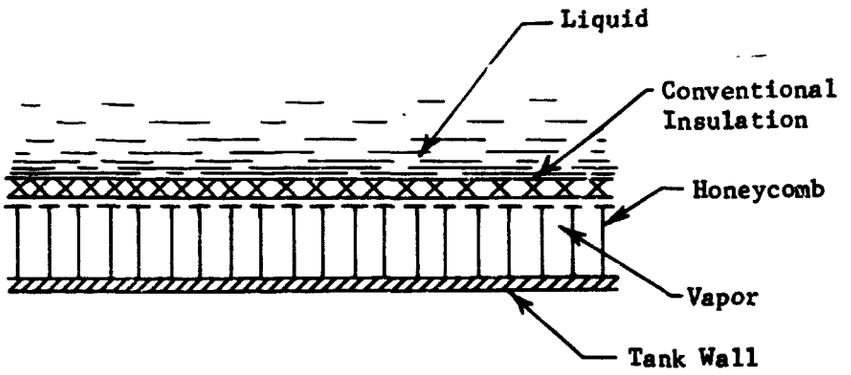

c

Figure II-20 Honeycomb Internal Capillary Insulation Concept

It was found to be impossible to maintain liquid in a stable condition above the gas when a wetting liquid such as methanol was used. When the tube, initially empty of liquid, was immersed in methanol with the open end up, the liquid entered and eventually filled the tube completely.

Because the contact angle of liquid hydrogen with all, or at least most solids, is in the vicinty of 0°, this configuration is not satisfactory. Figure II-20b shows the addition of a capillary barrier plate over the honeycomb. With this arrangement, the capillary stability occurs in a circular hole in the barrier plate. That this arrangement satisfactorily solves the interface stability problem can be demonstrated by assembling the honeycomb and barrier plate in the bottom of a container. With the honeycomb initially filled with air, the container can be filled with liquid, and very little, if any, liquid will find its way into the honeycomb cells.

However, when this system is applied as internal tank insulation, it is assumed that the gas in the cells is (or could be) vapor of the liquid being contained. In this case, it is clear that the boiling temperature exists at the interface. Considering the relatively high thermal conductivity of the liquid (in a zero-gravity environment, or convection in a one-g environment), a rather strong heat flux would be required to maintain this temperature at the interface if the bulk liquid were subcooled. If the liquid at the interface becomes cooler than the saturation temperature, condensation will begin to occur, allowing liquid to enter the honeycomb cell. Depending on the magnitude of the heat flux, a percolating action would probably follow, with liquid alternately entering and being evaporated or displaced from the cells until the liquid in the vicinity of the barrier plate comes to the saturation temperature. Therefore, this concept (as shown in Figure II-20b) does not appear to be adequate if subcooled liquid is to be stored.

For the application of the honeycomb insulation concept where subcooled liquid is to be contained, a thermal barrier must be interposed between the capillary barrier plate and the bulk liquid. Figure II-20c shows the use of a conventional insulation material such as foam for this purpose. This insulation layer need not be sealed, and would in fact be intentionally perforated if not inherently porous. This layer of insulation must be sufficient to result in a temperature drop equal to the difference between the boiling and bulk temperatures of the liquid at the minimum heat flux at which the system is to be operated. When the heat flux is increased above the minimum design level, boiling may occur in the space between the barrier and the supplemental layer of insulation.

This would cause the liquid-gas interface to intermittently move away from the capillary barrier opening, but would not result in liquid entry into the honeycomb cell. When liquid later returns to this vicinity, the interface will immediately form again at the barrier, assuming a sufficiently small hole size.

The capillary screen concept for positioning a gas layer at the tank wall is equivalent to the honeycomb system with the honeycomb removed. The capillary barrier or screen is positioned away from the tank wall with suitable standoff mounting posts, and the additional insulation is positioned above this point. A small spacing between the barrier and the conventional insulation layer may or may not be desirable, depending probably on the properties of the conventional insulation material. For the zero-gravity case where natural convection would not be expected, the two systems should be almost equivalent, with a weight advantage for the screen system. An advantage of both of these concepts is that sealing to prevent migration of fluids across the boundaries is not required. All parts of the systems operate at essentially tank pressure and if the tank pressure should change, the pressures through the insulation would respond accordingly.

For application in a one-g environment, the honeycomb cells would be sized so as to effectively eliminate convection as a heat transfer mechanism. The dimensionless parameter, Rayleigh number, characterizes the natural convection of a cell. This number is defined as follows:

$$Ra = \rho^2 \, Cp \, g \, d^3 \, \Delta T / k \, \mu_T$$

where:

ρ = density of gas
Cp = thermal capacity of gas
g = gravitational acceleration
d = characteristic dimension of cell
ΔT = difference in temperature across cell
T = mean temperature
k = thermal conductivity of gas
μ_T = viscosity of gas at temperature T

From Reference 7, it is estimated that the onset of convection in a typical honeycomb cell occurs at a Rayleigh number of 7,000 to 10,000. For Rayleigh numbers sufficiently below this value, the thermal conductivity through the honeycomb would be expected to

approximate the thermal conductivity of the propellant vapor. In the capillary screen concept, it is unlikely that convection could be prevented in a one-g environment. This system would therefore only be considered for zero-gravity applications.

2. Application of Internal Insulation

An analytical study was conducted to determine the potential for improvement of a liquid hydrogen orbital storage system by use of internal insulation in the vicinity of strong heat leak points. For this analysis, the heat leak was assumed to be a pipe segment connected to the bottom of the tank. The liquid hydrogen was assumed to be at 40°R and the opposite end of the pipe connected to a constant temperature source at 400°R. For purposes of the analysis, the bottom of the tank was simplified to a disk. Internal insulation was applied concentrically about the pipe center, and its thickness and diameter were varied as parameters. External insulation with an assumed effective thermal conductivity of 5×10^{-5} Btu/hr ft°R and 2-in. thickness was applied to the tank. The pipe was assumed to be perfectly insulated.

A steady-state thermal network analysis program was used to determine the heat leak due to the pipe, first with no internal insulation and then with the insulation applied. The pipe was divided into 20 segments of equal length, and the thermal conductivity was calculated for each segment as a function of temperature. The tank wall and the internal insulation were also divided into 20 ring segments each, with thermal conductivities calculated as a function of temperature. The internal insulation in all cases was assumed to have a thermal conductivity equivalent to that of hydrogen vapor.

Approximately 25 cases with variation of the various parameters were evaluated. Table II-3 gives the results of the more significant of these cases. Inspection of these results leads to the conclusion that at best, the use of internal insulation would result in a small improvement in overall performance. For those cases where a significant improvement is shown, an intolerable heat leak exists with or without the internal insulation. Unless a combination of materials were chosen to give a high heat input with a tank wall of low thermal conductivity, the improvement clearly does not justify the insulation.

Table II-3 Effect of Internal Insulation in Vicinity of Outlet Pipe

Case	Tank Material	Tank Wall Thickness (in.)	Pipe Material	Pipe O.D. (in.)	Pipe Wall Thickness (in.)	Pipe Length (ft)	Insul-ation Thickness (in.)	Insul-ation Diameter (ft)	Pipe Heat Leak Without Insulation (Btu/hr)	Pipe Heat Leak With Insulation (Btu/hr)
1	Aℓ	0.C75	S.S.	10	0.188	5	1	12	16.16	15.76
2	Aℓ	0.075	S.S.	10	0.188	5	2	12	16.16	15.71
3	Ti	0.075	S.S.	10	0.188	5	1	12	16.16	13.66
4	Ti	0.125	S.S.	10	0.188	5	1	12	16.16	14.31
5	Aℓ	0.075	S.S.	10	0.188	3	1	12	26.94	25.82
6	Aℓ	0.075	S.S.	10	0.188	1	1	12	80.8	71.20
7	Aℓ	0.075	S.S.	3	0.030	3	1	12	1.3	1.295
8	Aℓ	0.075	Aℓ	10	0.100	3	1	12	105.19	89.9
9	Aℓ	0.075	S.S.	10	0.188	3	1	6	26.94	26.23
10	Aℓ	0.075	S.S.	10	0.188	1	0.5	12	80.8	72.46

Note: Aℓ - aluminum
Ti - titanium
S.S. - stainless steel

Although it is concluded that the internal capillary insulation concept is not applicable to long term space storage of liquid hydrogen, other potential applications seem more promising. This insulation system appears to offer advantages in cryogenic booster tankage systems and for ground storage and transport of mild cryogens. Subsequent to the effort described above and in Chapter IV, the concept has been investigated in greater detail for liquid methane storage. At the time of this writing, the merits of the internal capillary (honeycomb) insulation system for that application appear to warrant further research and development.

III. PRELIMINARY DESIGN

A. INSULATION HEAT EXCHANGER AND TRUSS

A conceptual design and weight analysis was undertaken on a heat exchanger to be mounted between the insulation blankets. Because of the large difference in surface area between the hemispherical tank dome and cylindrical shroud plus the ends, it is desirable to incorporate into this heat exchanger a means for supporting the outer insulation blanket in the dome areas. The proposed design is shown in Figure III-1. Arbitrary insulation blanket thicknesses are shown, and a probable minimum tube spacing of 18 in. has been selected for the study.

The dome tubing is supported on the insulation support truss. The truss is a six-strut design with ring frames on 36-in. spacing. The six struts are pin-joined at the dome-barrel junction as shown in details A and B of Figure III-1. The strut-ring frame joint including a typical tube support is shown in section C-C; section D-D shows a typical ring frame insulation support member joint. The inner strap stabilizes the inside frame flange. The dome truss assembly complete with tube spiral and insulation is installed by means of bolts at the six pin joints. Support dome section details are given in Table III-1.

The barrel section tubing wrap is supported by the six tension rods. The end joints of the rods are shown in details A and B of Figure III-1. The rods are bolted to the tank truss at the aft end (detail B), and an adjustable screw fitting is provided at the forward end (detail A). The rods are pretensioned to 42,000 psi stress at installation to allow a small tension load to remain after tank shrinkage during cool down. Relative positions of tank to shroud frame are shown in detail A for room temperature installation, tank cool down (-423°F) and cold tank plus 40 psi pressurization. Detail E shows a typical ring joint at the aft end of the truss to accommodate the tank drain line.

The installation procedure is described in the following steps:

Step 1 - With insulated tank suspended within a handling ring at the upper dome-barrel intersection, install and adjust barrel section of heat exchanger;

Figure III-1 Insulation Heat Exchanger and Dome Truss Assembly

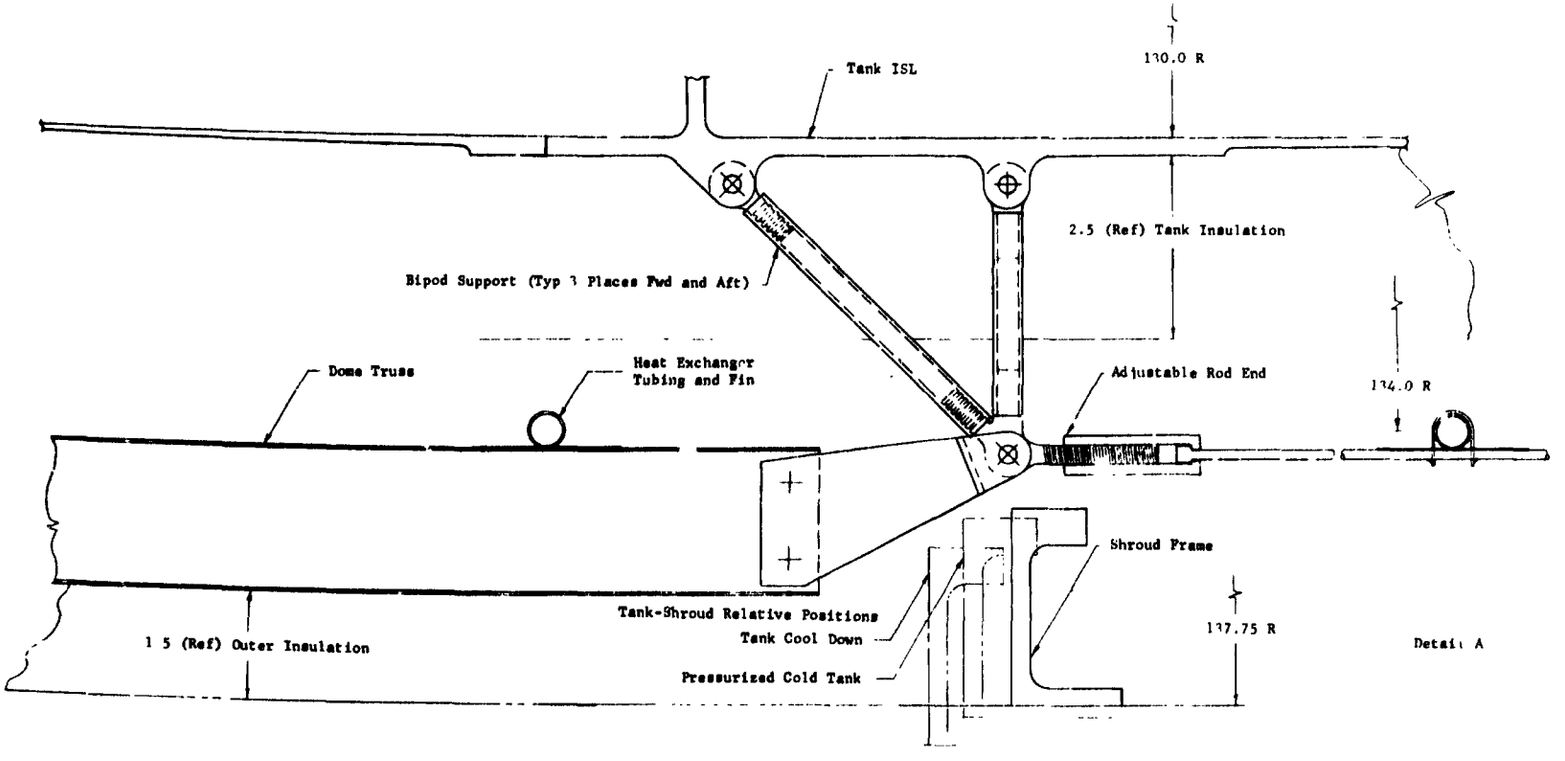

MCR-69-405

Figure III-1 (continued)

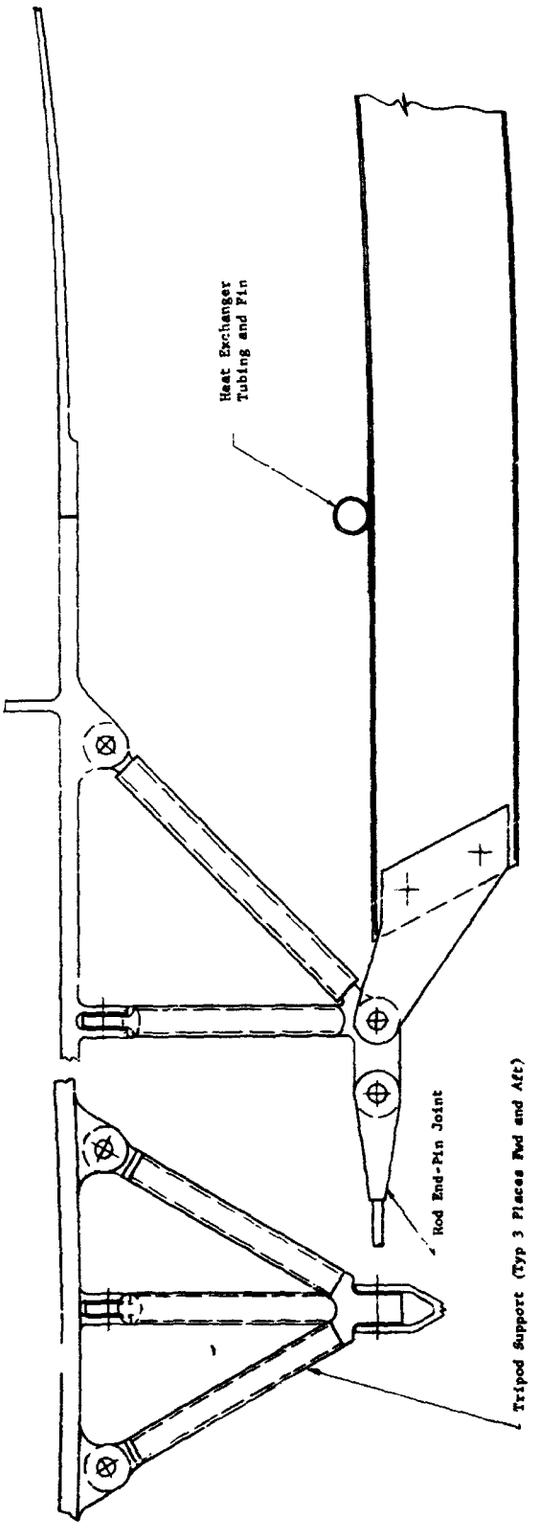

Figure III-1 (continued)

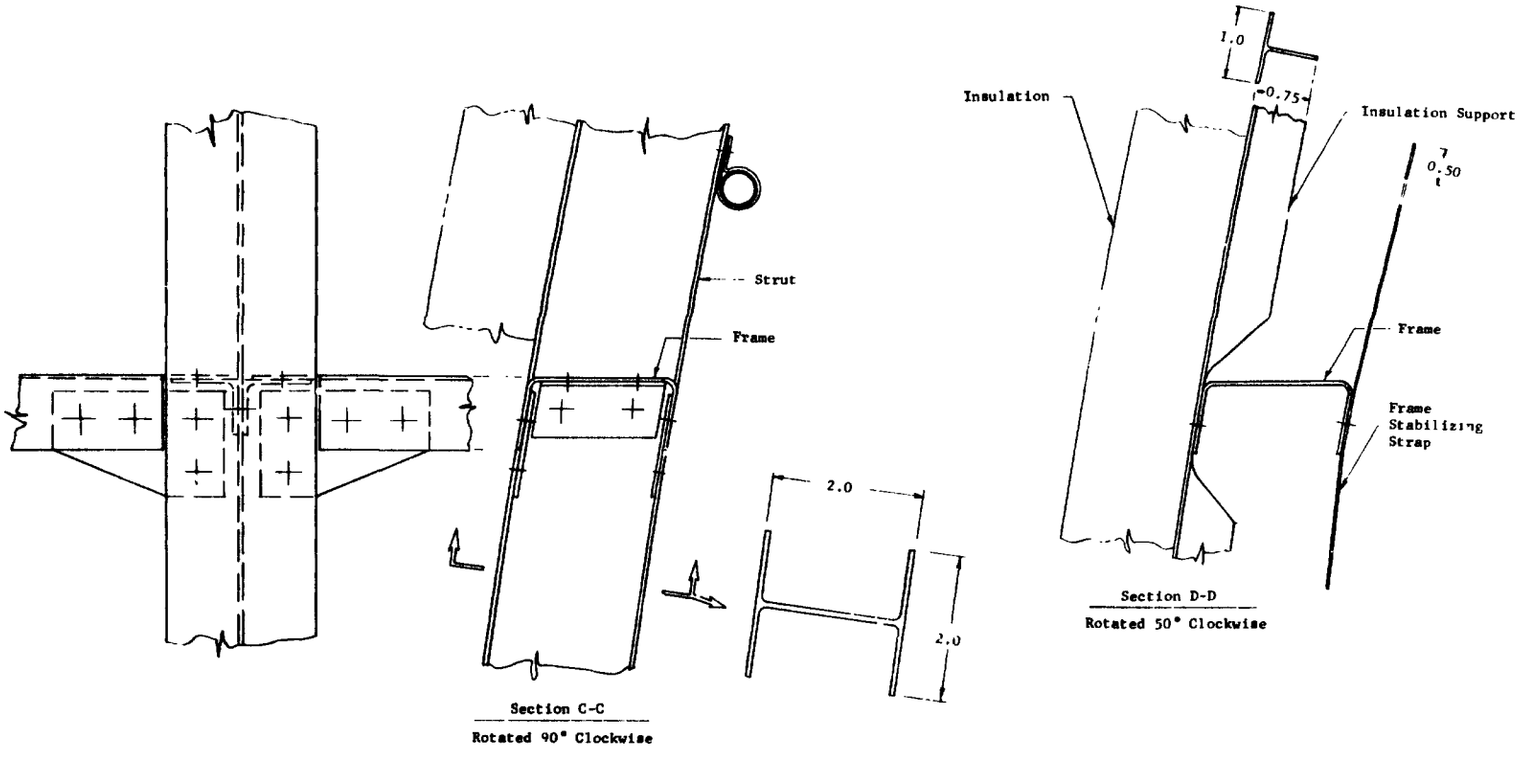

Figure III-1 (continued)

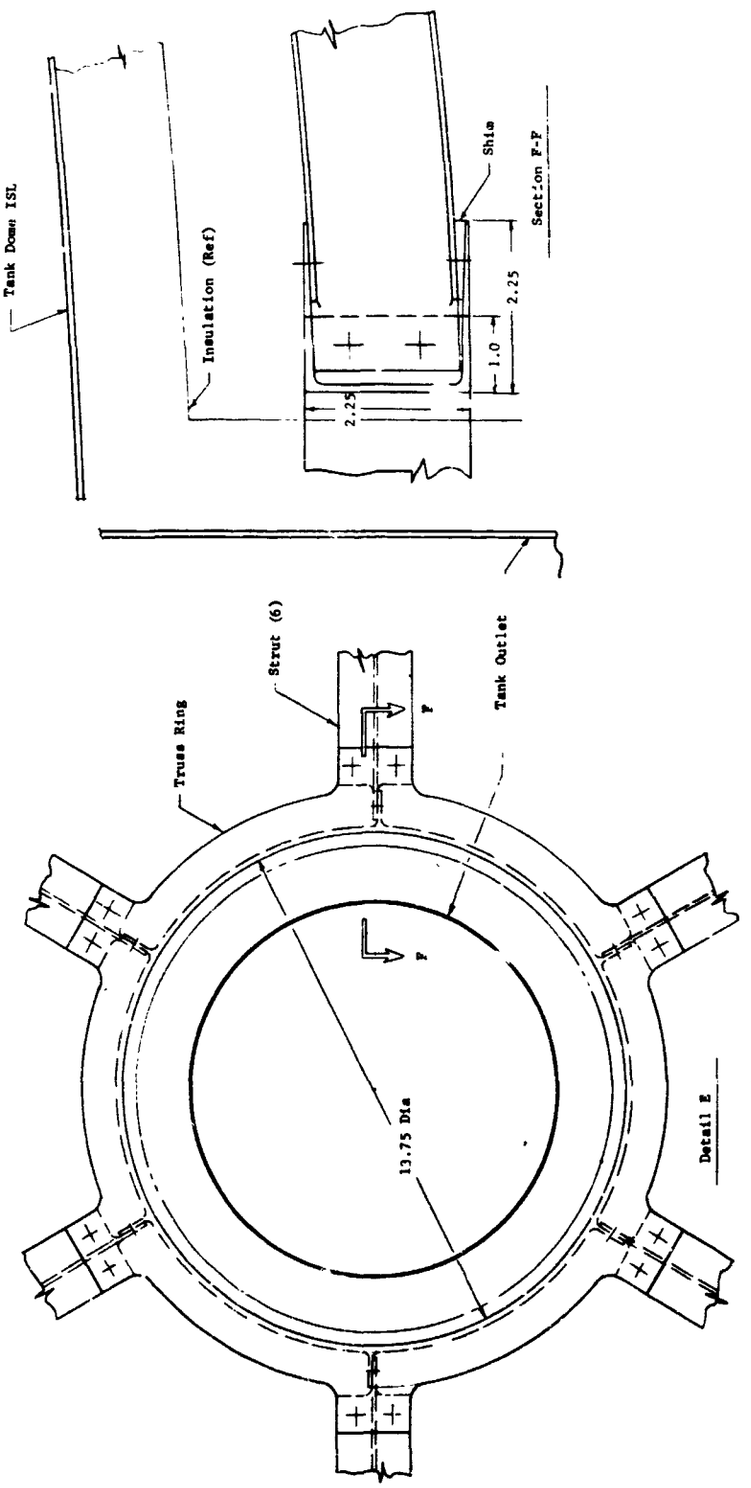

Figure III-1 (concluded)

Table III-1 Insulation Support Dome Truss Details

Location and Remarks	Frame	Strut
Frame 1 From the upper ℄ to the upper frame, the strut cross-section is a full I-beam.	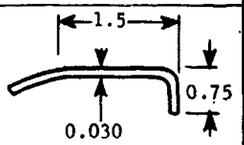	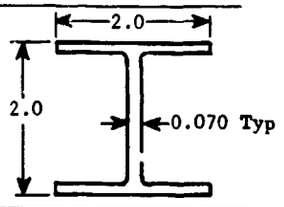
Frame 2 One flange of the strut I-beam from frame 1 to frame 4 is tapered.	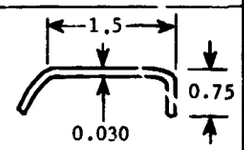	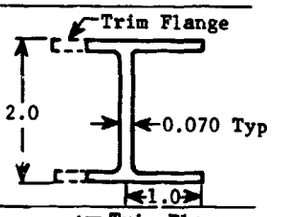
Frame 3	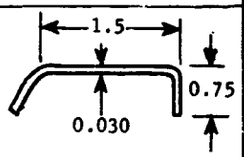	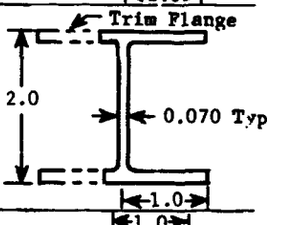
Frame 4 Strut has been trimmed to a channel section at this point.	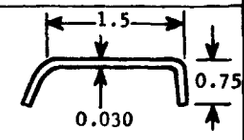	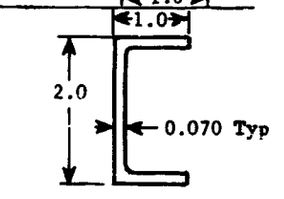
Frame 5	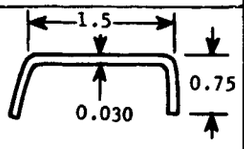	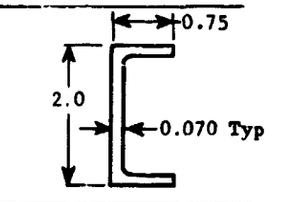
Frame 6.	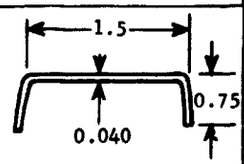	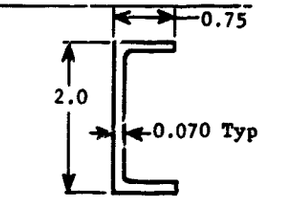

Step 2 - Position insulated tank and heat exchanger in shroud section of approximate length of tank barrel with shroud insulation installed;

Step 3 - Attach and adjust lower and then upper tank supports;

Step 4 - Install preinsulated lower dome truss. Close out heat exchanger connections. Close out truss-mounted insulation blanket to form staggered butt joint with shroud-mounted insulation blanket;

Step 5 - Install lower shroud skirt. Transfer load from handling ring and remove;

Step 6 - Install upper dome truss as in Step 4;

Step 7 - Install upper shroud skirt.

The support trusses and rods were constructed of 7075-T6 aluminum alloy material and the small standoff attachment trusses of glass filament composite rods. The heat exchanger configuration shown, considered to be an adequately conservative design, consists of approximately 2000 ft of 0.75 in. O.D. x 0.035 in. wall aluminum tubing. The fin is a 0.005 x 4 in. aluminum sheet brazed to the tube. The tube and fin are painted flat black to maximize radiative heat transfer. Lengths of tubing are joined by brazing with sleeve couplers. Except for the close-out connections, these joints can be adequately leak checked prior to installation.

The heat exchanger tube is internally plated with platinum or coated with a more active catalyst to effect continuous conversion of the vent gas to its equilibrium para-ortho composition. The chemical kinetics of this catalytic conversion process were not fully evaluated. Since flow in the tube is laminar in most instances, the incorporation of turbulence promoters at the tube joints may be necessary to achieve near complete conversion. In any event, testing of the catalytic converter design will be required.

The heat exchanger installation weight is itemized in Table III-2. From this design analysis, it is concluded that a radiative heat exchanger structure supported from the tank at the upper and lower barrel-dome junctions is practical and can be fabricated at an attractive weight when compared to predicted boiloff loss reductions.

Table II-2 Weight Statement, Liquid Hydrogen Tank Heat Exchanger and Insulation Truss (18-in. Tubing Spacing)

	Weight (lb)
Top Dome	
Structure:	
Struts	48.0
Ring Frames	39.0
Insulation Supports	12.0
Tank Attachment	2.5
Heat Exchanger:	
Tubing	45.4
Fin	11.8
Barrel	
Structure:	
Rods	2.0
Fittings	4.5
Heat Exchanger:	
Tubing	95.2
Fin	24.4
Aft Dome	
Structure:	
Struts	48.0
Ring Frames	39.0
Insulation Supports	12.0
Tank Attachment	2.5
Heat Exchanger:	
Tubing	45.4
Fin	11.8
Total	443.5

B. INSULATION SYSTEM DESIGN

A number of attractive concepts for assembling blankets of high performance multilayer insulation have been developed. All are based on the use of lightweight reflective foils such as aluminized mylar. The primary point of departure among these concepts is in the method of minimizing conductive heat transfer between the foils. It has not been an objective of this study to evaluate the various insulation systems, such as crinkled mylar, net or foam spacers or flocked foils. Rather, insulation has been considered parametrically in terms of its properties. However, in evaluating the design of an integrated hydrogen storage system, consideration was given to the assembly and installation of the insulation.

For purposes of this study, an insulation system made up of aluminized mylar and a net spacer material has been chosen. Such systems, on the basis of past investigations, offer acceptable thermal performance and ease of handling. The foil and net spacer system can be fabricated and installed as preformed panels and may offer advantages in blanket thickness control. The following paragraphs present a design concept for application of this type of insulation to the two-blanket configuration required for the cooled insulation scheme.

Double aluminized mylar, 0.15-mil thick with 800 Angstrom aluminum thickness on each side, is used for the radiation shields. The 0.15-mil mylar appears to offer adequate strength and a weight improvement over 0.25-mil material. Contact with water causes serious degradation of the reflective characteristics of the aluminum film. It is therefore assumed that the quality of the reflective film will be continuously monitored during fabrication of the blankets, and that the insulation will be maintained in a moisture-free environment at all times thereafter. This would be accomplished by maintaining a dry nitrogen purge on the system during storage, shipment, and assembly of the stage. Because of the large expense and time that would be required to replace the insulation on a large scale tank, the use of gold rather than aluminum for the reflective coating must be considered. Though less data is available on gold-plated foil, its advantages in durability and improved performance are well established. In the large quantity required for an SIV-B scale tank insulation system, the additional cost may not be a highly significant factor.

Nylon netting has been assumed as the spacer material. This material is readily available, but has disadvantages in terms of weight, thermal contraction, and outgassing. Silk and dacron nets have also been used. It is suggested that a knitted net offers advantages in the formulation of a lightweight insulation blanket, but that the selection of materials commercially available at this time is not adequate to permit optimization of this type of insulation system. Compared to the cost of assembly and installation of a space vehicle insulation system, the setup charge for fabrication of netting to new specifications is negligible. The determination of specifications for an optimum spacer material is not straightforward, however. Variations include material, yarn size and type, mesh, knit pattern and finish, with an unlimited number of possible combinations. Research and development in the area of knitted spacer materials for high performance insulation systems is therefore recommended.

The proposed blanket assembly is depicted in Figure III-2. It consists of an inner and outer structural net with alternating layers of aluminized mylar and spacer material. Depending on the spacer characteristics, an advantage may be gained by using two nets per foil, particularly toward the cold side. The blanket is assembled with closely spaced threads (possibly 3 or 4 in. spacing) tied between the structural nets or between plastic disks attached to the structural net. Thickness of the blanket is controlled by mechanically gaging the length of the thread. A small preload is designed into the blanket to improve dimensional stability. Diagonal threads are installed in the direction of the primary load on the blanket to limit slippage and compression of the blanket during boost loads. A hot needle is used to penetrate the mylar foils through which the threads pass. This technique will provide a reinforced hole with much greater strength than the torn opening made by a cold needle.

For a long term mission, perforations for venting the insulation should be kept to a minimum. This minimum perforated area would be greatly affected by any long term outgassing tendency of the spacer material. For the purge system to be described below, the perforation requirement may be determined by the purge gas flow requirements. In both instances, experimental data will be required.

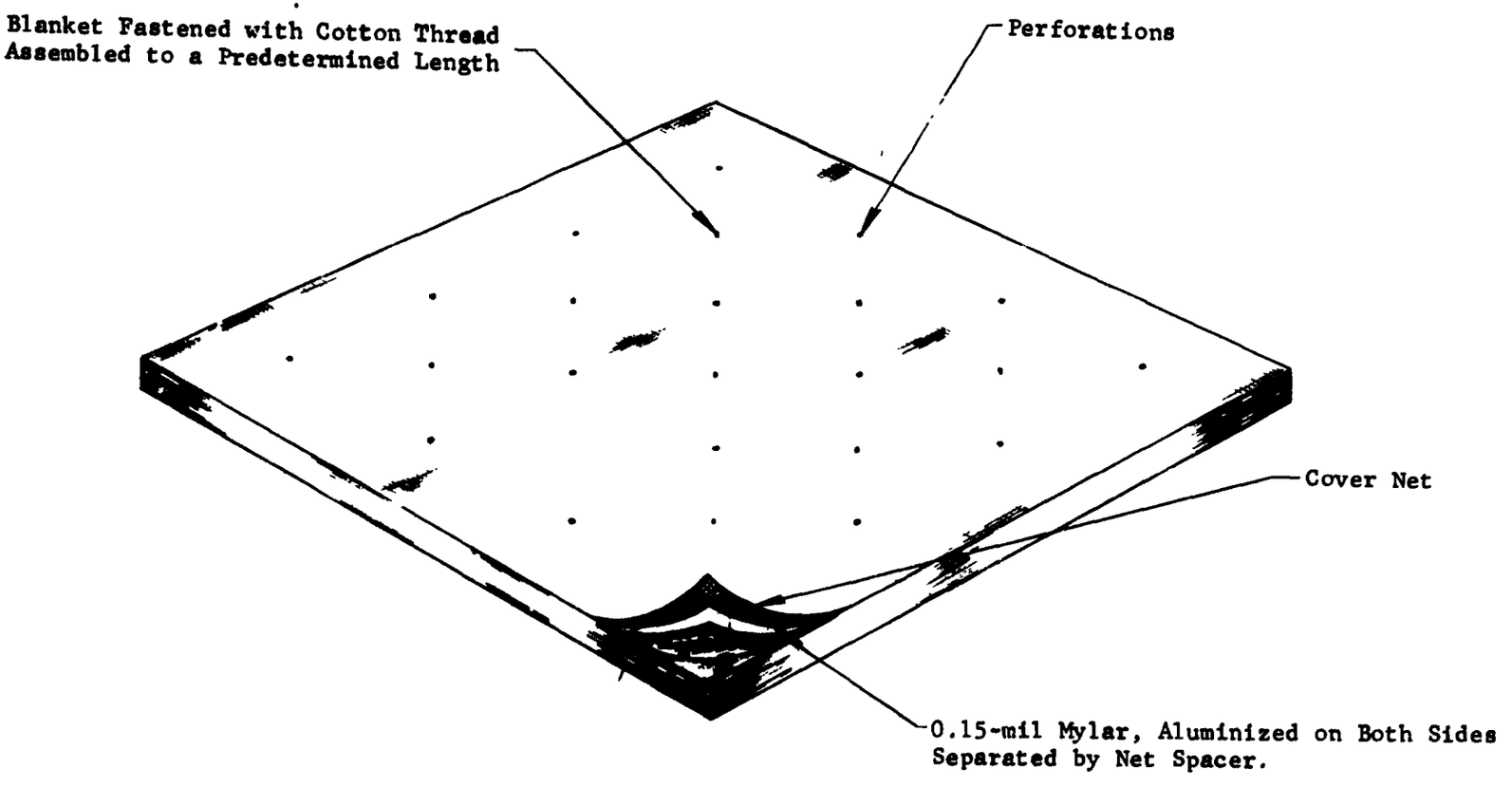

Figure III-2 Insulation Blanket Design

The tank-mounted insulation is prefabricated into 14 (or fewer) form-fitting panels as shown in Figure III-3. Insulation lay-up mandrels, as suggested by Figure III-4, will be required for the various forms. Handling fixtures will also be required to transfer the insulation blankets from the lay-up mandrels to the tank for installation. The shroud- and truss-mounted insulation blankets would be similarly treated.

C. INSTALLATION OF INSULATION

Attachment of the insulation blankets is as shown in Figure III-5. The primary structural attachment is by means of snap and curtain fasteners attached to dacron ribbons which, in turn, are fastened across the full length or breadth of the panel. These fasteners are located on all sides of each blanket, with mating pins bonded to the tank or shroud. At frequent intervals (approximately 1 ft) over the surface of the blanket, Velcro pile strips are bonded. Velcro hook strips are mounted on the tank or shroud at right angles to permit engagement with small alignment errors.

The junction between insulation panels is a butt joint with strips of aluminized mylar interleaved adjacent to each aluminized mylar foil. These strips are secured in place with small strips of mylar tape at appropriate intervals. This technique for minimizing radiation leakage through the blanket has been successfully applied to the integrated insulation system test (tank-mounted insulation) and is judged to be fully practical with regard to manufacturing methods. Inner and outer structural nets of adjacent panels are stitched together over the full length of the butt joints.

D. PURGE AND VENT SYSTEM

Figure III-6 depicts the overall insulation configuration for the purge and vent system. The outer insulation blanket is mounted to the shroud in the area of the tank barrel section. In the vicinity of the tank domes the blanket is mounted to the hemispherical heat exchanger truss. Near the tangency point between the shroud cylinder and the heat exchanger truss, the blanket swings freely between the two, to permit the two blankets to be joined. A staggered butt joint is employed at this close-out junction, without interleaving.

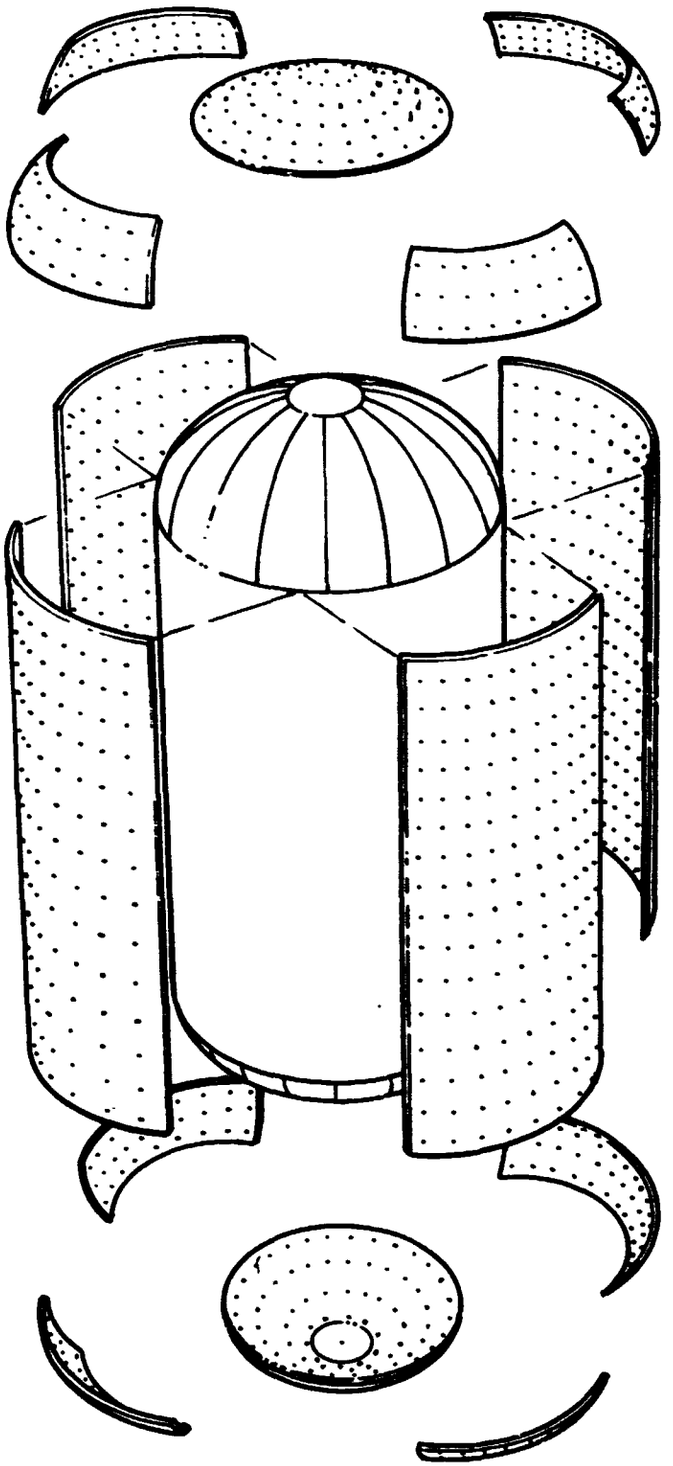

Figure III-3 Preformed Tank Insulation Panels

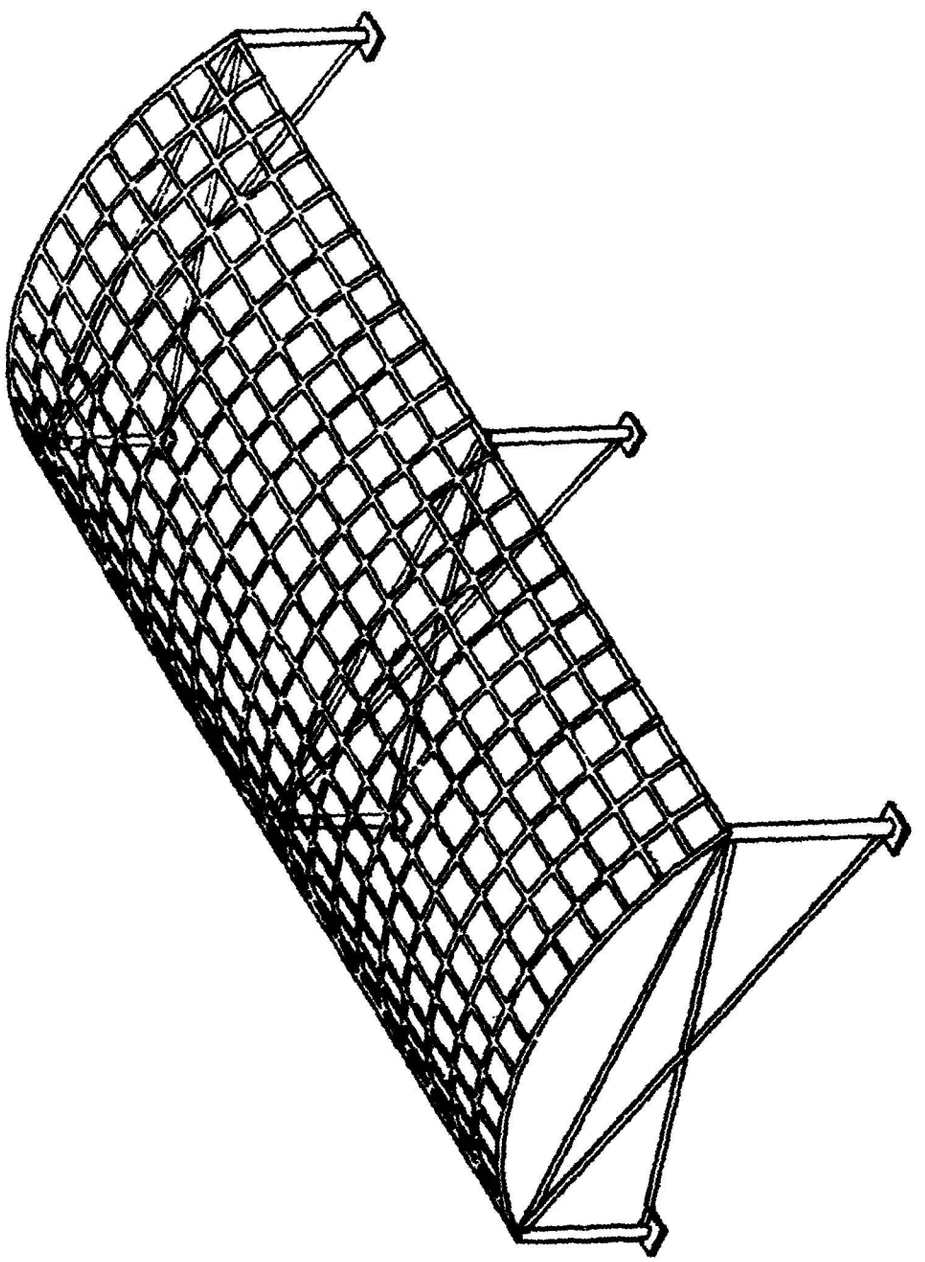

Figure III-4 Insulation Blanket Lay-up Mandrel

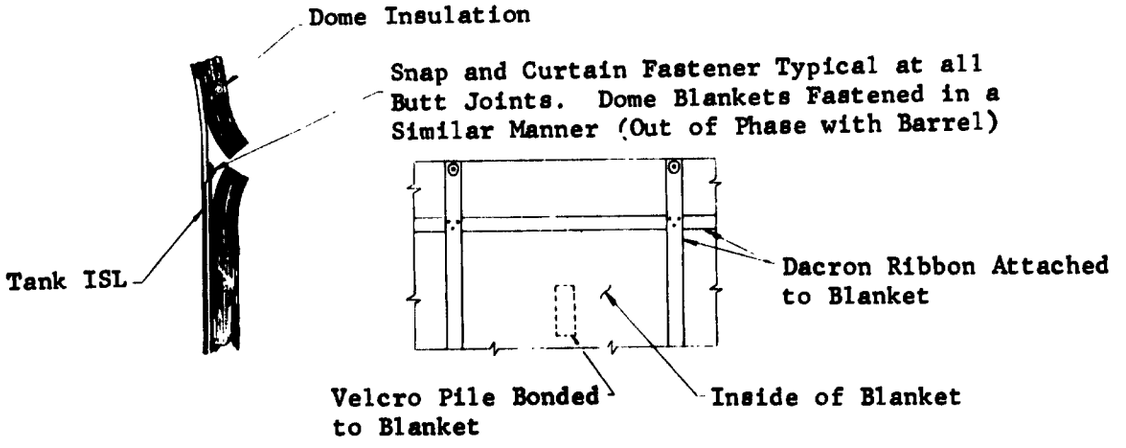

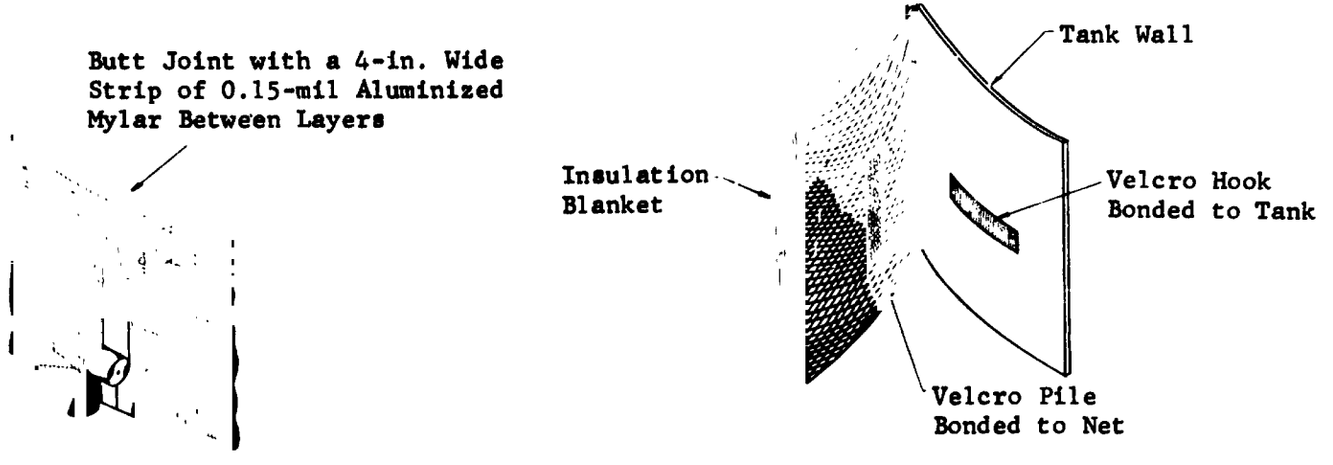

Figure III-5 Insulation Installation Details

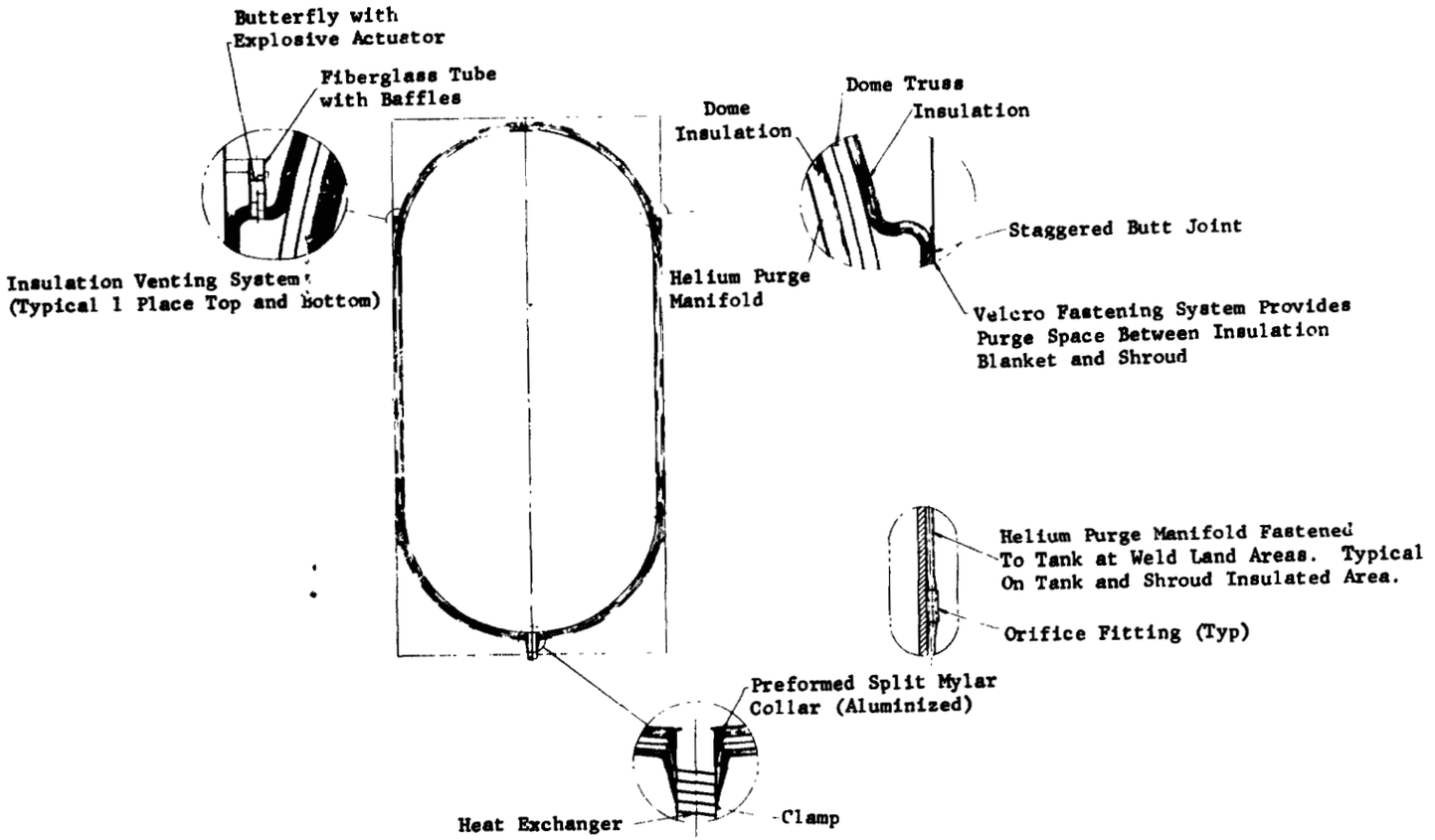

Figure III-6 Insulation Purge and Vent System

Conical insulation blankets are attached with clamps to the major pipe penetrations. These blankets are designed to approximately preserve the temperature gradient within the insulation blanket, resulting in a fixed heat flux per unit area and minimum heat flow along the insulation layers. These cones are joined to the tank and shroud blankets by interleaved preformed split collars of aluminized mylar. A simple coiled stainless steel tube heat exchanger is welded or brazed to the tank drain line to intercept and reduce heat leakage from that source.

The helium purge gas is fed through aluminum tubing distribution manifolds attached to the tank and to that area of the shroud on which insulation is installed. Orifices are located uniformly over these areas to meter a continuous flow of purge gas. The orifices are sized to require a significant pressure drop, allowing the manifold to operate at a pressure that is high compared to flow losses through the system. In this manner, the pressure is nearly constant at all points and the flow distribution will be uniform throughout. A secondary purpose of the close spaced Velcro fasteners is to provide a spacing between the insulation blanket and tank or shroud to improve the distribution of the purge gas.

The path of the purge helium is as follows: The gas that is distributed over the tank surface flows through the tank-mounted insulation into the region between the blankets. That gas which is distributed on the shroud surface likewise flows through the insulation to the region between blankets. To escape from this area, all of the gas then flows through the forward and aft truss-mounted insulation blankets into the shroud ends. These regions are assumed to be ventilated, or to be connected to a helium recovery system. Flow rate and pressure drop through the insulation must be adjusted so that the static pressure in the region between insulation blankets is sufficiently great to minimize hydrostatic effects on the purge flow pattern.

To assure proper venting of the insulation system in space, vent valves are installed through the outer insulation blanket as shown in Figure III-6. These valves, installed in fiberglass ducts with radiation barriers, are actuated by a pressure (altitude) switch with explosive actuators. If the shroud ends are not sufficiently open to the environment, additional valves or an alternative installation of the above ducts to the outside, will be required.

E. INTERNAL HEAT EXCHANGER

The thermodynamic vent system requires a heat exchanger either within or on the tank wall to assure vaporization of all vent fluid at the tank temperature. The heat exchanger shown in Figure III-7 represents a simple, lightweight approach to the problem. In the actual design of a space vehicle, this heat exchanger could be mounted on slosh baffles or other internal hardware. In the present design, approximately 600 ft of 0.75-in. O.D. x 0.035-in. wall aluminum tubing makes three passes through the tank. In this manner the vent fluid is used to transmit heat from warm to cold areas of the tank to minimize temperature gradients, and to limit to a small amount any uncooled pockets of fluid near the tank wall. The weight of this heat exchanger is estimated to be 83 lb.

Thermal analyses on the internal heat exchanger indicate that this design is adequate to remove all heat reaching the tank and to limit thermal stratification to a maximum temperature differential within the tank of approximately 5°R. Thus, when the highest liquid temperature is being held to 40°R by the control system, some liquid may be as cold as 35°R. However, such analyses are based on assumptions as to the nature of heat transfer and liquid position in a weightless environment. Any design of a thermodynamic vent system should take into account the best data then available, hopefully from large scale orbital experiments.

F. VENT CONTROL SYSTEM

Analysis has shown that efficiency of the heat intercepting vent system is greatest when the vent flow rate is constant. This would suggest that a throttling control system be used to minimize cycling. However, the complexity of throttling valves and controllers is not attractive for a long term space operation. Figure II- 8A illustrates a proposed system using on-off pressure switches and valves to achieve a reasonable approximation to steady-flow conditions. By utilizing three properly sized flow restrictors, flow rates of 0, 75, 125, and 400% of the nominal flow rate can be obtained. Under normal conditions, then, the flow will cycle in the range of nominal ±25%. For transient or off-normal conditions, the 0 and 400% positions permit control of tank pressure to be maintained.

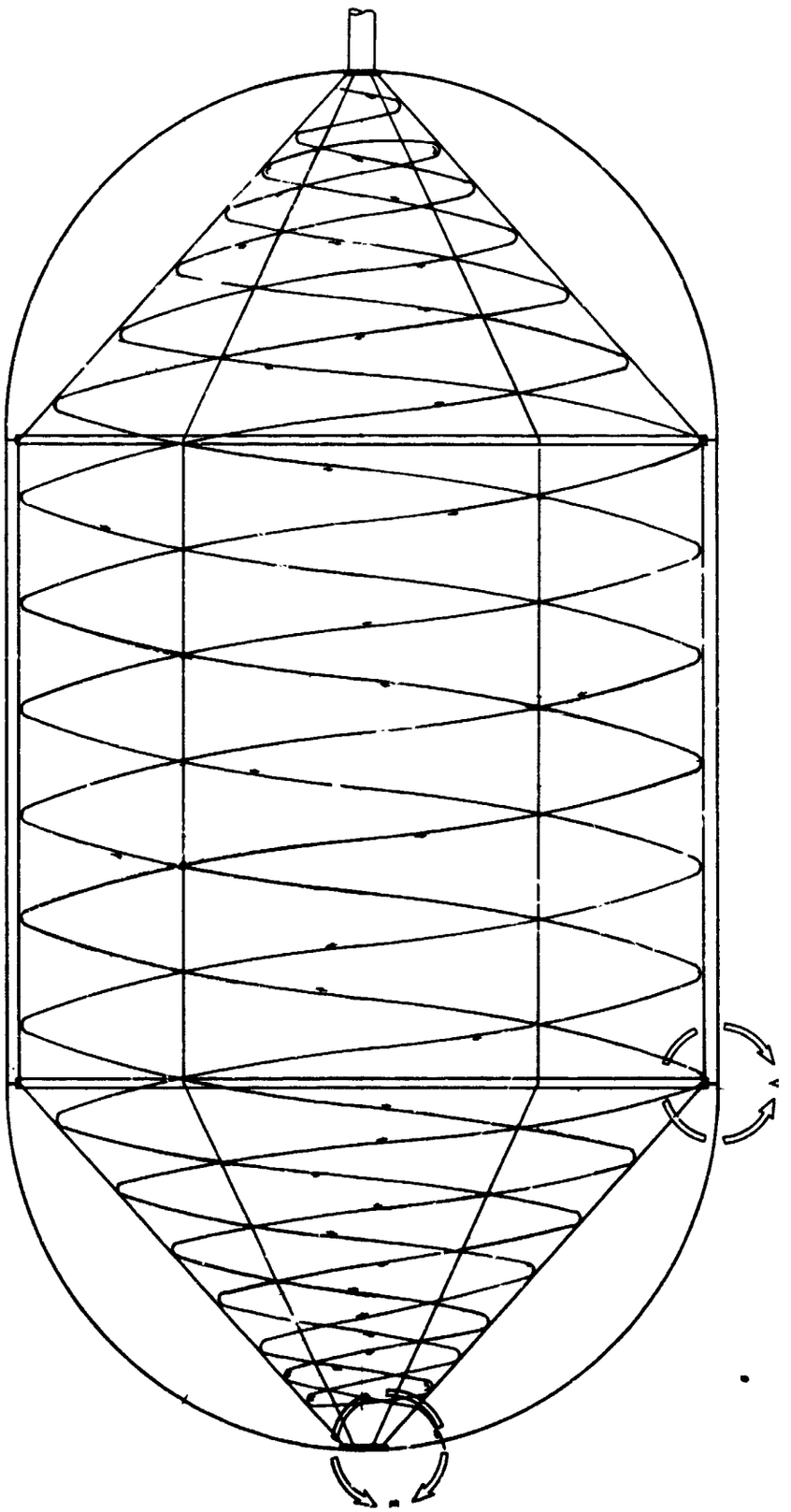

Figure II"-7 Internal Heat Exchanger

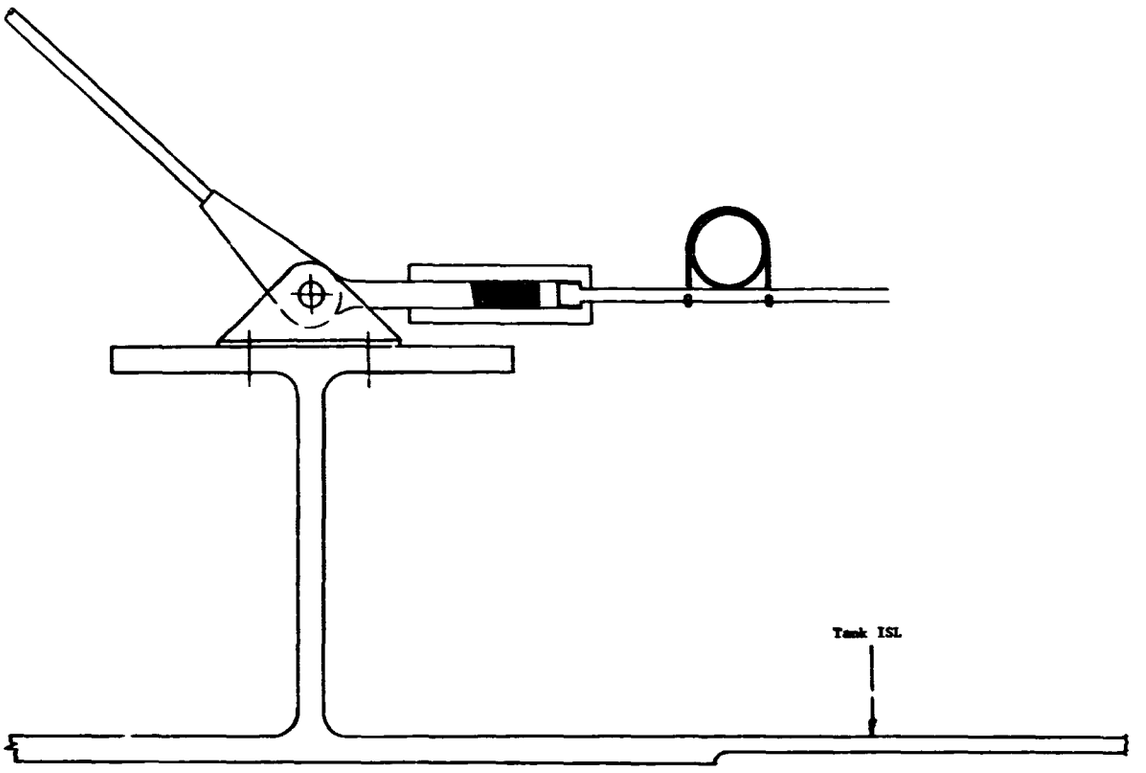

Detail A

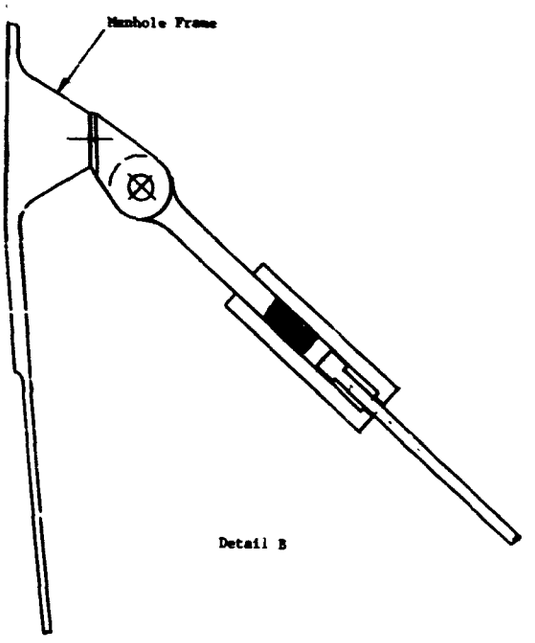

Detail B

Figure III-7 (concluded)

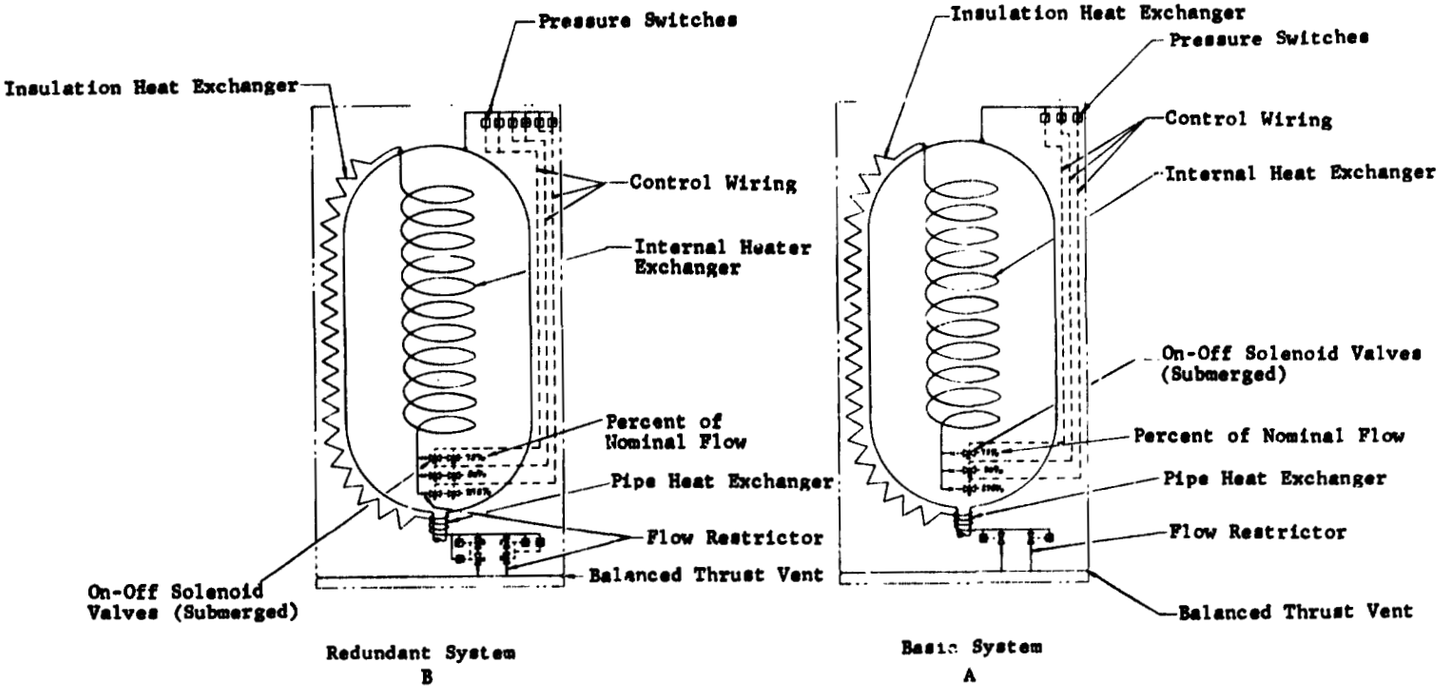

Figure III-8 Vent Control System

In order to eliminate the problem of possible freezing of hydrogen in the system due to low back pressure, a two-stage, on-off, back pressure regulation system is included. Since back pressure is not as critical as flow rate on system efficiency, cycling of these valves to hold the pressure within reasonable bounds should be acceptable. Figure III-8B illustrates the same system, but with redundant components for increased reliability.

G. NONMETALLIC COMPOSITE TANK SUPPORTS

In the reference vehicle previously described, a significant amount of heat reaches the tank through the titanium tank support members. Further, the thermal performance of the titanium system is dependent on the thermal contact resistance offered by a series of stainless steel washers. The actual force acting on these washers, and consequently the heat leak, is difficult to predict. The structural and thermal properties of several nonmetallic composite materials appear attractive as a means of reducing structural heat leak. In addition to the thermal analysis reported in Section II, which indicated that a significant gain might be achieved, a design analysis was undertaken.

Primary considerations are the same as for the metal support design. The new material should have as good as or better strength characteristics and lower thermal conductivity, and should lend itself to reasonably simple manufacturing techniques and low cost producibility and maintenance. Two materials from the composite material field were selected for design evaluation: boron and S-glass. These materials have high strength-to-weight ratios and low thermal conductivity; however, both have some drawbacks. S-glass has a very low modulus of elasticity, making is susceptible to buckling. Boron fibers are brittle and fragile in many applications where a small bend radius is required. In spite of these problems, however, recent literature indicates that boron eventually may become very prominent for designs such as struts, landing gear, and column applications.

In reviewing the history of boron as a structural material, we find that initially it was almost impossible to produce boron fibers with constant strengths and modulii. External flaws could be traced to deposition techniques of the boron-to-tungsten core. Large residual stresses were also encountered during the production operations due to heat. At first, acid etching processes were developed to rid fibers of surface flaws, but boron fiber producers have made excellent progress in solving this problem and the residual stress problem, and are now producing high quality fibers without flaws and of good consistancy. Other problems facing the producers were oxidation and physical damage during handling. Sheath coating processes have successfully been developed and fibers can now be grouped and wound around large diameter spools for safe handling.

The next step was to discover useful and practical ways to use boron fibers. The answer was boron composites, both metallic and nonmetallic. For the purpose of this study, to reduce heat transfer, a nonmetallic boron composite is the most beneficial form. A unidirectional boron fiber, resin-impregnated tape was found to be the best choice for this application. Constant strength and modulus are required of an efficient composite. Through testing of boron composites, it has been increasingly evident that the strength and modulus are highly dependent on precise spacing of the filaments so that each filament can react loads equally. Unequal loading can cause a breakdown in the matrix system and expose filaments to failing shear loads. Testing of good quality boron filaments indicates an average tensile stress of 400,000 psi and one of the more successful projects using boron tape on filament-wound pressure vessels shows an average fiber tensile stress of 236,000 psi at 75°F and 273,800 psi at -320°F (Ref 8).

Fiberglass-reinforced composites are not new to the airborne structural field. Composite structures have been used in fairings, rudders, and heat shields for aircraft. One of the latest glass composites that has been developed for higher strength potential is S-glass or S-994. S-glass is a fiberized glass composed of 65% SiO_2, 25% Al_2O_3 and 10% MgO. The principal attraction of S-glass composite is its tensile strength, but it also offers low density, appreciable corrosion resistance, and low fabrication and maintenance cost. Tested tensile values of S-glass composites have ranged in the neighborhood of 280,000 psi to 290,000 psi (Ref 9), more than twice that of titanium. Compressive stress is also slightly higher than that of titanium at approximately 136,000 psi; but, with only an 8×10^6 psi to 9×10^6 psi modulus (Ref 9), S-glass composite becomes somewhat undesirable for stiffness applications.

For the stress analysis, allowables used for both composites are as presented in Table III-3 taken from Ref 9. The allowables are room temperature values. However, all indications are that at cryogenic temperatures the values become slightly better.

Table III-3 Mechanical Property Comparison

Property	Titanium	Boron Composite	S-Glass Composite
Young's Modulus, psi	16×10^6	39.2×10^6	8.42×10^6
Ultimate Tensile Stress, psi	130×10^3	186×10^3	280×10^3
Ultimate Compressive Stress, psi	126×10^3	230×10^3	136×10^3
Density, lb/in^3	0.160	0.076	0.074

The design of the boron epoxy lower support tube is shown in Figure III-9. A primary problem to be resolved in this design is the equal distribution of tension and compression loads through the fibers. For maximum strength, the fibers are aligned parallel to the load axis. The design concept presented here relies on a metal insert with a curved profile to transfer tension loads to the fibers. The boron fibers, in a preimpregnated tape form, are laid up over a thin wall aluminum mandrel, and overwrapped on the ends to conform to the profile of the metal insert. Overwrapping of the boron in this area with graphite and epoxy results in a restraint of the longitudinal fibers, and a tension failure of the graphite must occur before the joint can fail. After curing of the assembly, the aluminum mandrel is etched away. The boron fibers are preloaded due to the curvature resulting from conformance to the end fitting, and a degradation of load carrying capacity therefore results.

After curing of the epoxy, the ends, including metal, boron, and graphite, are machined to a flat surface perpendicular to the tube axis. Assembly of the threaded end pieces into the tube inserts provides for compressive loading of the fibers. To compensate for irregularities in the machined tube end surfaces, a room temperature curing epoxy filler is applied before assembly of the end fittings. Depending on the characteristics of the bond between the metal inserts and the boron epoxy, a small slippage of the insert may occur when the tube is initially loaded in tension. Therefore, as part of the manufacturing procedure, each part should be loaded to its design load in tension prior to machining the ends. Experience indicates that after the initial loading, no further slippage will occur.

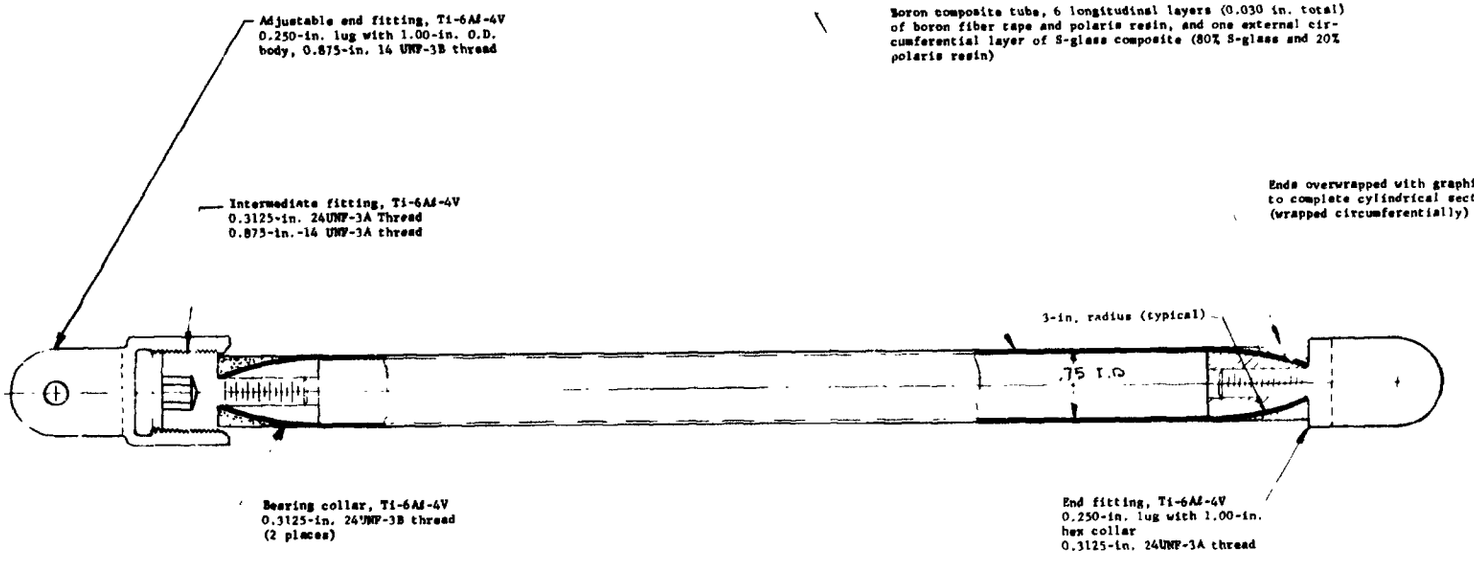

MCR-66-405

Figure III-9 Lower Support Tube, Boron Epoxy

Because of the high compressive strength of the boron epoxy composite and primarily tension loading on the lower supports, the design of the boron support was governed by tension requirements. Therefore, a minimum tube diameter was chosen. A 50% volumetric fiber content is assumed. This is achieved by use of boron tape, 0.125-in. wide and approximately 0.005-in. thick. The tape is made up of approximately 25 to 29 boron fibers about 0.004-in. maximum diameter and bonded together to form a boron tape. The boron tape is then laid up using the polaris resin system for the composite matrix. The polaris resin system consists of EPON 828 and 1032 with methyl nadic anhydride in proportions of 50, 50, and 90, respectively. This resin system was selected on the basis of its good bonding adhesion to the boron fibers, plus its applicability to cryogenic applications and its desirable overall properties. Because the 0.004-in. fibers are formed over a 3-in. radius, a degradation of strength of about 16% will result. The metal inserts and end fittings are of 6Al-4V titanium heat treated to a 160,000 psi tension allowable. Titanium is used because its thermal expansion characteristics are most compatible with those of the composites.

The glass epoxy lower support tube design is shown in Figure III-10. The material used is 20 end roving S-glass. Again the polaris resin system was chosen for the reasons noted above. The same concept is used for transmitting tension and compression loads to the fibers as that described above for the boron tube. Because of the small fiber diameter, the degradation of fiber strength caused by conformance to the 3-in. radius of the metal insert is expected to be negligible. Compression loading governs the design of the S-glass epoxy lower support. The section has been sized for the condition that the local critical crippling stress equals the Euler stress, resulting in a minimum column section area.

An alternative design for the upper tank support of S-glass epoxy is shown in Figure III-11. This tube is loaded in tension only and is therefore designed with a minimum diameter. Tension loads are transmitted to the glass fibers in the same manner as the composite lower strut designs. Because of the lower elastic modulus and the greater tensile strength of the glass epoxy, maximum tank motion is 0.310 in., compared to 0.100 in. for the titanium stabilizer system. Because the upper support is loaded in tension only, no advantage would result from the use of boron epoxy. A weight estimate for the composite structural elements is tabulated.

	Weight (lb)
S-glass epoxy lower support	0.63
Boron epoxy lower support	0.56
S-glass epoxy upper support	0.32

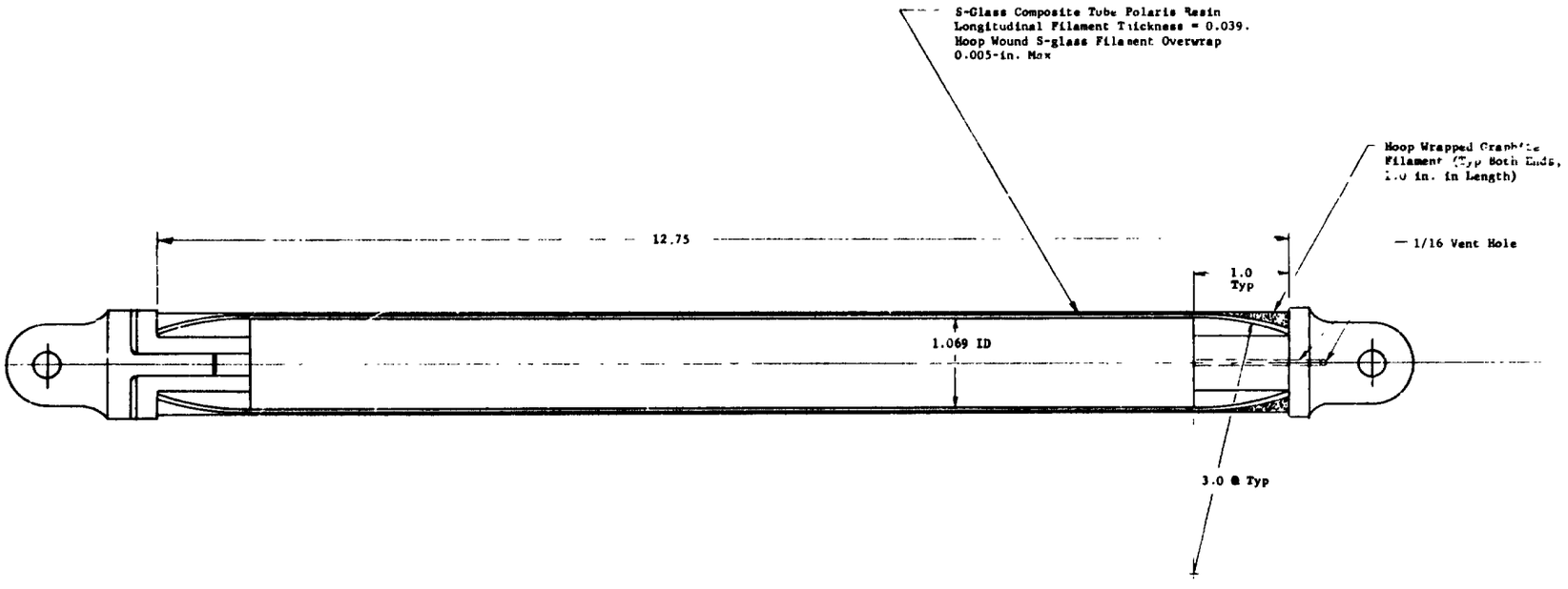

Figure III-10 Lower Support Tube, S-Glass Epoxy

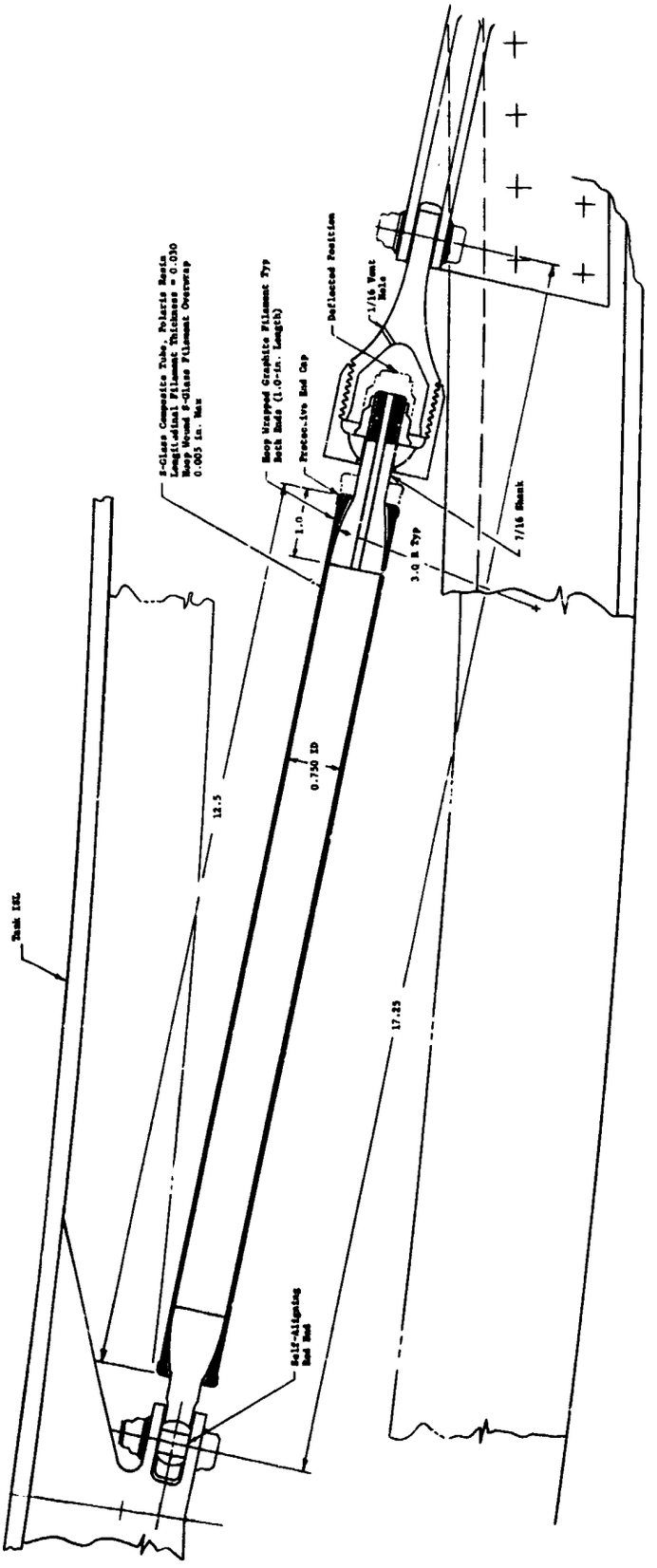

Figure III-11 Upper Stabilizer Support, S-Glass Epoxy

IV. EXPERIMENTAL PROGRAMS

A. INTERNAL CAPILLARY INSULATION, FEASIBILITY DEMONSTRATION TESTS

Small scale table top tests were conducted to demonstrate the feasibility of the honeycomb and the capillary screen concepts for positioning a gas layer between the liquid and the tank wall. The basic test apparatus for the honeycomb concept is shown schematically in Figure IV-1. It consisted of a cubical plexiglas box with inside dimensions of 6 in. The insulation specimens to be tested were mounted on the bottom and one wall of this box. Each specimen of insulation was made up as follows: A piece of 0.5-in. thick plate glass was used as a base. A heating wire of 30-gage nichrome wire was attached to the outer side of the glass with Delta Bond 152 epoxy adhesive. Honeycomb material, 0.5 in. thick, was attached to the inner side of the plate glass. The honeycomb was made of phenolic impregnated cloth with flattened hexagonal cells approximately 0.3125 x 0.1875 in. in size. The glass was coated with a thin layer of Narmco 7343 adhesive and the honeycomb pressed into the adhesive. The open end of the honeycomb was closed with a capillary barrier sheet of 5-mil mylar sealed to the honeycomb with a thin layer of Narmco adhesive. Figure IV-2 shows two specimens in various stages of construction. A small hole was drilled through the mylar into each cell with a number 76 size (0.020 in.) drill. A 0.25-in. thick piece of cork board was installed over the mylar sheet with a separation of approximately 0.0625 in. Figure IV-3 shows the assembled test article with foam insulation. This insulation proved to be unsatisfactory and was replaced with cork.

Sixteen copper/constantan thermocouples were used to measure the temperature at various levels in the specimen. The arrangement of these thermcouples is shown in Figure IV-1. Wattmeters were used to determine the heat load applied to the specimen by the integral heaters.

Pentane was used as a test fluid because of its near ambient boiling temperature. The test vessel was filled with pentane and the heaters activated. In order to purge the air from the cells, the honeycomb temperature was brought to about 125°F then allowed to cool. At times it was necessary to run this heating and cooling cycle several times before the cells were filled with liquid. When the cells were filled, the power to the heaters was adjusted to the desired setting and the test was run until the temperatures throughout the test specimens were steady.

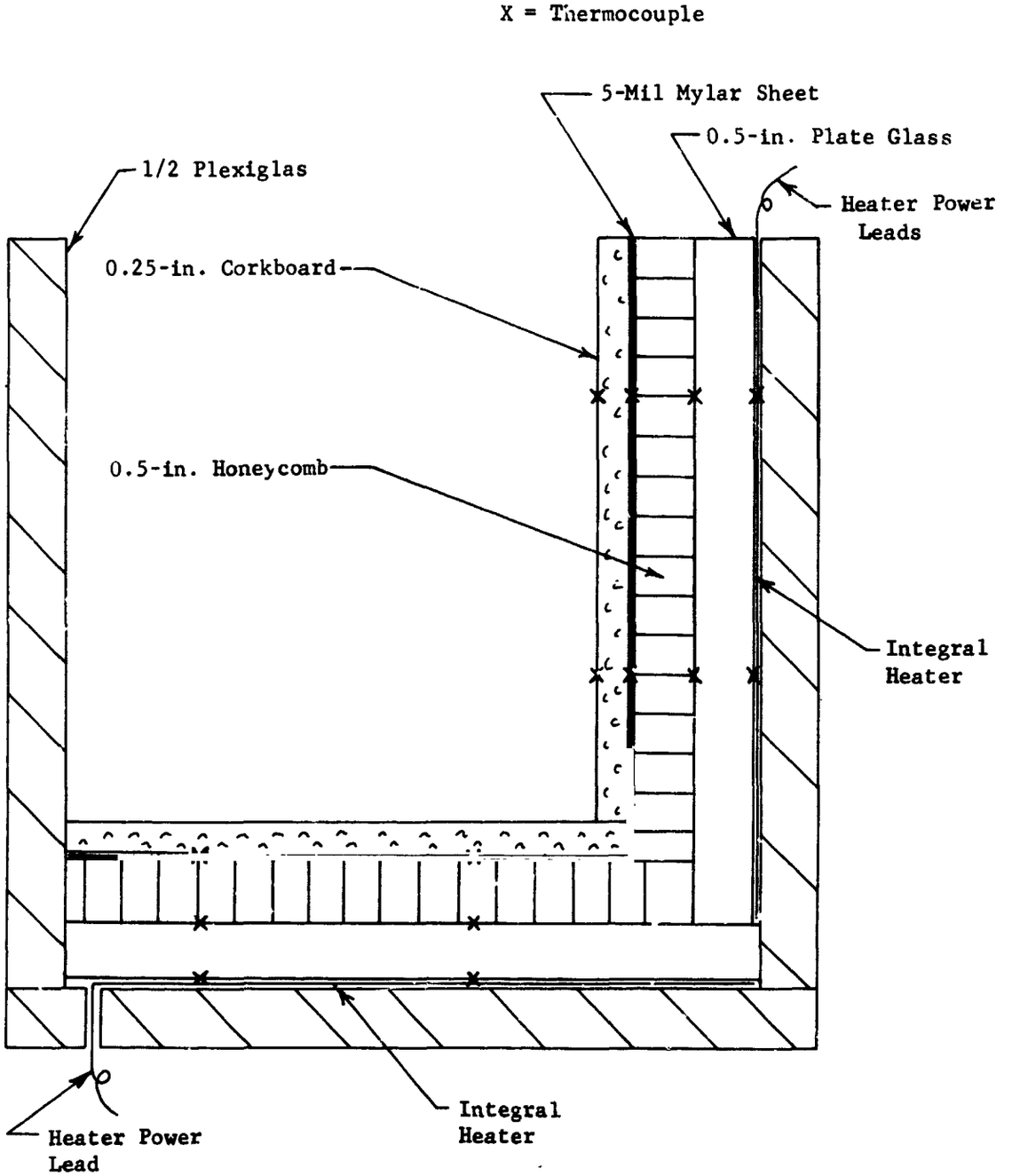

Figure IV-1 Honeycomb Internal Capillary Insulation, Feasibility Test Schematic

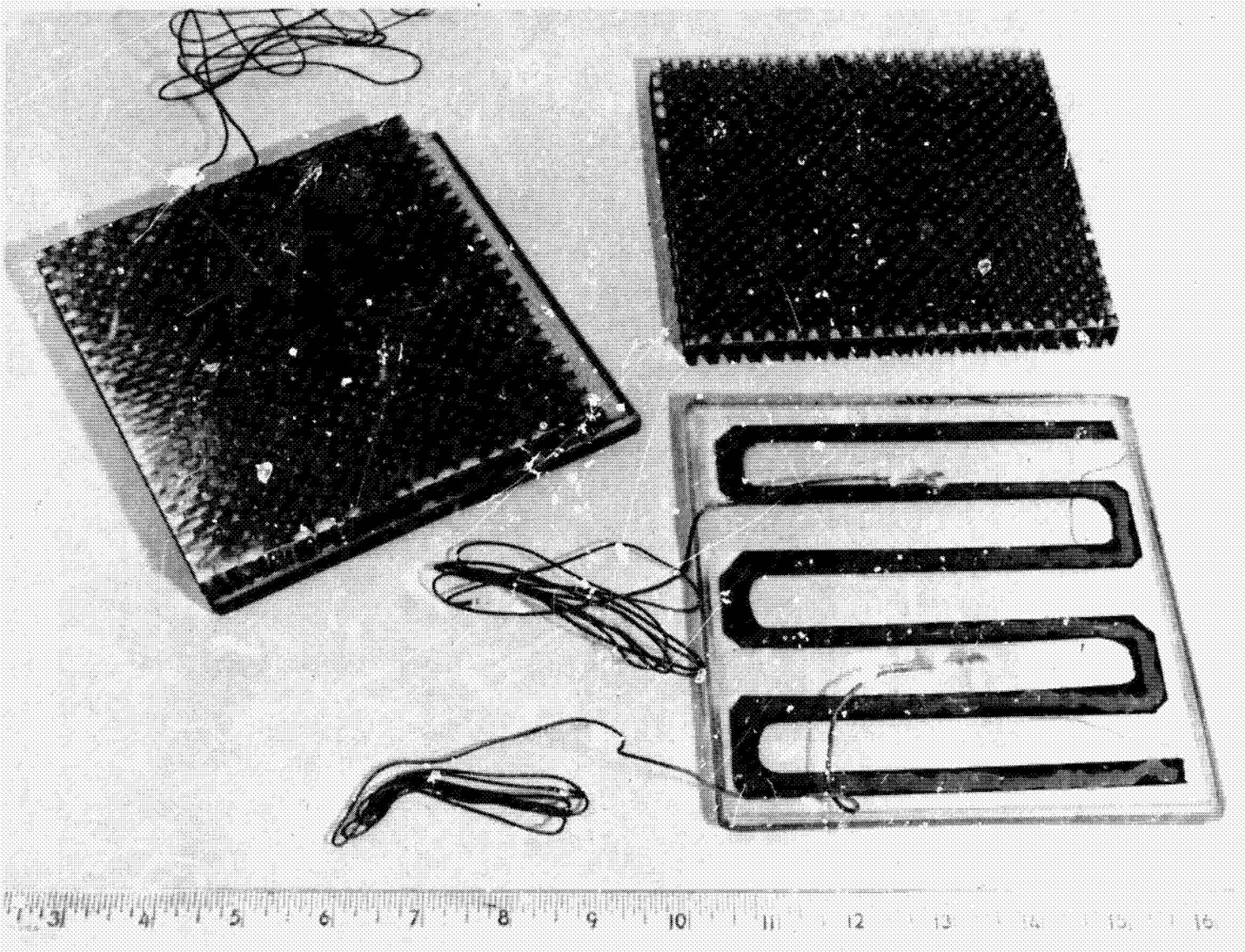

Figure IV-2 Partial Assembly of Honeycomb Internal Capillary Insulation, Feasibility Test Article

Figure IV-3 Honeycomb Internal Capillary Insulation Concept Test Article

Figure IV-4 Partially Completed Feasibility Test Article
Internal Capillary Insulation, Screen Concept.

1. Results of Test No. 1

This test was designed primarily to check out the test apparatus and determine if the liquid can be driven from the cells. With the cells full of liquid, the bottom heater was energized with 100 watts. In 20 minutes all of the cells appeared to be empty. The temperature of the hot side of the honeycomb was 300°F.

The second part of this test was conducted to determine if the vertical section of insulation would perform as predicted. The plan was to apply 40 watts of power to the vertical heater and take motion pictures to visually record the emptying of the cells. However, the heater was not needed as when the sun gun, used for illuminating the cells, was turned on, it supplied sufficient radient energy to force the liquid from the cells.

2. Results of Test No. 2

This test was made to obtain motion pictures of the evacuation of the horizontal honeycomb section. With the cells filled with liquid, 120 watts of power was applied to the heater. It required approximately 20 minutes at this power setting for the liquid in the cells to be evaporated. This test run was also photographed. When the liquid had been evaporated, the power was reduced to 40 watts, the system wrapped in foam insulation, and allowed to reach steady state. After 2 hours, the temperatures were relatively constant at the values listed.

Liquid side of cork insulation	- 78°F
Space between cork and barrier plate	- 85°F
Junction of honeycomb and glass plate	- 102°F
Outside of gla[illegible] plate	- 190°F

3. Results of Test No. 3

Starting with all cells filled with liquid, power was applied to bottom heater (30 watts). In approximately 35 minutes most cells were dry so power was reduced to 20 watts. After 100 minutes some cells appeared to be refilling. Power was increased to 25 watts. After 30 minutes there appeared to be no change so power was increased to 100 watts to dry cells. After 15 minutes, cells were dry so power was reduced to 30 watts for 40 minutes then 28 watts for 40 minutes. Temperatures appeared stable, so test was secured. The steady-state temperatures are listed.

Liquid side of cork insulation	- 78°F
Space between cork and barrier plate	- 85°F
Junction of honeycomb and glass plate	- 141°F
Outside of glass plate	- 160°F

From these tests it can be concluded that the insulation system tested did indeed function to impose a gas layer between the liquid and the heated tank wall. When the heat flux was above a minimum level, the tank wall could be maintained considerably above the boiling temperature of the liquid, and the system was operable with the bulk of the liquid below the boiling temperature. The results of test No. 4 verify that there is a minimum heat flux at which the system is operable. Because this test was not designed to give accurate data, the actual threshold flux could not be measured. Similarly, because of heat leakage to the surroundings, an apparent thermal conductivity of the honeycomb-gas layer could not be determined. However, this k value was estimated at 0.1 to 0.2 Btu/hr ft°F, much higher than the conductivity of pentane vapor. The Rayleigh number was calculated to be in the range of 12,000 to 15,000, whereas natural convection is predicted to become significant at a critical Rayleigh number of 7,000 to 10,000. It is therefore assumed that much better performance could be obtained by reducing the cell size.

A model to determine feasibility of the capillary screen concept was also fabricated and tested. This model was made identical to that for evaluating the honeycomb concept, except that a single layer of 325 x 2300 mesh dutch twill stainless steel filter cloth was substituted for the honeycomb and capillary cover plate. Figure IV-4 shows this model, completed except for the layer of cork supplemental insulation. Instrumentation and power supplies were identical for the two test setups.

The same tests reported above were attempted for this concept. The vertical compartment was observed to very quickly pump out the originally contained liquid. However, when dry, the gas layer did not remain stable. After a short time, depending on the heat flux, the compartment would suddenly refill (at least partially). Then the emptying process would begin again, and the system would continue to cycle from empty to full to empty. The bottom compartment appeared to be cycling also, but did not become totally dry.

An explanation is offered for the failure of the capillary screen system to function as predicted. Boiling occurs in the space between the screen and the cork, as was observed in the honeycomb system. When bubbles are formed in this region, the screen tends to heat to a temperature greater than the boiling point of the liquid. The screen then becomes totally dry in this spot, and no capillary action is possible. No difference in pressure across the screen can then exist. Thus, in a still wet region, liquid moves through the screen due to hydrostatic forces. In the honeycomb system, this same drying of the capillary openings occurs, but because the cells are isolated from each other no breakdown occurs.

It is therefore concluded that the capillary screen internal insulation concept previously described is not suitable for one-g applications. Whether this same behavior might occur in a zero gravity environment is subject to question. However, a similar behavior might be predicted. In the zero-g case, capillary wicking action in the space between the screen and tank wall could replace the gravity effect to cause liquid to flow into that region when the screen develops dry spots.

B. STRUCTURAL MATERIALS AND COMPONENTS THERMAL CONDUCTIVITY TESTS

In the analytical evaluation of heat leak through the structural support members, it became apparent that available test data on the thermal conductivity of nonmetallic composite materials were inadequate, particularly at low temperatures. Information was likewise scarce regarding the thermal contact resistance afforded by multiple stacked washers and self-aligning bearings. A limited test program was undertaken to develop additional thermal conductivity data for these materials and components. Composite materials chosen to be tested were S-glass epoxy, boron epoxy, and graphite epoxy. A commercially available self-aligning spherical bearing, and an assembly of two groups each consisting of 150 stainless steel washers arranged for transmission of tension and compression loads, were also tested. In the case of the latter specimens, force applied axially on the specimen was varied as a parameter. All specimens were tested at reduced temperatures, 175°R or below.

In the case of the nonmetallic materials, a cylindrical tube section was chosen as the specimen configuration because the shape and method of laying up the composite materials could influence their thermal conductivity. Therefore, these specimens were fabricated in a manner similar to, and in the approximate size of, actual structural support members.

A schematic description of the thermal conductivity test apparatus is shown in Figure IV-5. A liquid hydrogen tank provides the heat sink and reduced temperatures necessary for the test. The measurement assembly is attached below the hydrogen tank and consists of the specimen, upper and lower heaters, and a shroud. The entire assembly is insulated and installed in a vacuum chamber. The test is conducted by applying power to the lower heater and measuring the temperatures of each end of the specimen. An upper heater and a thermal resistance are installed between the shroud and the hydrogen tank. This arrangement permits the test section temperature to be raised to a value above that of the hydrogen tank with application of power to the upper heater. The boiloff rate and the power to the upper heater are not parameters required to determine the thermal conductivity of the specimen. The shroud is thermally well connected to the upper mounting plate, and the entire enclosure operates within a few degrees of the upper surface temperature. The specimen is insulated; the insulation is in a thermal environment approximating the temperature of the cold end of the specimen.

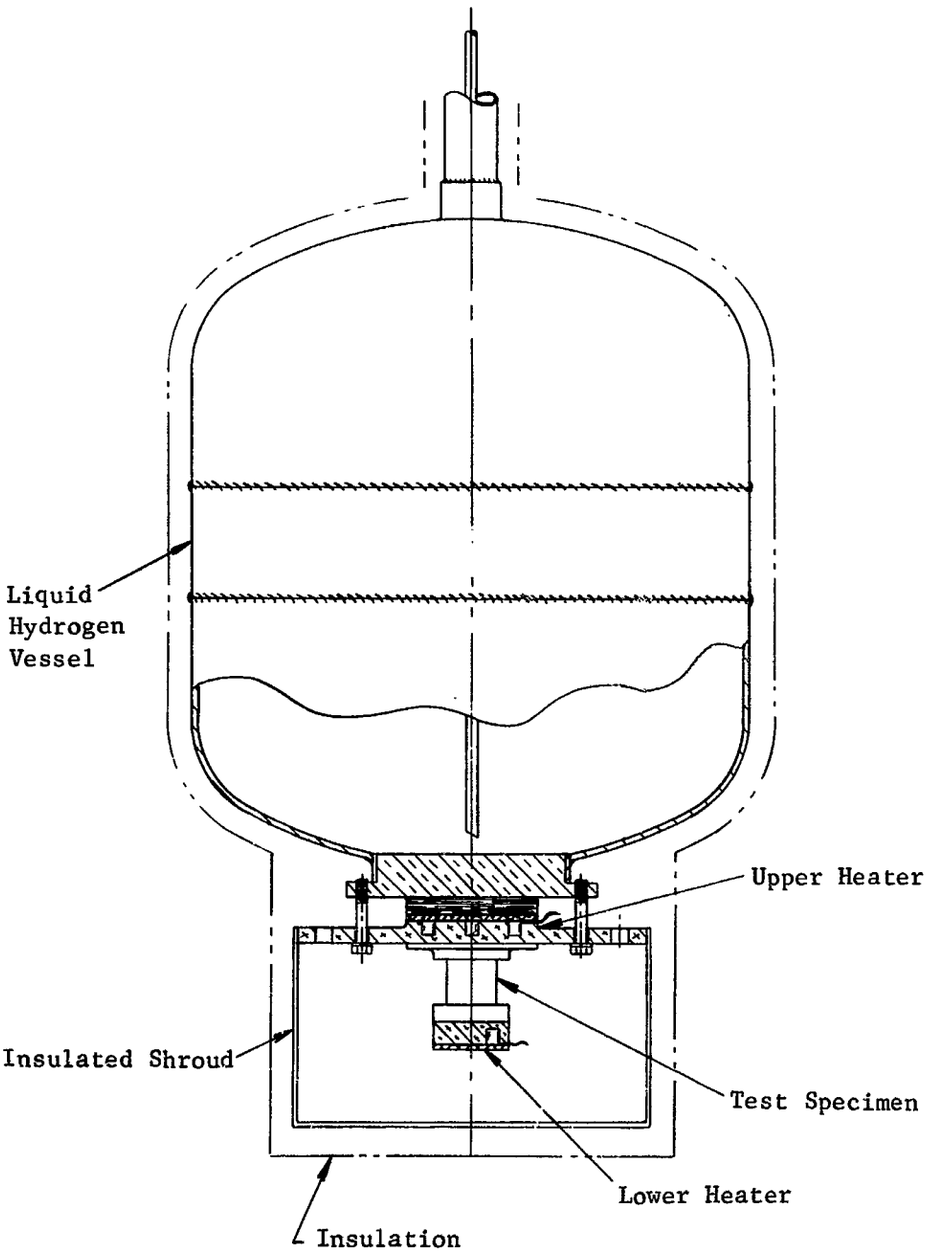

Figure IV-5 Thermal Conductivity Test Apparatus for Nonmetallic Composite Tube Specimens, Schematic Diagram

Instrumentation consists of chromel constantan thermocouples to measure the specimen end fitting temperatures and voltage, and current measurements to determine the power to the lower heater. In the first checkout test, a number of thermocouples were installed on the shroud and hydrogen tank, and additional thermocouples and resistance thermometers were installed on the specimen end fittings. It was found that two thermocouples at each end of the specimen were adequate as they closely followed each other and the resistance thermometers. Test data were recorded on strip chart recorders and/or logged manually from digital voltmeter readings.

The assembly and installation of the test specimen is illustrated schematically in Figure IV-6. Aluminum rings, machined to provide an interference fit with the inside of the specimen, are first shrink-fitted into each end of the specimen (Figure IV-7). These rings are 0.125-in. in length and 0.125-in. in wall thickness, and serve to provide thermal contact with the inside of the specimen. The specimen, with rings in place, is bonded into the upper end piece that is made of aluminum, and is in the form of a flange for attachment to the upper mounting plate. Tolerances are controlled so that the inner ring and that part of the end piece which fits over the specimen align within 0.005 in., to provide thermal contact over a fixed length of the specimen. The active length of the specimen is the distance between the metal end pieces.

The specimen is internally insulated with alternate discs of aluminized mylar and nylon netting. Ventilation is provided through a 0.0625-in. hole drilled in the lower end fitting. The lower fitting is then bonded to the specimen with the internal ring in place. A high thermal conductivity epoxy, Delta Bond 152, is used in the assembly of the specimen. While high for epoxy, the thermal conductivity of the bonding material is little higher than that of the specimens (if not lower). However, effects of this thermal resistance are kept to a negligible value by maintaining small clearances on the mating pieces, so that the ratio of the area of the epoxy to its thermal path length is very great. The lower heater, consisting of a pair of electrical resistors bonded to the lower fitting, and the thermocouples are now installed.

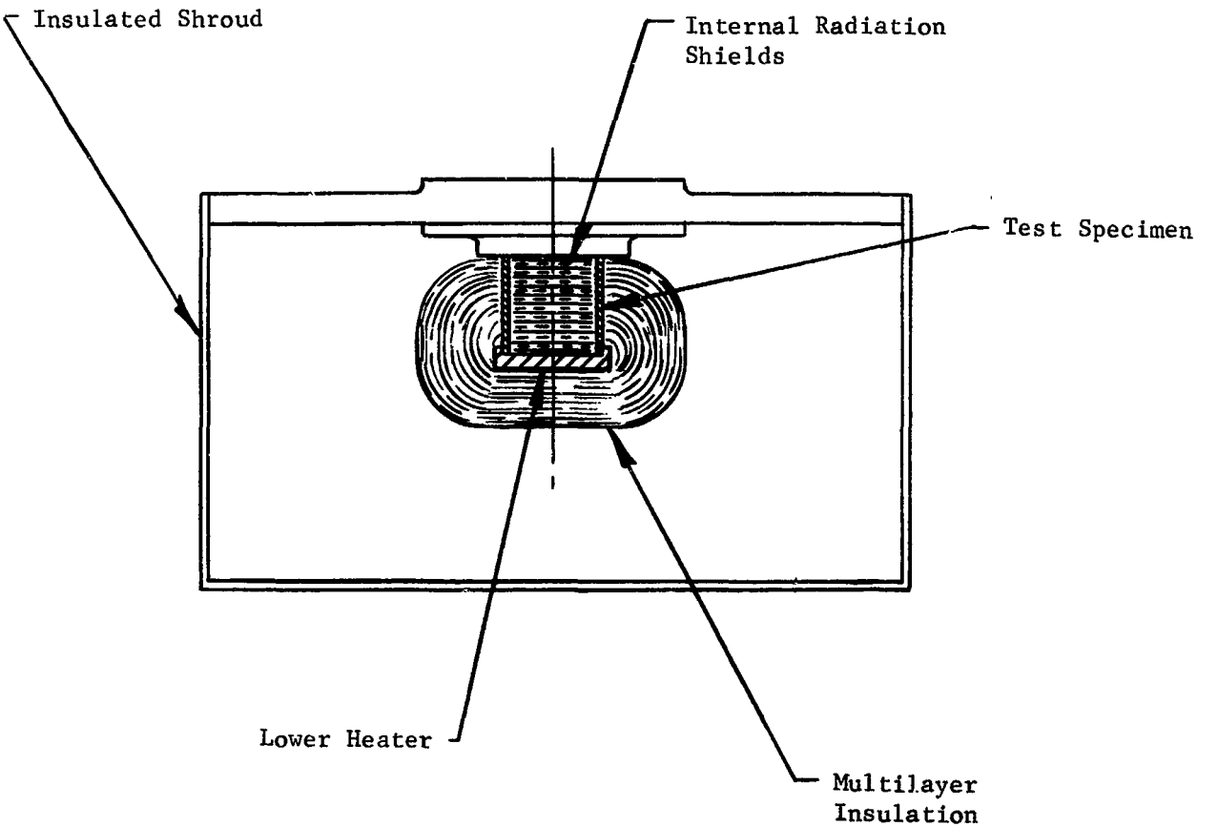

Figure IV-6 Thermal Conductivity Test Specimen Installation, Schematic Diagram

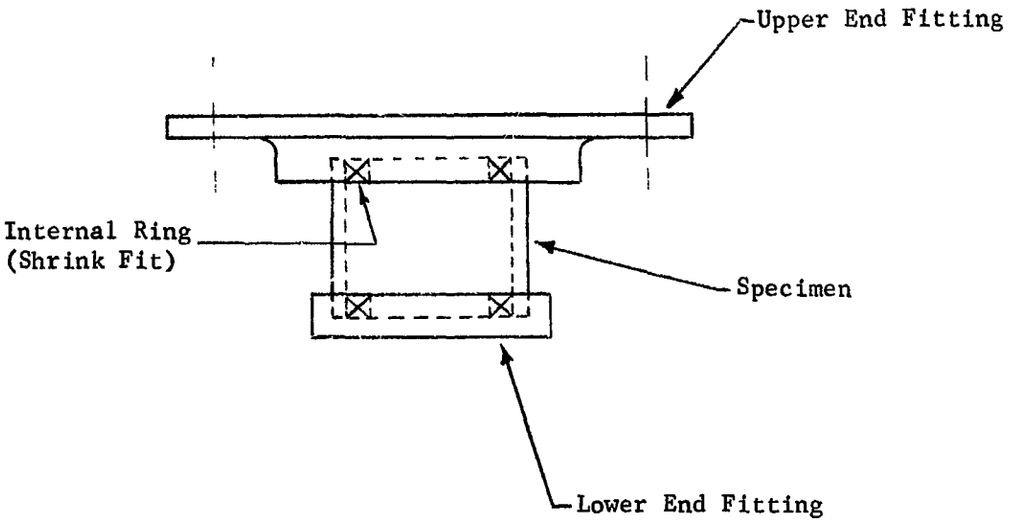

Figure IV-7 Specimen Assembly Details

Next the specimen is externally insulated. As shown in Figure IV-6, individual insulation layers are formed so as to make concentric bags around the specimen and lower heater. This is accomplished by first cutting squares of adequate size of aluminized mylar and nylon netting and perforating each with a hole of the same diameter as the outside of the tube specimen. A short radial cut from the hole is made in each foil and spacer, to permit assembly over the tube. All layers of the insulation are then assembled flat over the specimen with each layer of mylar separated by two spacers. The foils are rotated so that the radial cuts are not aligned. The cuts are repaired with mylar tape as the foils are properly positioned. Starting from the lower end, each layer is formed so as to enclose the heater. Excess material is trimmed and the closure is secured with mylar tape. The instrumentation and heater lead wires, which must be folded through the insulation, are not shown in the schematic. This is done in such a manner that at least 1 ft of each wire is enclosed in the insulation. A typical specimen after insulation is shown in Figure IV-8. The shroud is then installed and insulated as shown in Figures IV-9 and IV-10. Finally, the entire assembly is installed in the vacuum chamber.

Figure IV-8 Composite Material Thermal Conductivity Specimen After Insulation

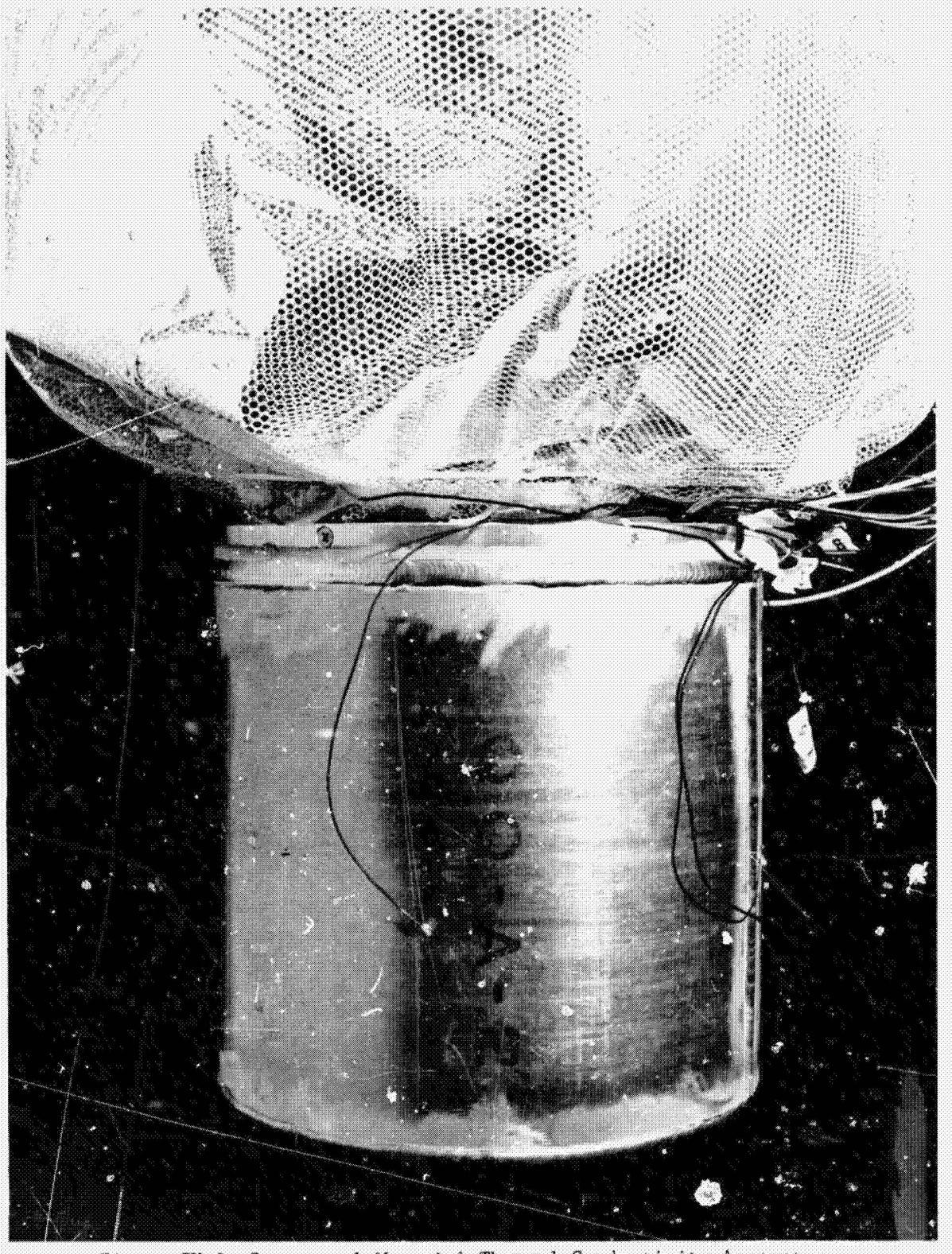

Figure IV-9 Structural Material Thermal Conductivity Apparatus with Shroud in Place

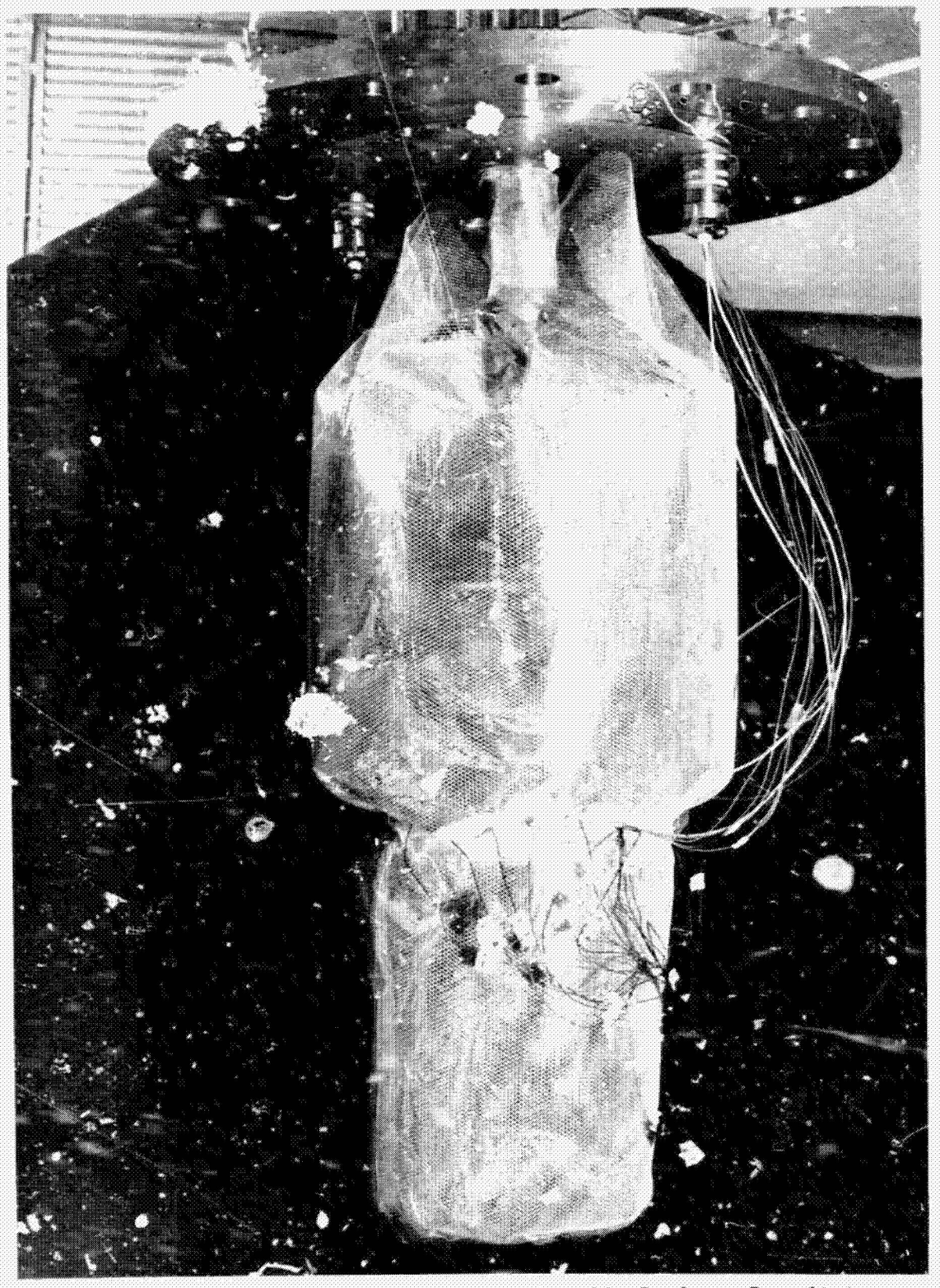

Figure IV-10 S.. .tural Materia' Test Assembly Ready to Install in Vacuum Chamber

For the stacked washer and self-aligning bearing tests, a dual bellows force mechanism is added to the test assembly as shown schematically in Figure IV-11. Determination of the thermal conduction of the component is again accomplished by measurement of the temperatures at each end of the component and the electrical power applied to the lower heater. The flange below the lower heater is connected to the bellows assembly by an S-glass epoxy tube, to minimize the loss of heat to the bellows unit. In principle, this test configuration is insulated in the same manner as described above for the tube specimens. In practice, however, the insulation of these specimens was much more difficult to accomplish and the thermal leakage through the insulation to the surroundings was more difficult to estimate. Figure IV-12 shows the force mechanism with the stacked washer specimen installed, prior to insulation. A force was applied to the specimen by pressurizing one or the other of the bellows, depending on whether a tension or compression loading was desired. The other bellows, exposed to local atmospheric pressure, was purged with helium to prevent condensation of air in the bellows.

The structural materials and components tests were conducted on a three-shift basis because each test ran at least 48 hours. Using the above described equipment, the tests were accomplished in the following manner. After installation in the vacuum chamber and pump down to a pressure of 5×10^{-5} mm hg, or below, the hydrogen tank was purged with helium and then filled with liquid hydrogen. No power was applied to either heater until all parts of the system had come to their equilibrium temperatures. At this point, data recording and/or logging was begun. To obtain the lowest temperature data point, a power was established and then applied to the lower heater to result in an expected temperature difference of 10 to 20°R across the specimen. This power level was maintained until the entire system again stabilized. A second power setting was then based on the actual temperature difference attained during the first test. After obtaining data with two or three power levels on the lower heater and with the upper heater unpowered so as to maintain a minimum cold end temperature, power was applied to the upper heater to raise the cold end temperature. After several steady-state tests had been completed with the cold end temperature below 100°R, the hydrogen was transferred out of the tank. The rate of temperature rise of the cold end of the specimen was then regulated by adjustment of the power applied to the upper heater. Since the natural warmup time of the system was on the order of 5 to 7 days, almost any desired temperature rise rate could be programed.

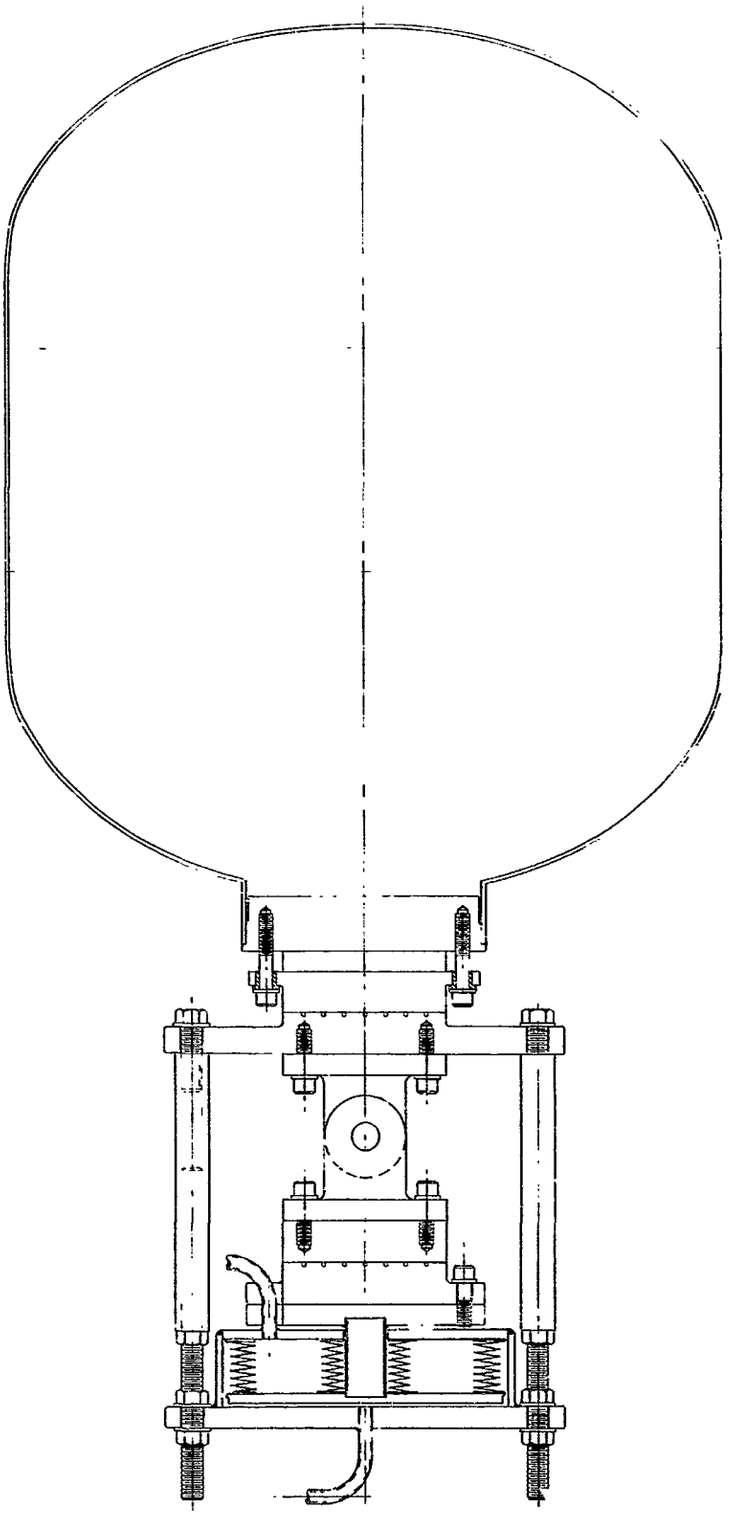

Figure IV-11 Structural Component Test Configuration with Force Mechanism, Schematic Diagram

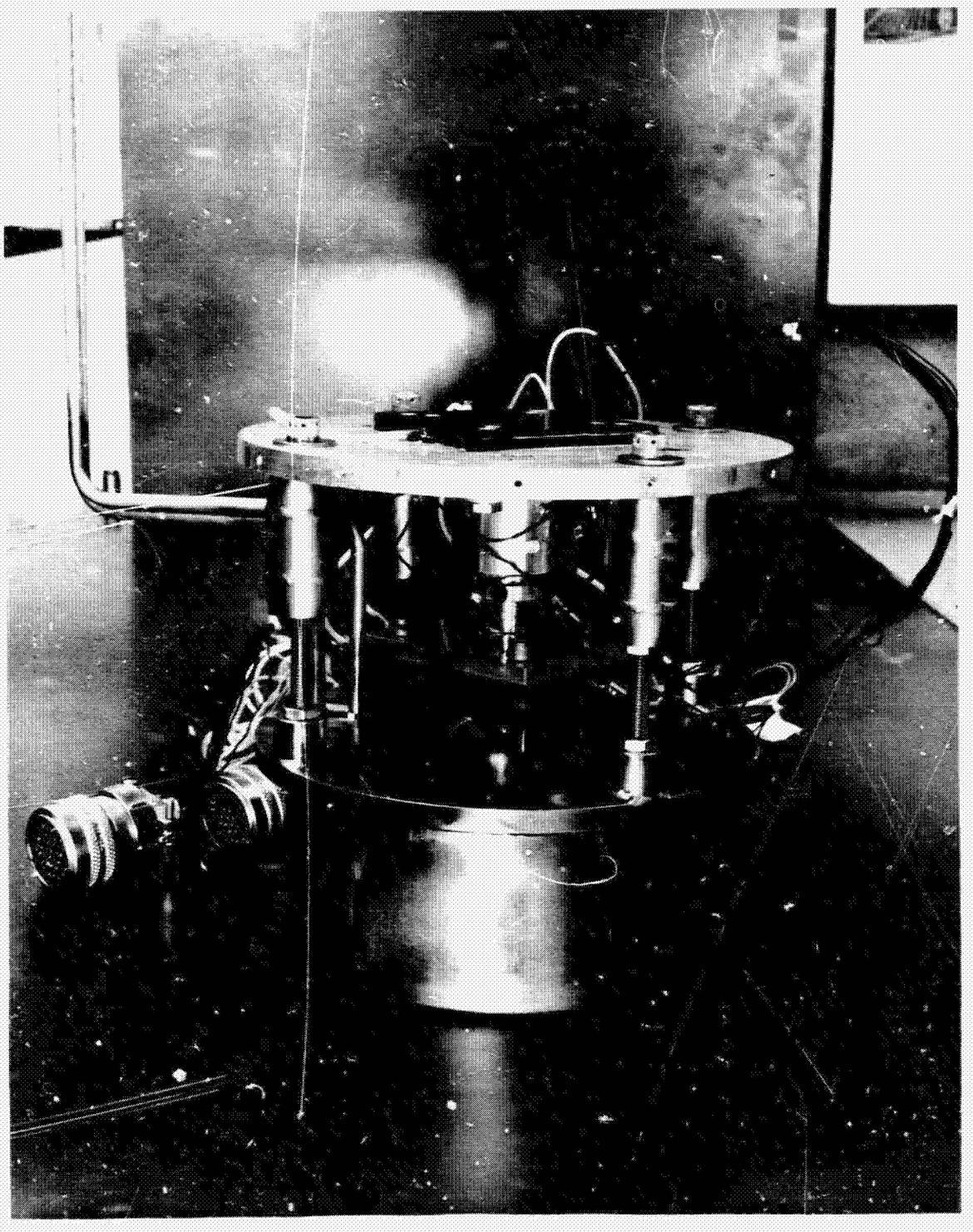

Figure IV-12 Force Mechanism with Stacked Washer Specimen Installed

From this point, a test plan was followed that was designed to obtain the maximum data coverage possible in the time available before weekend shutdown or programed termination of the test. Data was acquired under transient and near steady-state conditions that could be obtained by careful regulation of power input. The temperature difference across the specimen was also varied during transient data recording and between steady-state data points.

Data Reduction - For those test data obtained under steady-state conditions, i.e., steady power input and constant end temperatures, direct computation of the thermal conductivity of the specimens could be made without consideration of the energy required to change the temperature of the various thermal masses associated with the hardware. Some of the data, however, were recorded during the transition from one point to another. Reduction of the composite tube specimen data was accomplished by a computer program that included correction for losses through the insulation installed around the specimen and through the power and instrumentation lead wires. In addition, the program provided compensation for the energy absorbed or given up by the thermal masses. The effective thermal mass consisted primarily of the aluminum end piece, but also included the insulation, a portion of the lead wires, a portion of the sample, etc. Therefore, the actual thermal mass used was varied during repeated iterations. Its initial value was taken as that of the aluminum end piece, and it was increased upward by steps. The thermal capacity of this mass was considered to have the characteristics of aluminum. Thus, by plotting the apparent thermal conductivity versus temperature for the various trial values of the mass, a family of thermal conductivity versus temperature curves was obtained. That curve which smoothly passed through the steady-state data points was taken as the test result. For incorrect selection of the thermal mass, the curve would deviate above or below such a smooth curve for the transient data points. Because the data obtained from the test was not continuous, a certain amount of scatter occurred. Figure IV-13 is a typical plot obtained from the data reduction program. Because of the scatter and the large number of data points considered, the plots presented for the various specimens represent the best fit and do not show the individual data points obtained.

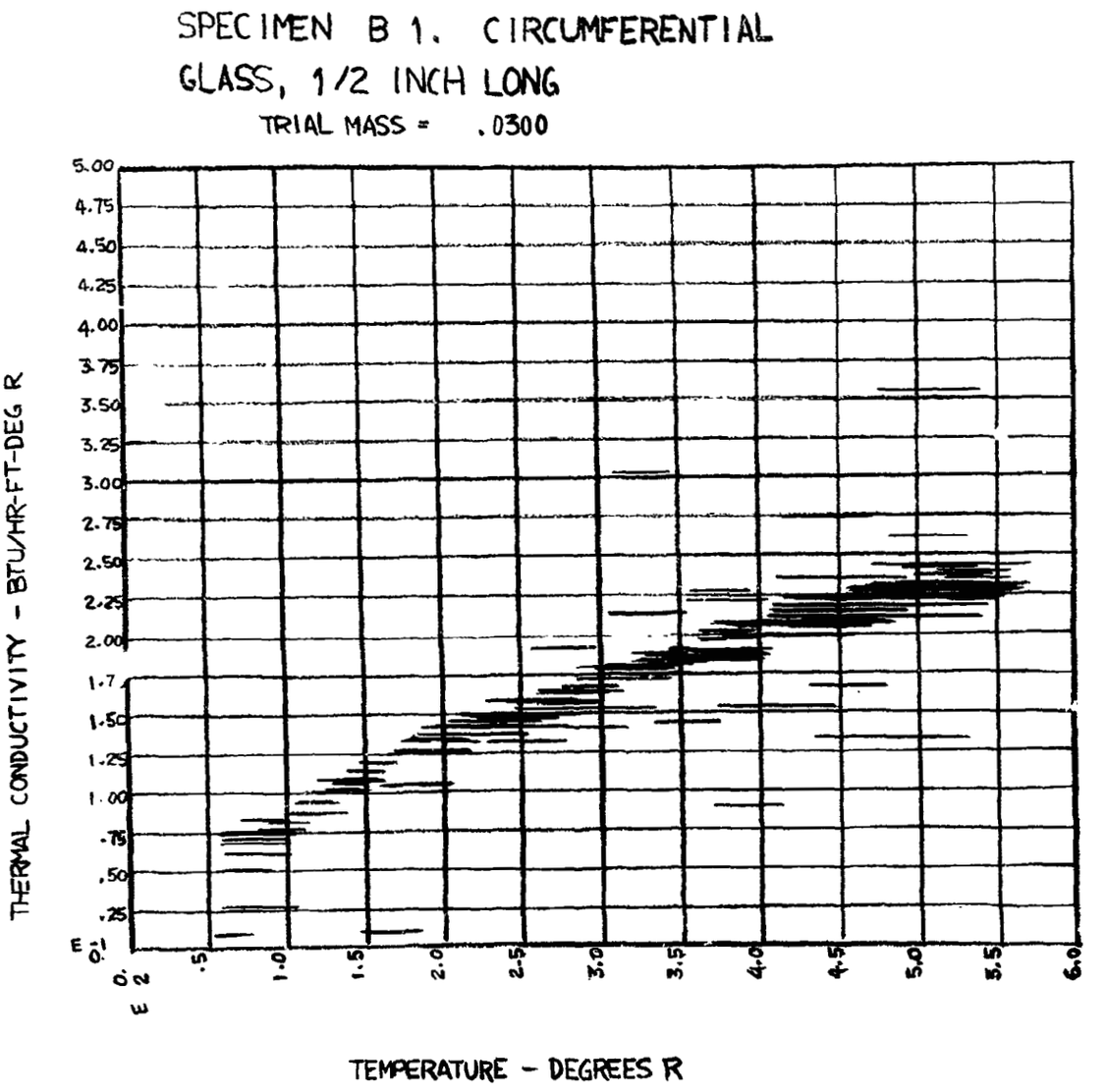

Figure IV-13 Typical Computer Plot for Composite Material Thermal Conductivity Test Data Analysis

Correction for the lead wire conductance and for the insulation heat leakage considered the temperature dependency effect on the conduction of these materials. The input data to represent the physical characteristics of the insulation and lead wire could not be highly accurate, but values were input based on approximate measured geometries and dimensions. In the test design, an effort was made to keep the extraneous heat fluxes to a small value, hopefully below 10% to minimize their effects. In reviewing the actual data reduction, the extraneous heat leak appears to have varied from below 5% to as much as 20% of the total heat flux through the specimen. This value is dependent on the thermal conductivity of the specimen, the operating temperature, and temperature difference across the specimen. In planning the transient phases of the tests, the temperature rise rate and temperature difference across the specimen were held to values for which the estimated effect of heat storage in the materials would not exceed 25% of the heat flux through the specimen.

If the data reduction technique was successful in reducing these error contributions each by at least two thirds, then their net contributions would be no more than 6.7% and 8.3%, respectively. Considering these independent error contributions along with estimated inaccuracies in temperature, power, and physical measurements of the specimen, an overall accuracy estimate of 10% to 12% can be made using the normal root-mean-square error analysis technique.

A specimen of a known thermal conductivity was not used for calibrating the apparatus and procedure. However, as a check on the accuracy of this thermal conductivity device, two S-glass epoxy specimens were cut from the same tube (specimens 2 and 3) in an effective length of 1-in. and 0.5 in., respectively. Since the heat flux under given conditions for the 0.5-in. specimen would be twice that for the 1-in. specimen, comparison of the two results provides a useful check on overall accuracy. Results for the two tests were within 3% at 100°R and 500°R.

Test data for the structural components, the stacked washer, and spherical self-aligning bearing specimens, were analyzed in the same manner. Corrections to account for the fiberglass tube between the specimen and the bellows assembly, and for areas which could not be fully insulated, were added to the thermal correction network. In addition to these extraneous heat fluxes, thermal masses were much greater. Although much of the test data, when reduced, appears to be consistent and realistic, some of the data appeared erratic. Most of the test data presented is believed to be of sufficient accuracy to be useful, but no estimate for the limit of inaccuracy is made.

Test Results - A description of the specimens which were tested and the test results for each is presented in the following paragraphs.

Several of the composite material tube specimens are shown in Figure IV-14. Figure IV-15 shows the method of assembly of the tubes and end fittings. The polaris epoxy system, as described in Chapter III, Section G, was used for all of the composite material specimens. Physical details and the reference to the proper thermal conductivity versus temperature graphs are given in Table IV-1. Attempts to produce a circumferentially wound boron epoxy specimen were not successful because of breakage of the fiber when wound on a 1-in. diameter mandrel.

Table IV-1 Physical Properties of Test Specimens

Specimen	Fiber Material	Fiber Orientation	Inside Diameter (in.)	Outside Diameter (in.)	Effective Length (in.)	Fiber by Weight (%)	Fiber by Volume (%)	Thermal Conductivity Curve (Figure No.)
1	S-glass	Circumferential	1.002	1.140	0.503	81.3	63.4	IV-16A
2	S-glass	Longitudinal	1.000	1.132	0.500	79.4	62.2	IV-16B
3	S-glass	Longitudinal	1.000	1.132	1.000	79.4	62.2	IV-16
4	Boron (0.004-in. dia)	Longitudinal	1.005	1.143	0.540	67.5	49.2	IV-17
5	Graphite (Thornel-50)	Circumferential	1.005	1.1137	0.635	60 (estimated)	53.4 (estimated)	IV-18
6	Graphite (Thornel-50)	Longitudinal	0.998	1.114	1.000	60 (estimated)	53.4 (estimated)	IV-19

Figure IV-20 presents a comparison of the thermal characteristics of the above specimens, with the exception of the longitudinally oriented graphite epoxy.

The self-aligning spherical bearing specimen is shown before assembly in Figure IV-21. The bearing was manufactured by Kahr Bearing Corporation under part number HSR-4-7. It is of stainless steel construction and has an outside diameter of 0.6562, a 0.25-in. bore and 0.5-in. ball diameter. The test assembly consists of the bearing, a steel bolt and nut, and aluminum end fittings. Because of the high thermal conductivity of the aluminum, the measured conductance was essentially that of the bolt and bearing combination. Catalog data recommends a bore of $^{+.000}_{-.0005}$ for the mating part at room temperature. The aluminum housing was bored to provide the recommended fit at 100°R, resulting in a clearance of about 0.001-in. at room temperature. Results of the thermal conduction tests for this specimen are presented in Figure IV-22.

Figure IV-14 Composite Material Tube Section Thermal Conductivity Specimens

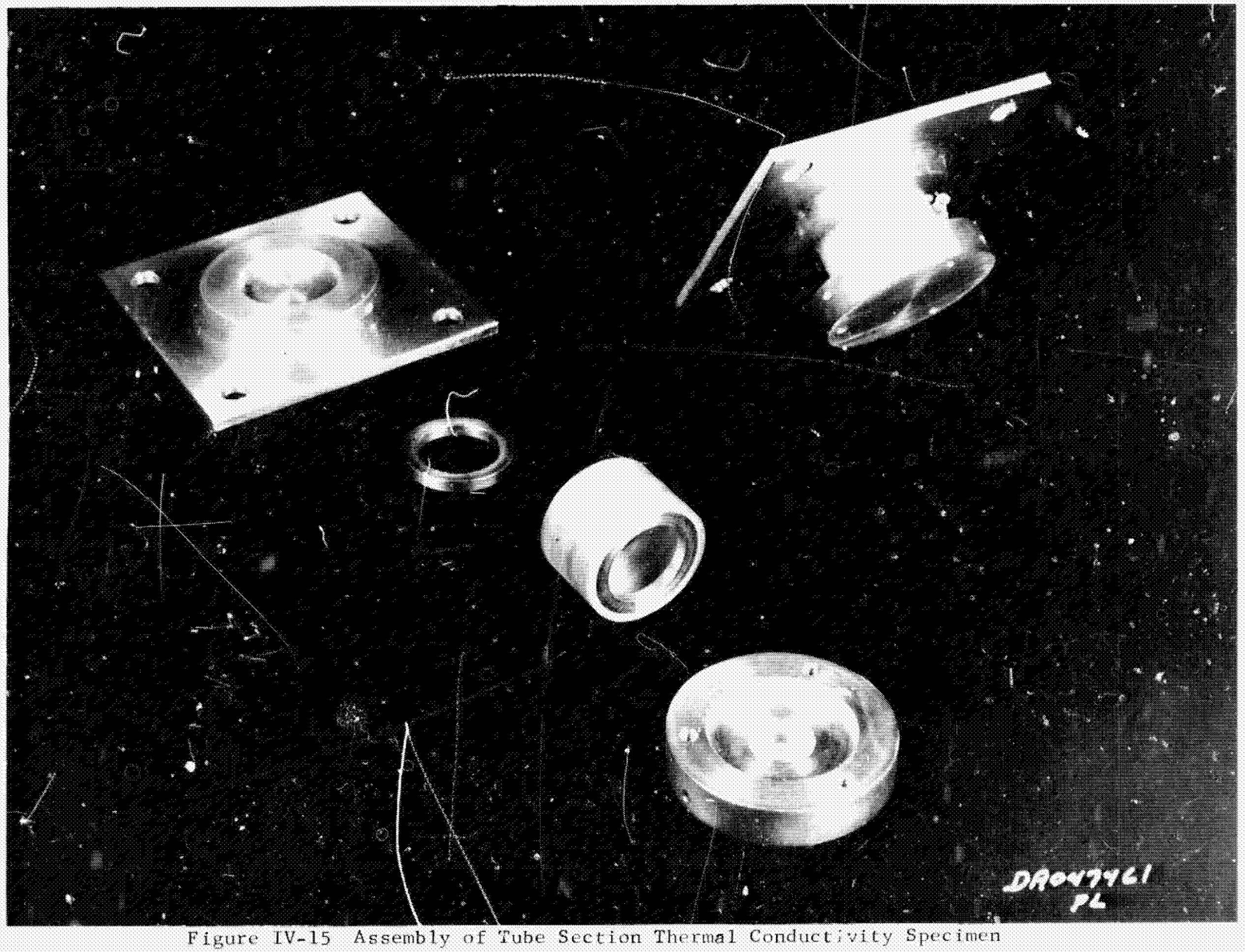

Figure IV-15 Assembly of Tube Section Thermal Conductivity Specimen

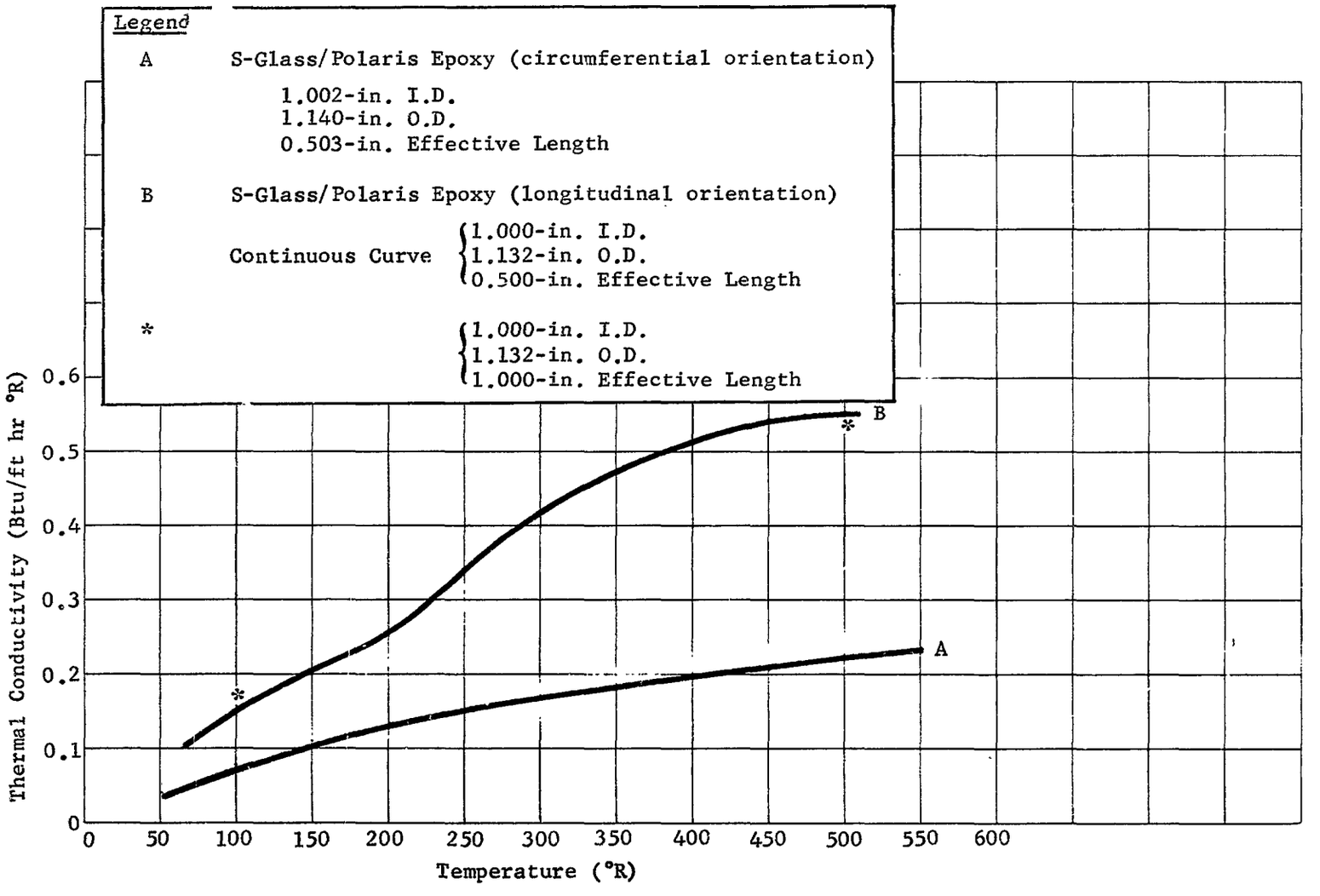

Figure IV-16 Thermal Conductivity vs Temperature for S-Glass Epoxy Composite Cylinders

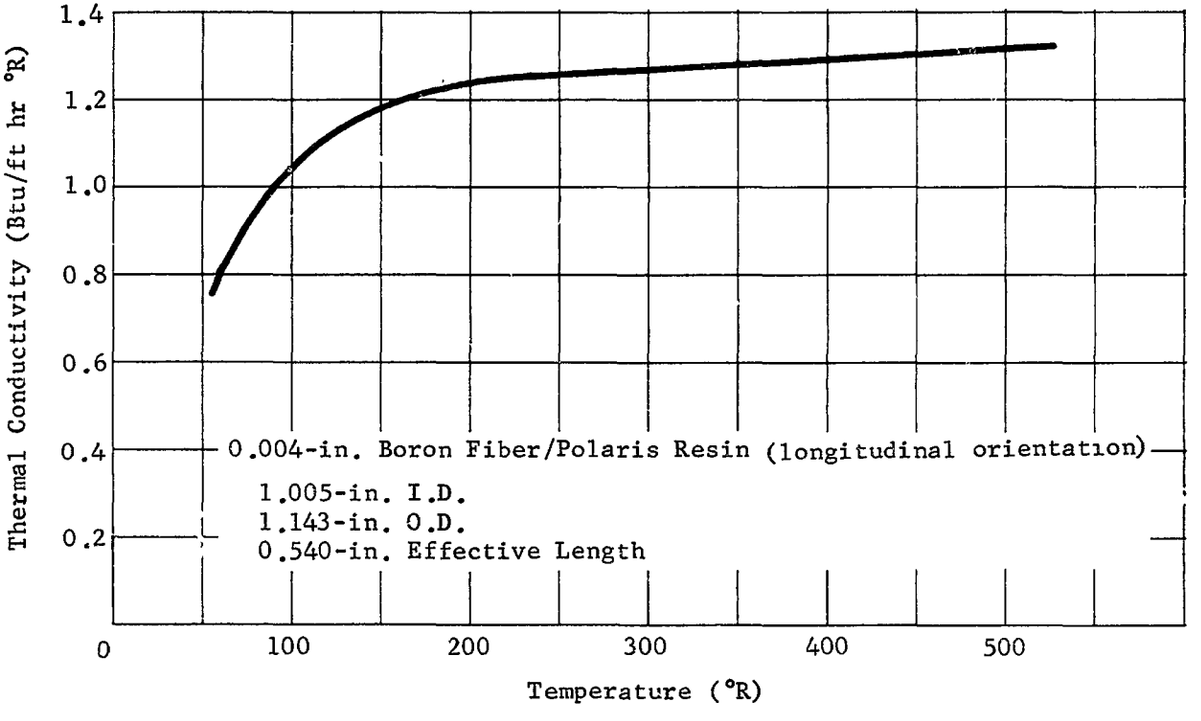

Figure IV-17 Thermal Conductivity vs Temperature for Boron Epoxy Composite Cylinder

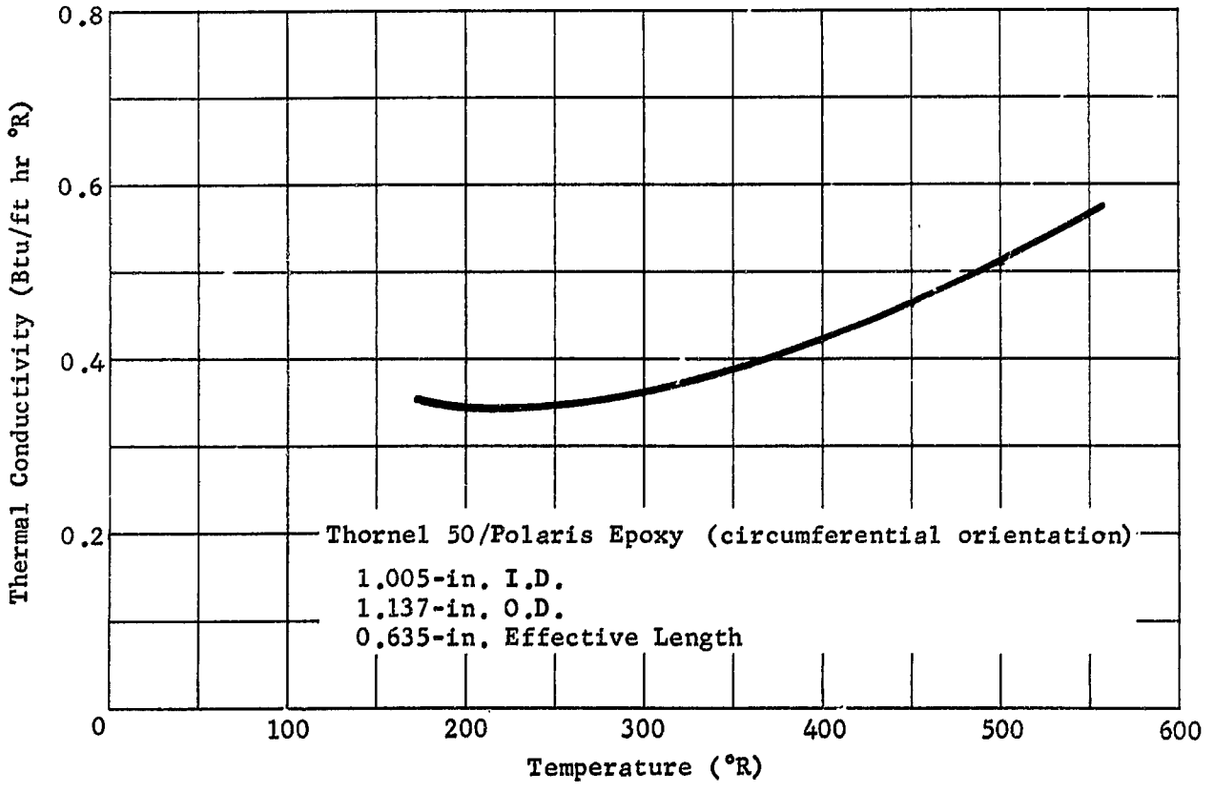

Figure IV-18 Thermal Conductivity vs Temperature for Circumferential Fiber Graphite Epoxy Composite Cylinder

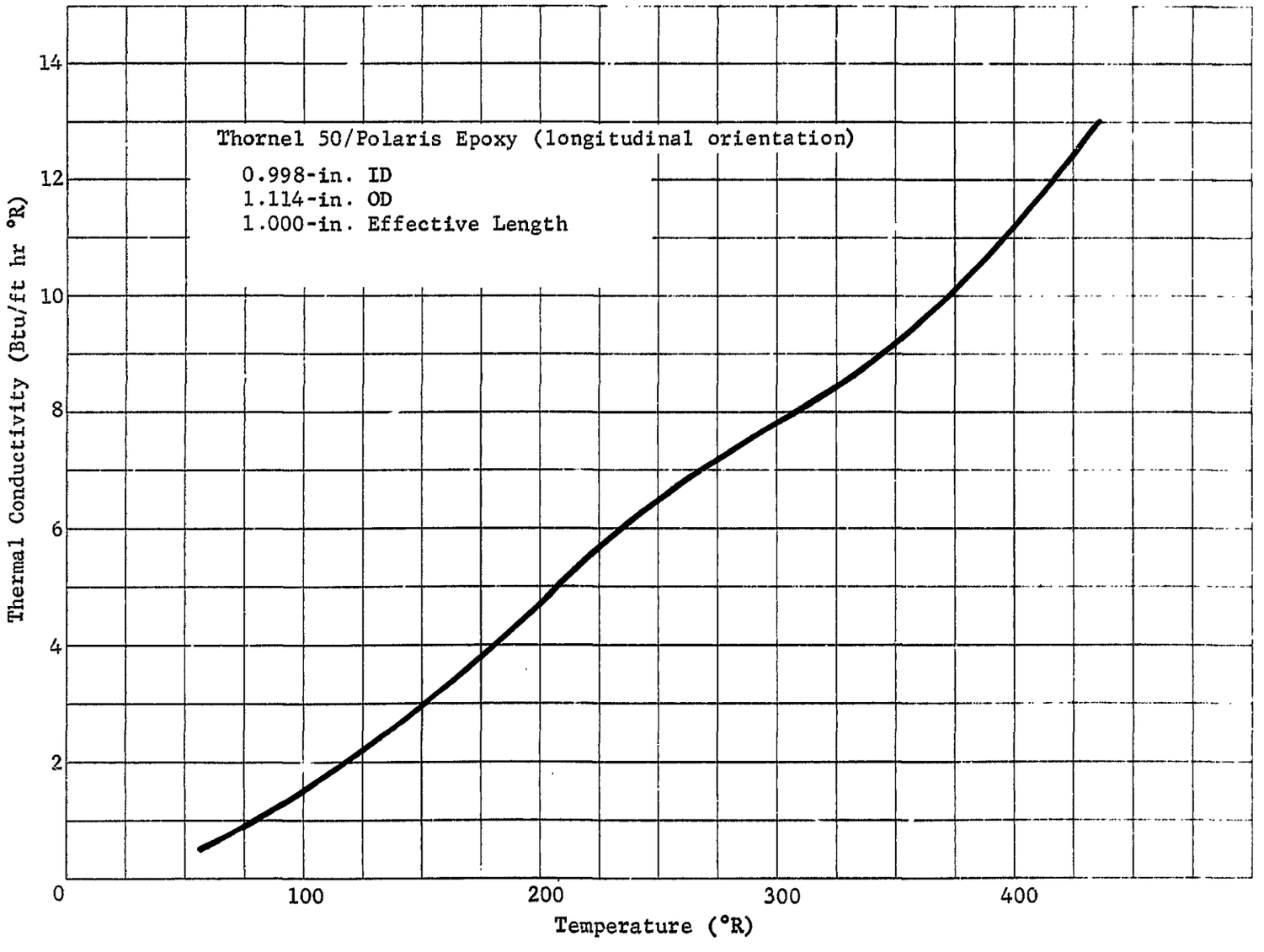

Figure IV-19 Thermal Conductivity vs Temperature for Longitudinal Fiber Graphite Epoxy Composite Cylinder

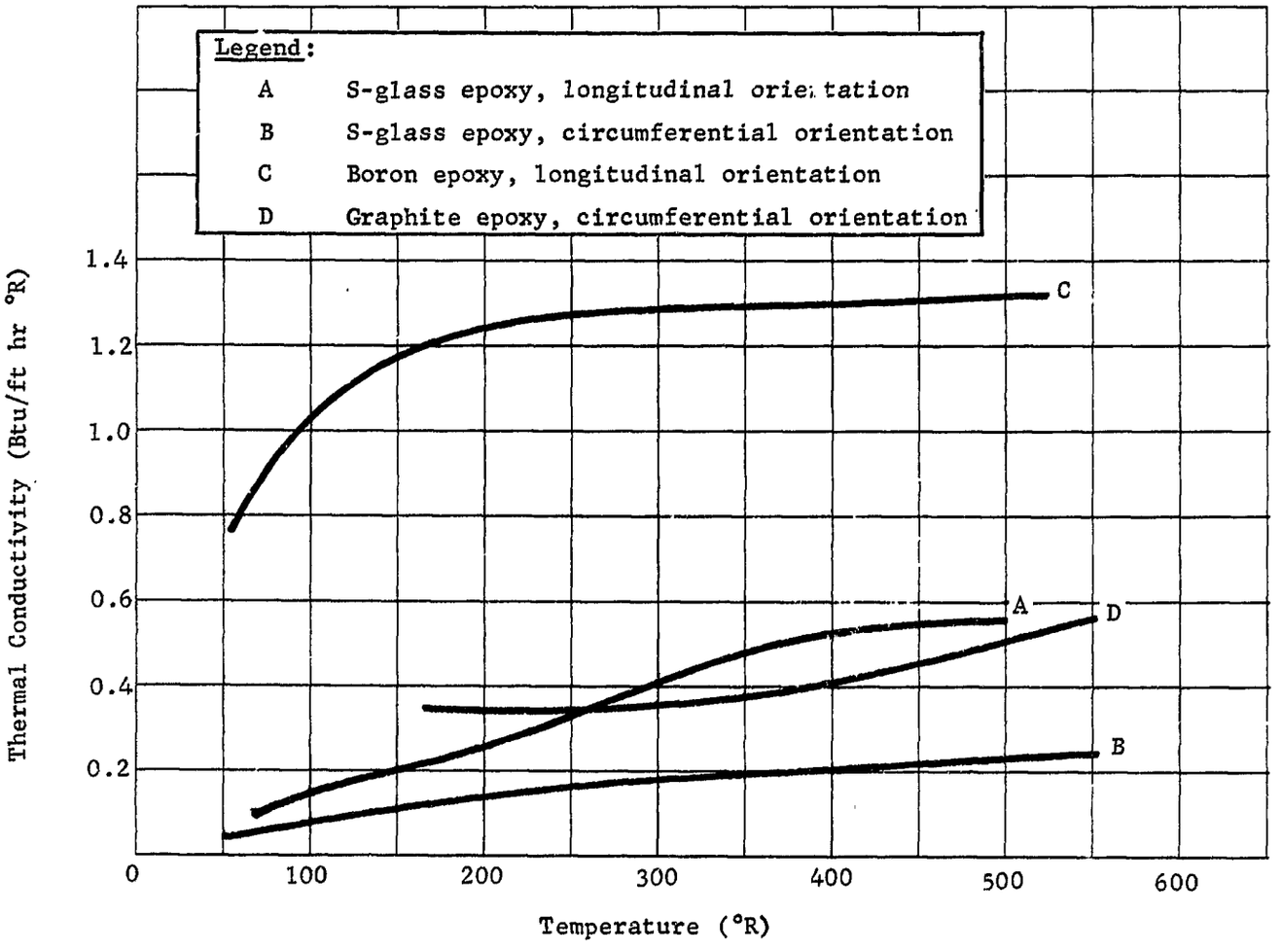

Figure IV-20 Comparison of Thermal Conductivity vs Temperature for Several Nonmetallic Composite Materials

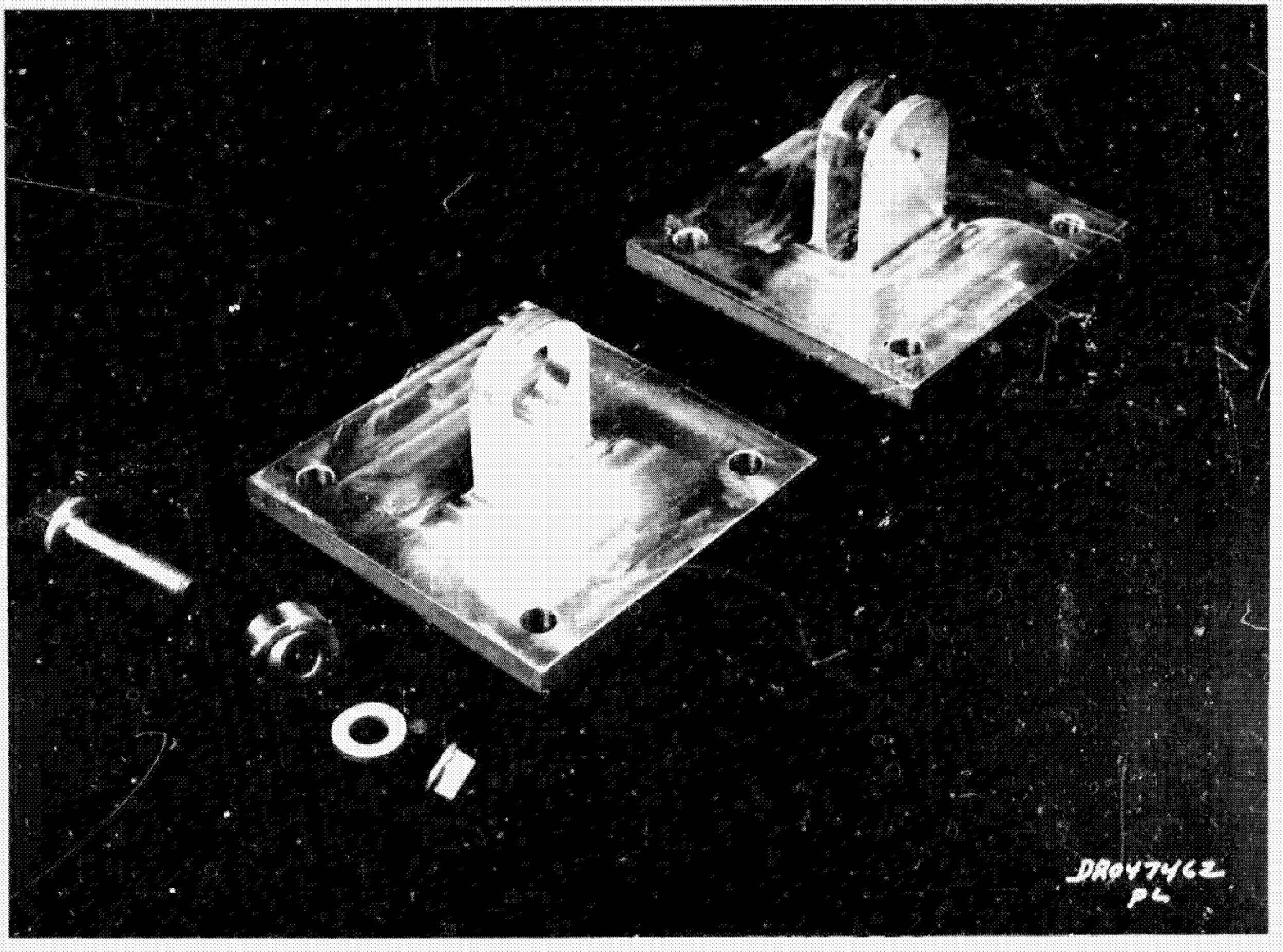

Figure IV-21 Spherical Bearing Thermal Contact Resistance Specimen Before Assembly

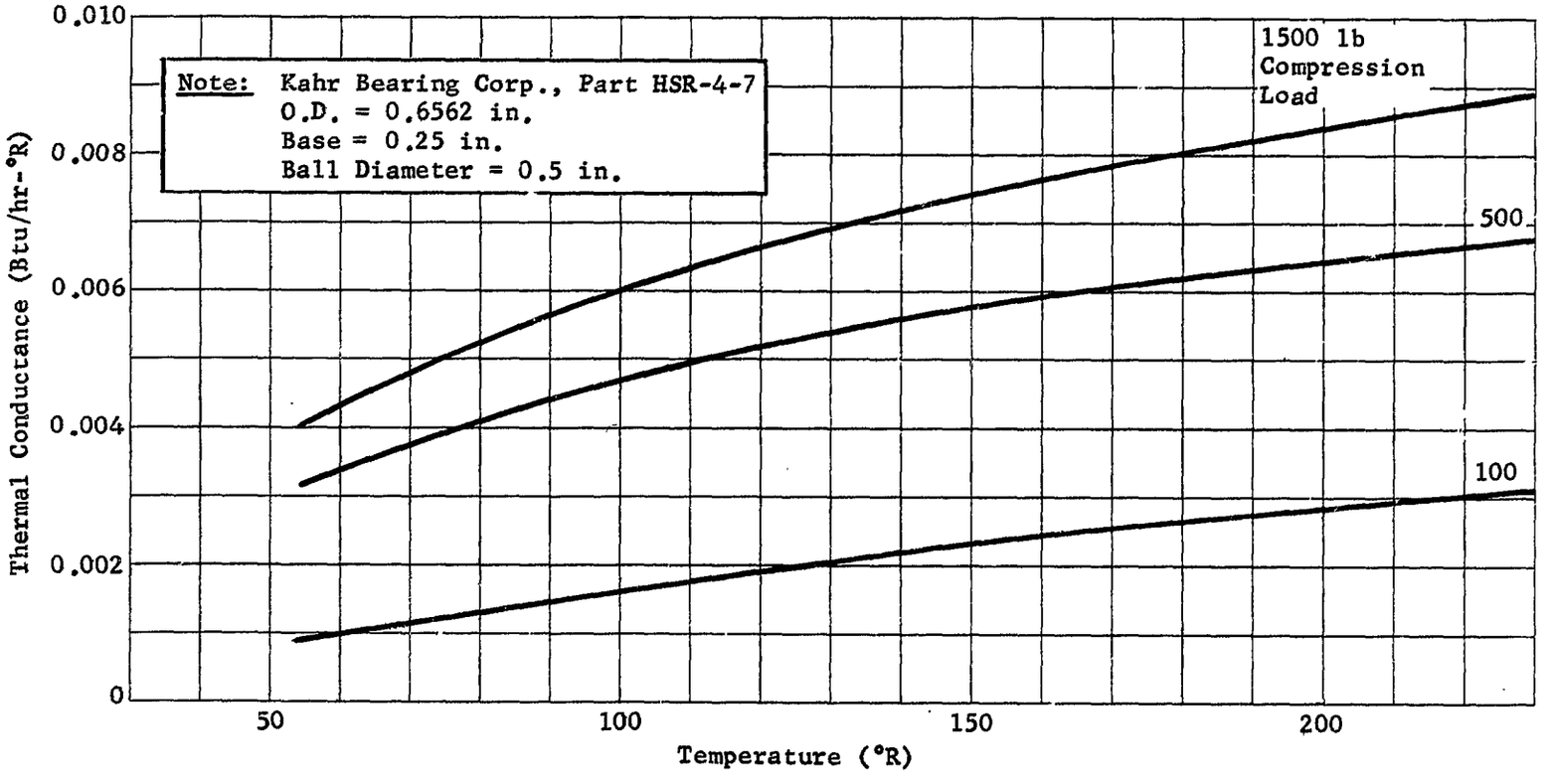

Figure IV-22 Thermal Conductance vs Temperature at Several Bearing Loads for a Spherical Bearing

The stacked washer test specimen is shown partially assembled in Figure IV-23. This specimen includes 300 0.004-in. stainless steel washers, 0.750-in. O.D. x 0.453-in. I.D. Washers (150) are assembled on each side of the intermediate fitting, as shown in Figure IV-24. Tests were conducted with various applied forces for two preload conditions on the washers. The first test was with essentially no preload. This was accomplished by first applying a torque of 100 in.-lbs or more to the nut, and then backing the nut off several times. The final backoff was to the point where negligible torque, less than 1 in.-lb, was observed. Test results for this preload condition are presented in Figure IV-25. For the second load condition, a torque of 50 in.-lb was applied to the nut. The 0.4375-in. 20 UNF nut was of the self-locking type, but was retapped to turn freely on the threaded stem. Results for this test condition are given in Figure IV-26.

The raw test data for these specimens was processed in the same manner as was that for the composite material tests. Again, the curves presented represent the best interpretation of a large number of somewhat scattered data points. As previously pointed out, corrections for extraneous heat leak and thermal capacity effects were more severe for these tests. In addition, there is some discrepancy of data for the lower applied force conditions. This was most likely caused by inaccuracies in the force determination, occurring as a result of inaccurate determination of effective bellows areas and differential thermal contraction effects.

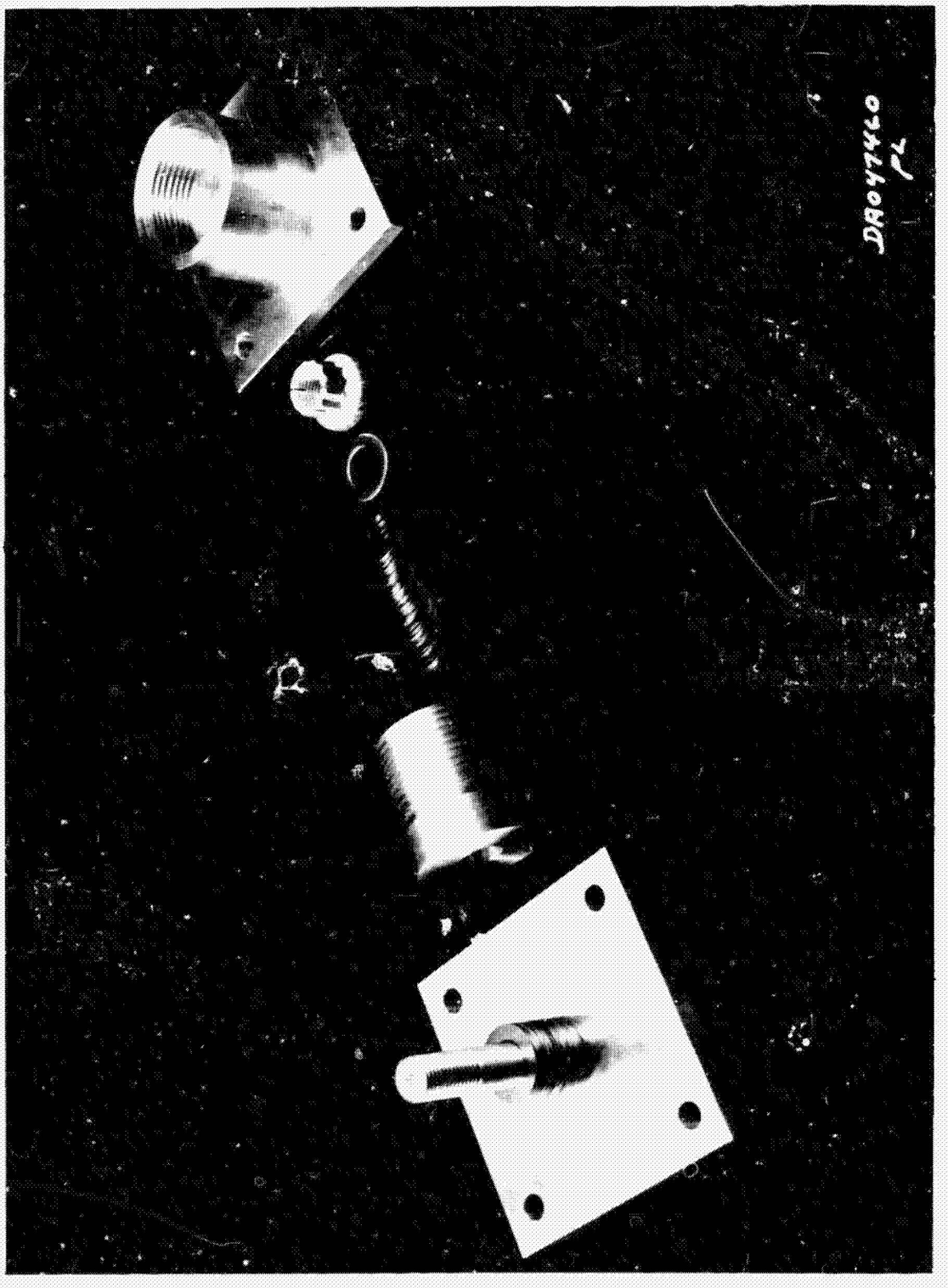

Figure IV-23 Assembly of Stacked Washer Thermal Contact Resistance Specimen

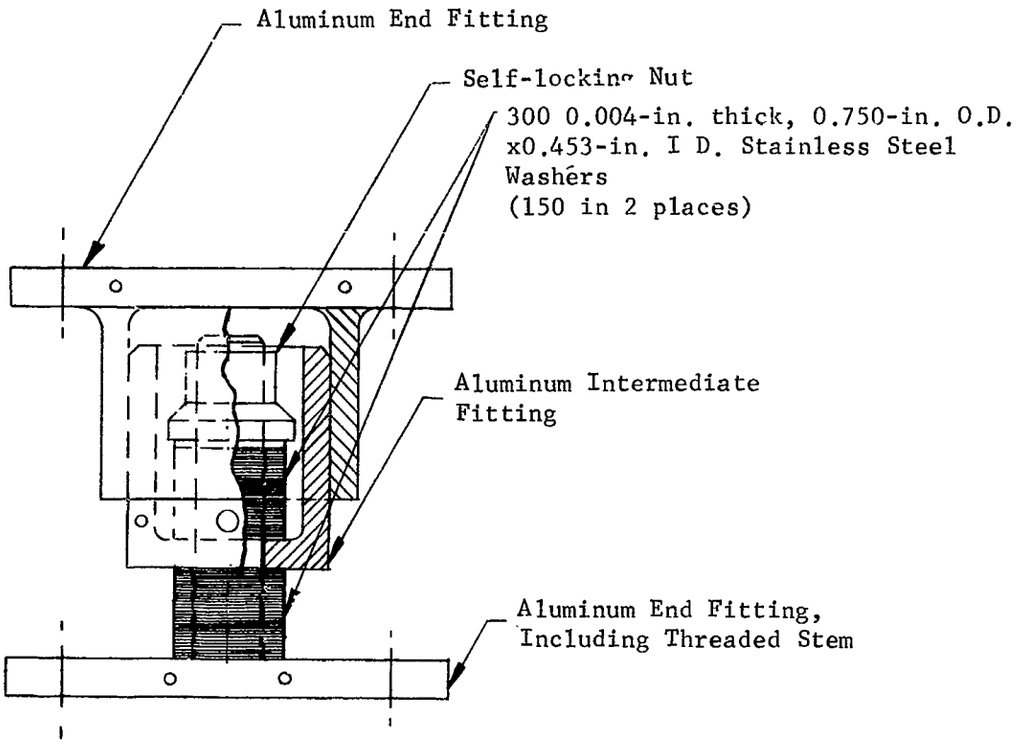

Figure IV-24 Stacked Washer Thermal Resistance Test Specimen

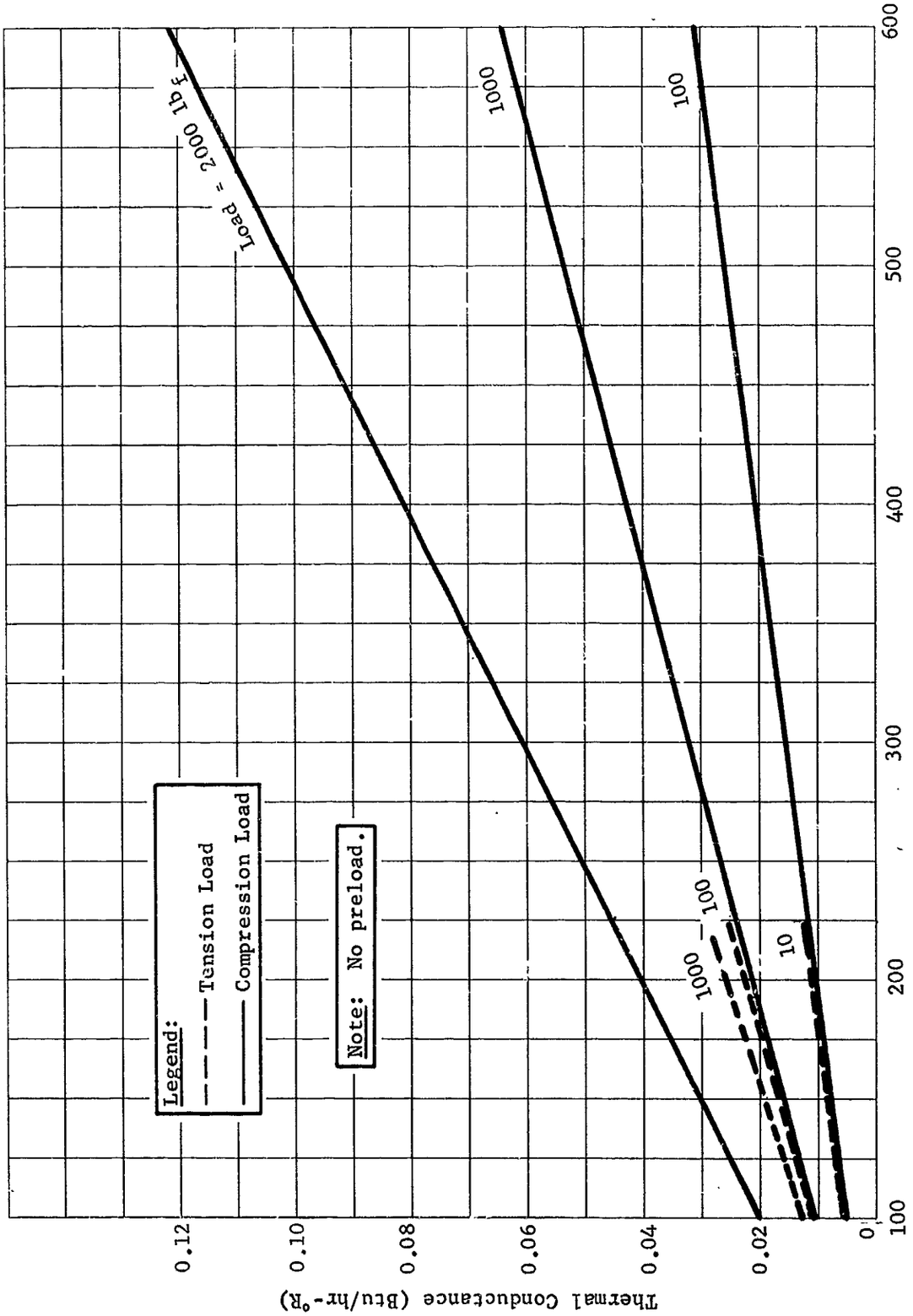

Figure IV-25 Thermal Conductance vs Temperature at Several Loads for Stacked Washers, No Preload on Washers

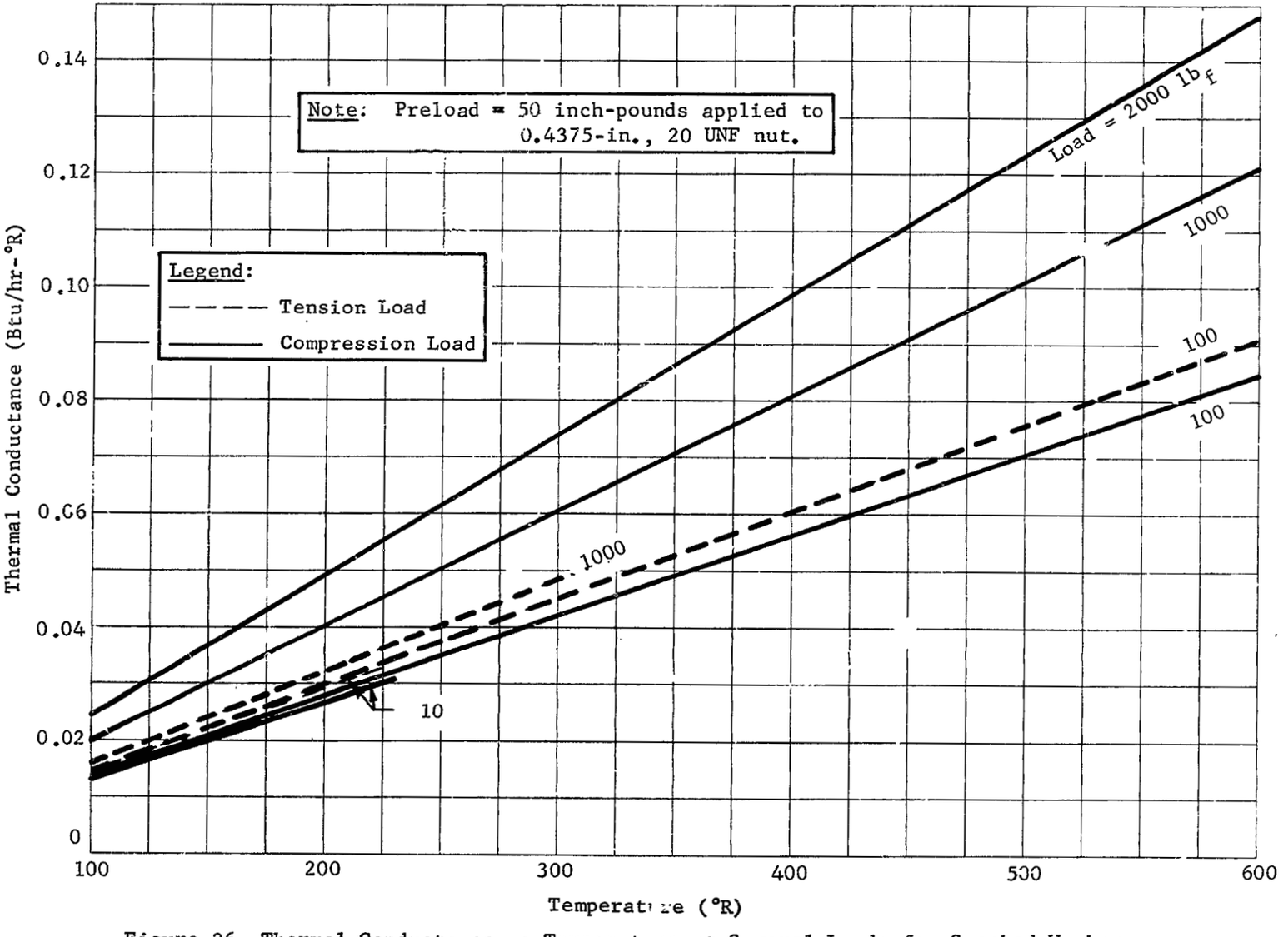

Figure 26 Thermal Conductance vs Temperature at Several Loads for Stacked Washers, 50 in.-lb Preload on Washers

C. INTEGRATED TANK INSULATION SYSTEM TEST

A major objective of this study has been the evaluation of means for utilizing boiloff gas to intercept heat leaking into a hydrogen storage tank, and thereby reduce the boiloff losses. Two of the most significant sources of heat into a typical large scale cryogenic tank are insulation and piping heat fluxes. The problem of utilizing the refrigeration capacity of the vent gas to reduce heat flux from these two sources has been analyzed in detail. The conclusion of the analytical studies is that for an optimized system, up to 50% reduction of boiloff can be achieved.

In particular, it appears attractive to intercept heat in the insulation system for large scale tankage. This can be accomplished by dividing the insulation into two parts -- a tank- and a shroud-mounted blanket. A heat exchanger can be installed on the surface of either of these blankets and physically connected to assure thermal contact. A more attractive approach, in many respects, is to mount the heat exchanger between the blankets with the thermal energy transported accomplished by means of radiation. This approach eliminates the need for physical connection between the insulation and heat exchanger and permits the heat exchanger to be supported in the most convenient manner. The preliminary design analysis previously described indicates that such an approach is feasible for the tankage system considered in this study.

Unfortunately, the thermal design of the radiatively coupled insulation cooling system is dependent on several variables which may be difficult to predict. Of primary inportance are:

1) Actual dependence of insulation conductivity on temperature;
2) Effective emissivity of insulation blanket surfaces, and directional effects;
3) Effective conductance along insulation surfaces, and through annular gap;
4) View factor from neat exchanger element to insulation blanket surface.

Since the uncertainty of these variables results in some uncertainty in the analytical results, it is desirable to obtain experimental data that can be compared with the analytical predictions. Therefore a small scale test program was undertaken to investigate experimentally the cooled insulation concept using radiation coupling with the heat exchanger. In addition, cooling of piping penetrations to the tank was included as part of the total system test.

1. Test Objectives

The objectives of this test program were to:

1) Demonstrate feasibility of using vent gas to effect a substantial reduction in boiloff losses through cooling of piping penetrations, and by use of a radiatively coupled heat exchanger between two tank protection insulation blankets to intercept a part of the heat reaching the tank through the insulation system.

2) Obtain sufficient detailed temperature and boiloff data to permit comparison with analytical predictions, and provide design data and/or insight regarding the important design parameters listed in the previous section;

3) Obtain performance data on the tank insulation system, with heat exchanger system inactive, as a basis for determining improvement realized with the heat interception devices active;

4) Determine general operating characteristics and unforeseen difficulties in application of the cooled insulation technique.

2. Description of Test Apparatus

To satisfy these objectives, a test article was fabricated, using an existing 4-ft diameter by approximately 6-ft long stainless steel hydrogen tank, and 6-ft diameter vacuum chamber. The overall layout of the test setup is shown in Figure IV-27. Basically the equipment consists of a liquid hydrogen tank mounted within a controlled temperature shroud, and insulated with tank and shroud insulation blankets of multilayer insulation. Additional thermal control is achieved through the use of vent gas heat exchangers that intercept heat before it reaches the tank.

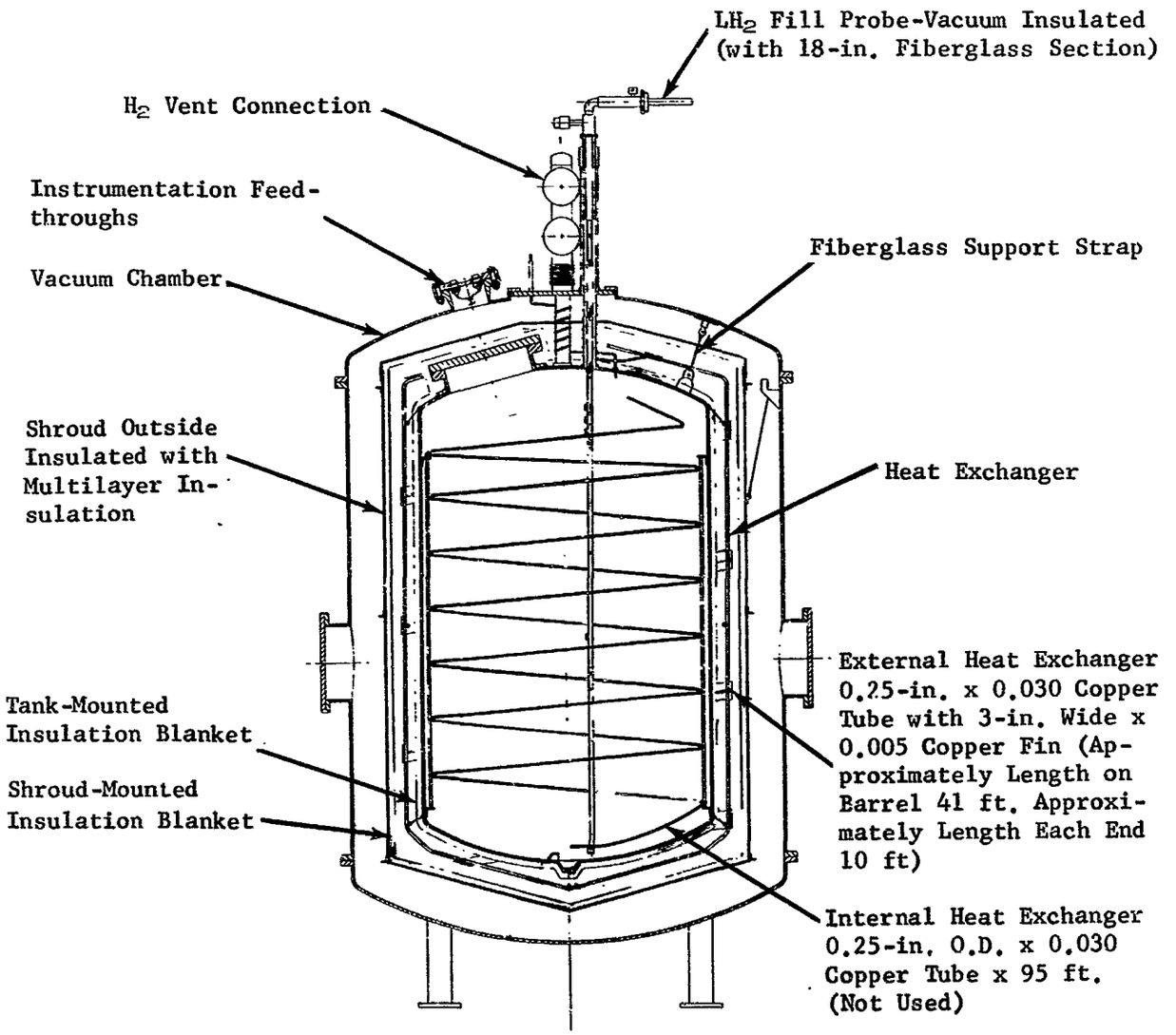

Figure IV-27 Integrated Tank Insulation System Test Installation

The tank, shroud, insulation, and heat exchangers are installed in a vacuum chamber to provide the proper operating environment.

The tank is an existing 4-ft diameter, 6-ft long, 304 stainless steel tank with 0.25 and 0.375-in. walls in the barrell and dome sections, respectively. A 14-in. manway permits access into the interior of the tank. Two stainless steel tubes, 2-in. and 2.5-in. diameter, enter the upper dome of the tank to provide for filling, venting and pressurizing the tank.

Electrical feed-throughs in these lines permit instrumentation wiring access to the tank. Liquid hydrogen is loaded through a 0.75-in. stainless steel tube, mounted concentrically within the 2-in. tube through the dome. This tube extends to the bottom of the tank to provide a means of draining the tank. An 18-in. section in the upper portion of the fill probe is constructed of epoxy filled fiberglass, 0.75-in. I.D. by 0.865-in. O.D., to minimize the heat leak through the line. The tank is supported by three fiberglass epoxy tension members, 5.875 in. long by approximately 0.187-in. diameter.

A shroud is installed between the vacuum chamber wall and the liquid hydrogen tank. This shroud serves two purposes: (1) it provides a constant boundary temperature during tests; (2) the shroud is used to support an outer blanket of insulation that is part of the tank insulation system.

The shroud, shown in Figure IV-28, consists of an aluminum framework supporting a sheet aluminum skin. It is supported from the walls of the vacuum chamber by three 0.1875-in. stainless steel cables. The shroud is heated by means of electrical heaters consisting of lengths of 22-gage copper wire, bonded to the outside surface of the shroud with a thermally conductive epoxy (Emerson & Cumming, Stycast 2850-FT). This heater is divided into three units: the barrel section of 500 watts capacity; one on each of the end cones, each capable of 100 watts power dissipation or more. These heaters are direct-current-powered and provide the capability of maintaining the shroud at a temperature of 75°F or greater. The completed lower half of the shroud is shown in Figure IV-29.

An insulation blanket consisting of five layers of aluminized mylar and 12 layers of nylon net is installed on the outside of the shroud to reduce the power requirements and aid in maintaining a constant shroud temperature.

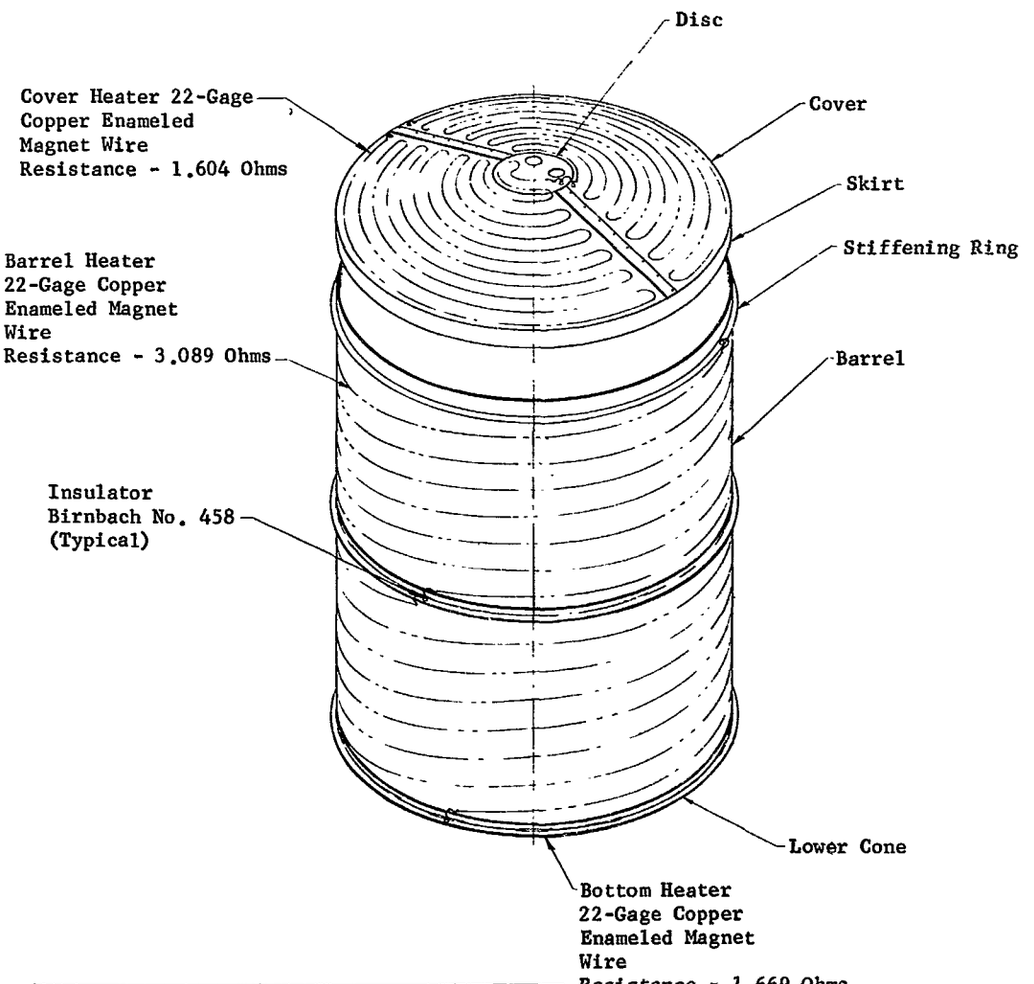

Figure IV-28 Shroud Assembly

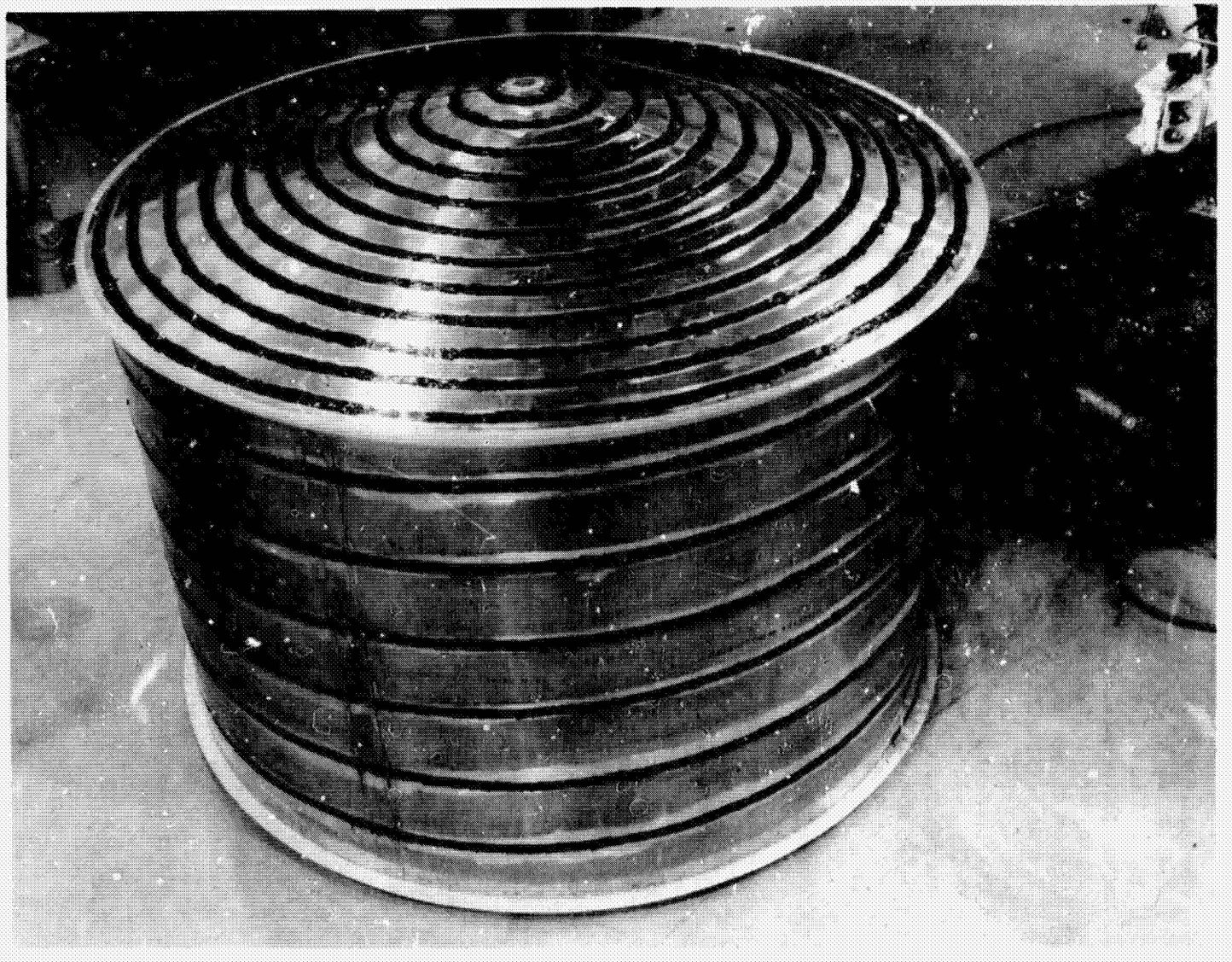

Figure IV-29 Lower Half of Shroud Assembly

This test article was originally designed to incorporate the thermodynamic vent system concept. Therefore, a heat exchanger, consisting of 95 ft of 0.25-in. O.D., 0.030-in. wall copper tubing was installed in the tank. This internal heat exchanger was mounted to vertical frame members attached to the tank wall. The tubing was installed with approximately uniform distribution from bottom to top in a spiral configuration. The thermodynamic vent system design included a submerged on-off solenoid valve and a Lee Jet (GW AA 4J) flow restrictor. The valve to be used was a Circle Seal model A649T 4 BP-AA, modified by the installation of Teflon seals. This valve was chosen because of its history of successful operation in a similar liquid hydrogen application. Unfortunately, however, neither the valve originally selected, nor several others which were tried, would shut off to an acceptable leak rate. The thermodynamic vent was therefore abandoned, and the internal heat exchanger was inactivated, but allowed to remain in place.

Three other heat exchangers are used to intercept heat that would normally enter the tank. The flow is divided, with part of the hydrogen being used for intercepting the tank penetration heat leak, and part being used for cooling the insulation. The heat exchangers on the tank penetration consist of 0.25-in. O.D., 0.030-in. wall stainless steel tubing silver-soldered to each of the two tank penetrations. Approximately 40 in. of tubing is coiled uniformly around each pipe from approximately 2 to 10 in. from the tank interface.

The insulation is cooled by means of a radiation heat exchanger located midway between the tank-mounted insulation and the shroud-mounted insulation. This heat exchanger, depicted in Figure IV-30, consists of 0.25-in. O.D., 0.030-in. wall copper tubing coiled around a stainless steel support frame. It is supported from the tank with dacron tension ties. Approximately 41 ft of tubing is used on the barrel section with approximately 10 ft on each dome. A fin of 4-in. wide by 0.005-in. thick copper is soft-soldered to the tubing parallel to the insulation surfaces. The fin tube assembly is painted with optically black paint. Each of the three heat exchangers is connected to a manual throttling valve outside the vacuum chamber to permit adjustment of the flow through the heat exchangers. A schematic diagram of the flow circuit is shown in Figure IV-31.

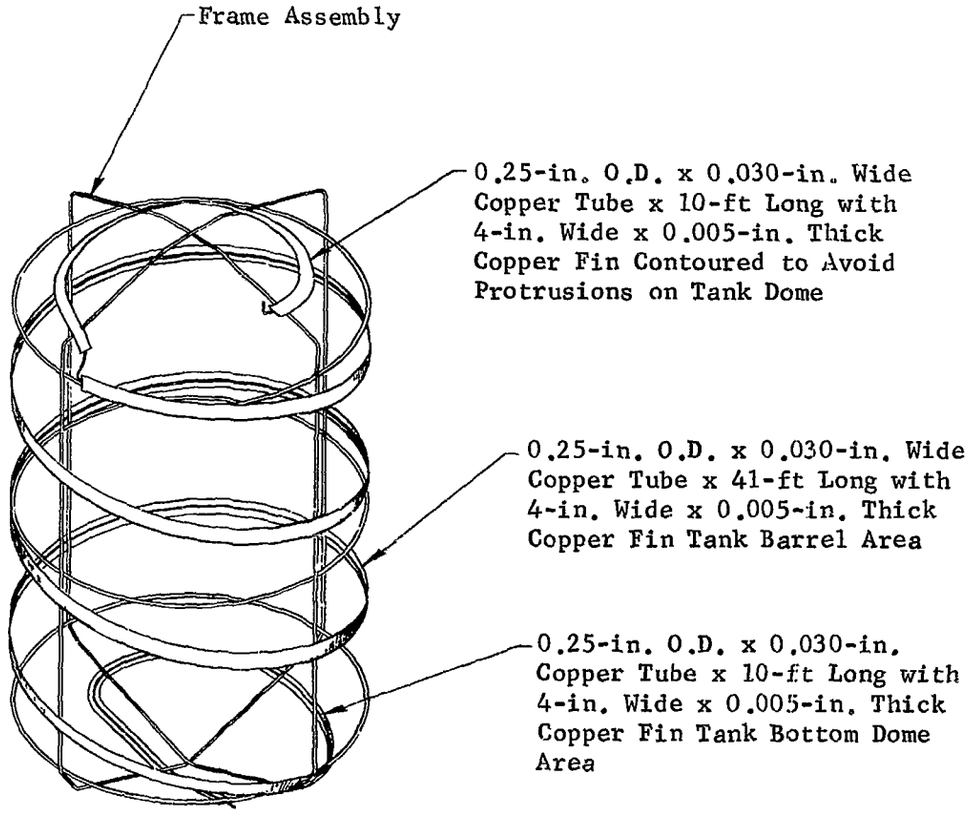

Note: Heat exchanger fins painted on both sides with Krylon No. 1602 ultra flat black enamel.

Figure IV-30 Radiatively Coupled Insulation Heat Exchanger Assembly

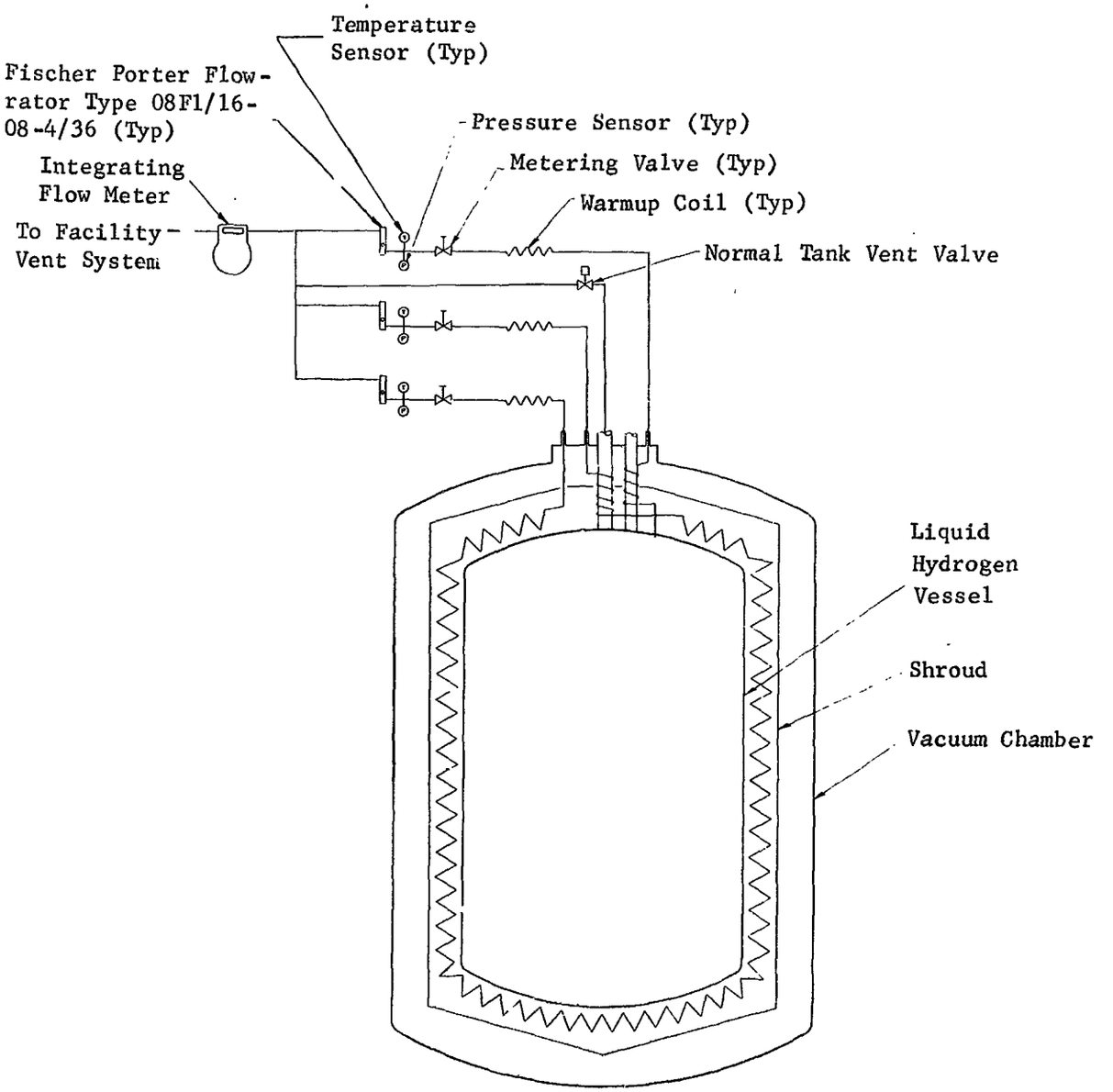

Figure IV-31 System Schematic

The tank was insulated with a multilayer insulation system consisting of 0.25-mil mylar film radiation shields, aluminized on both sides, and 14 x 14 mesh (0.007 in. approximately) nylon netting spacers. The tank-mounted blanket consists of 20 radiation sheilds with two layers of netting separating each shield and assembled to a thickness of 0.5 in. The shroud-mounted blanket is made of 40 radiation shields each separated by two layers of netting and assembled to a 1-in. blanket thickness. The aluminized mylar was perforated with 0.125-in. holes on 6 in. centers to assure adequate evacuation.

The tank insulation system was preformed into four panels -- two dome sections and two half-barrel sections. The dome assembly fixture is shown in Figure IV-32 with the manhole cover form installed. Figures IV-33 and IV-34 show insulation blankets partially assembled. Details of the insulation assembly and installation are given in Figure IV-35. Two layers of nylon net served as inner and outer covers for the insulation panels. Cotton thread was used to assemble the blanket in the following manner: Lengths of thread were first tied to the pair of nets forming the inner blanket cover at a spacing of approximately 4 x 4 in. for the dome panels and on 4 x 6 in. centers for the shroud panels. Each thread was then marked to the correct length (0.5 in. for tank panels and 1 in. for shroud panels). After all the foils and spacers were laid up, each thread was threaded into a needle, pushed through the blanket, and tied to the outer cover layers at the pre-marked length. This assembly method was not intended as a production procedure, but as a one-time approach to evaluating the predetermined length thread method of blanket assembly. The procedure proved to be even more tedious and time-consuming than had been expected. For production operations, a mechanized procedure using a heated needle to eliminate tearing of the mylar is visualized.

The insulation panels were assembled to the tank and shroud by use of Velcro hook and pile strips. For the tank-mounted insulation, the panels were trimmed to close fitting butt joints between panels. All joints were then interleaved, layer by layer, with 3-in. wide strips of aluminized mylar. These strips were held in place with mylar adhesive tape at appropriate intervals. The interleaving operation, surprisingly, proved faster and less difficult than had been anticipated. The insulated tank is shown in Figure IV-36.

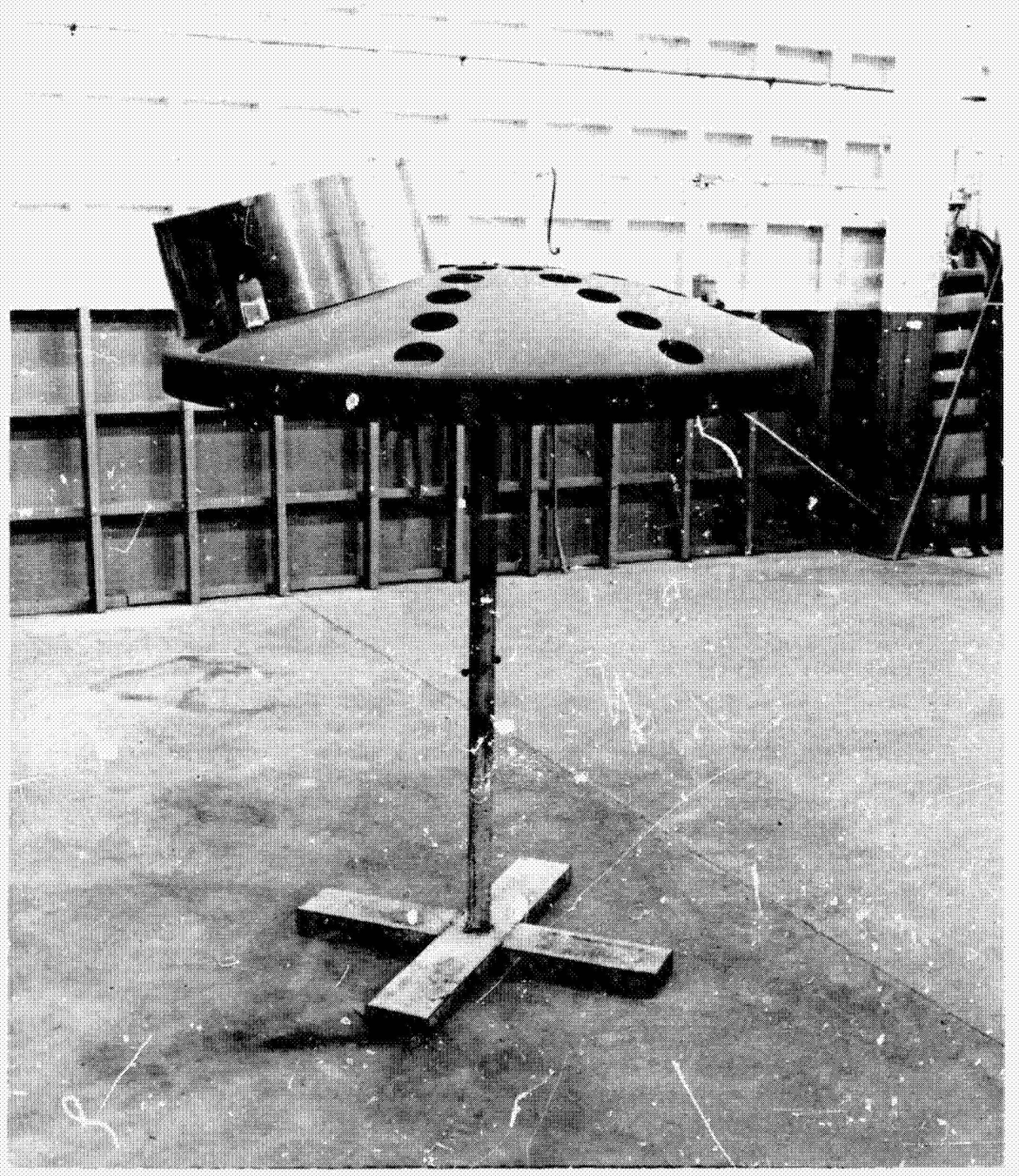

Figure IV-32 Dome Insulation Assembly Fixture with Manhole Cover Form

Figure IV-33 Partially Assembled Upper Tank Dome Insulation Panel

Figure IV-34 Partially Assembled Tank Barrel Section Insulation Panel

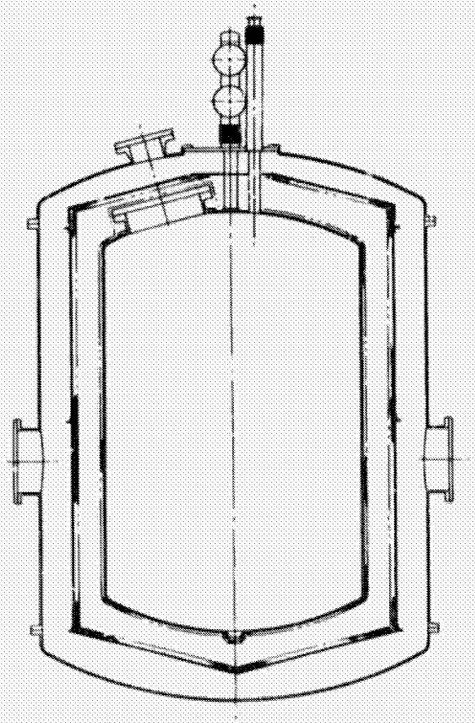

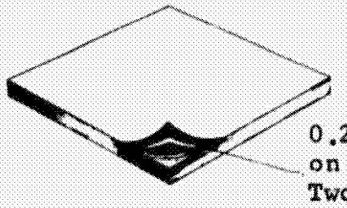

0.25-mil Mylar Aluminized on Both Sides Separated by Two Layers of Nylon Net

Typical Insulation Blanket

Cotton Thread Tied to a Predetermined Length

Blanket Tie Method

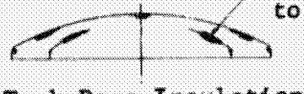

Insulation Tailored to Fit Mandrel

Tank Dome Insulation Layup

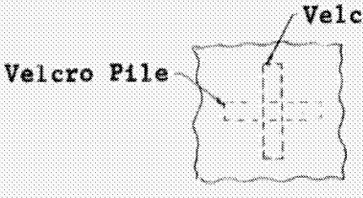

Velcro Hook

Velcro Pile

Insulation Fastening System

Blanket Butt Joint with 3-in. Wide Strip between Layers

Insulation Blanket Joint

0.75-in. Velcro Hook and Pile Strips Approximately 3 in. Long Cemented to Tank and Insulation Blanket with NARMCO 7343/7139 Adhesive (Shroud Insulation Applied in a Similar Manner)

Figure IV-35 Insulation Details

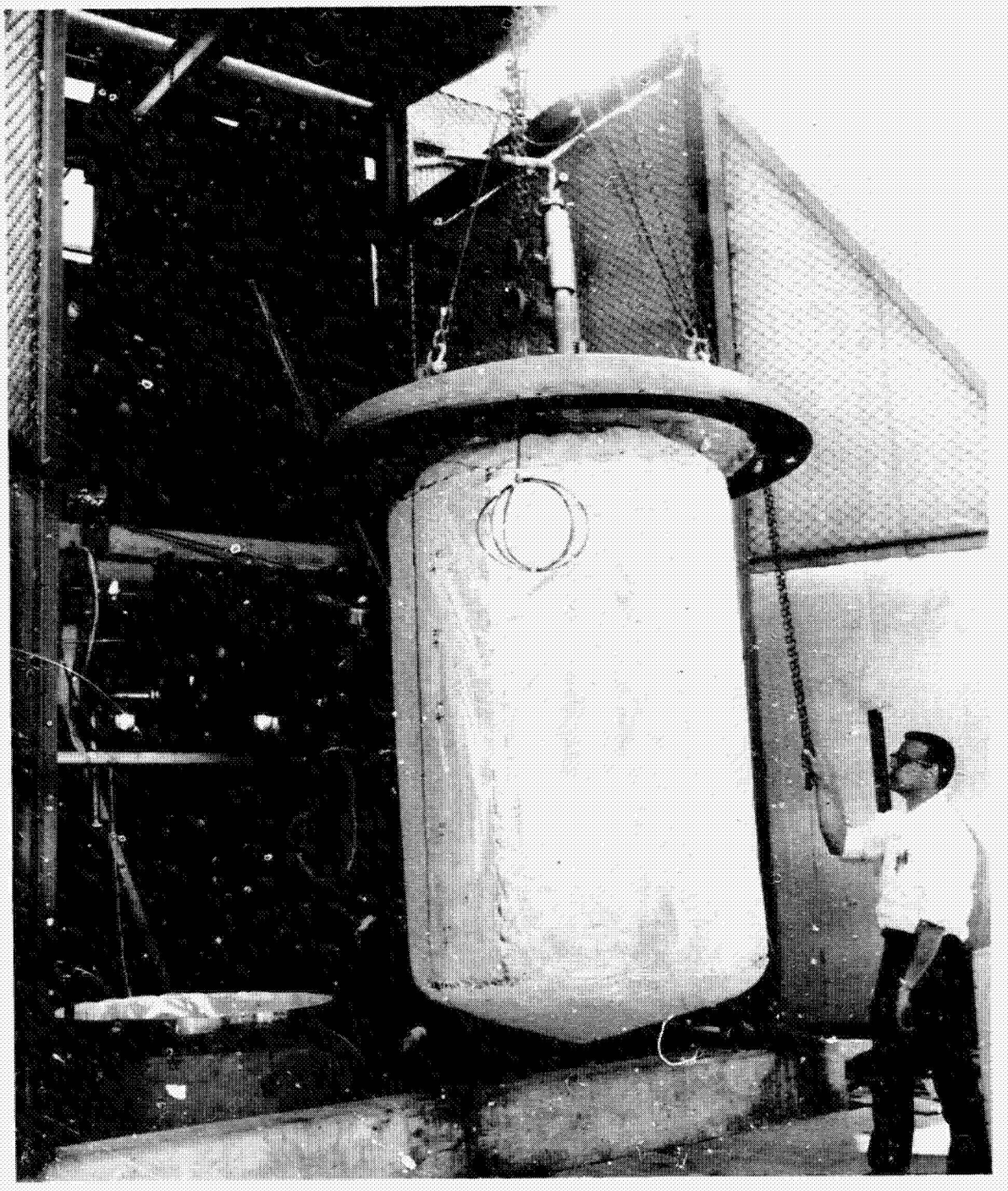

Figure IV-36 Insulated Liquid Hydrogen Tank

3. Instrumentation

Instrumentation for this test included measurement of temperatures, pressures and flowrates.

The low temperature measurements for this test were made with chromel/constantan thermocouples. Thermocouples were used to measure the temperature profile of the insulation and tank penetrations, and monitor the performance of the heat exchanger and the temperature of the shroud, tank, and bulk liquid. In order to obtain more accuracy in measuring the temperatures of the bulk liquid, each of the thermocouples in the tank was connected for differential temperature measurement and referenced to a cold junction located in the tank itself. The temperature of the cold reference was measured with a platinum resistance temperature bulb.

Temperature measurements were also made of the vent gas temperatures at the inlet of each flowmeter, using copper/constantan thermocouples.

The primary pressure measurement for this test was the hydrogen tank pressure. This measurement was made with redundant strain gage pressure transducers with a range of 0 to 50 psig plus a sensitive Bourdon tube gage. Vent gas pressures at the inlet of each flowmeter were measured with 0 to 15 psig Bourdon tube pressure gages.

Glass tube rotameters were used to measure the flowrates of the individual heat exchangers. In addition, the total vent flow was measured with an integrating positive displacement utility type gas meter.

Data was recorded on magnetic tape using a high speed data link from a subscriber station to a central data processing facility. Measured variables were converted from millivoltage to proper units by computer and displayed in tabular form. During long transient periods, this system was not used. Instead, only pertinent variables indicating overall status of the test were manually logged. In addition, flow rates and flowmeter pressure readings were manually recorded for all conditions.

After installation of insulation, heat exchangers and instrumentation, the test tank was installed in the 6-ft diameter vacuum chamber. Figure IV-37 shows the complete assembly at this point.

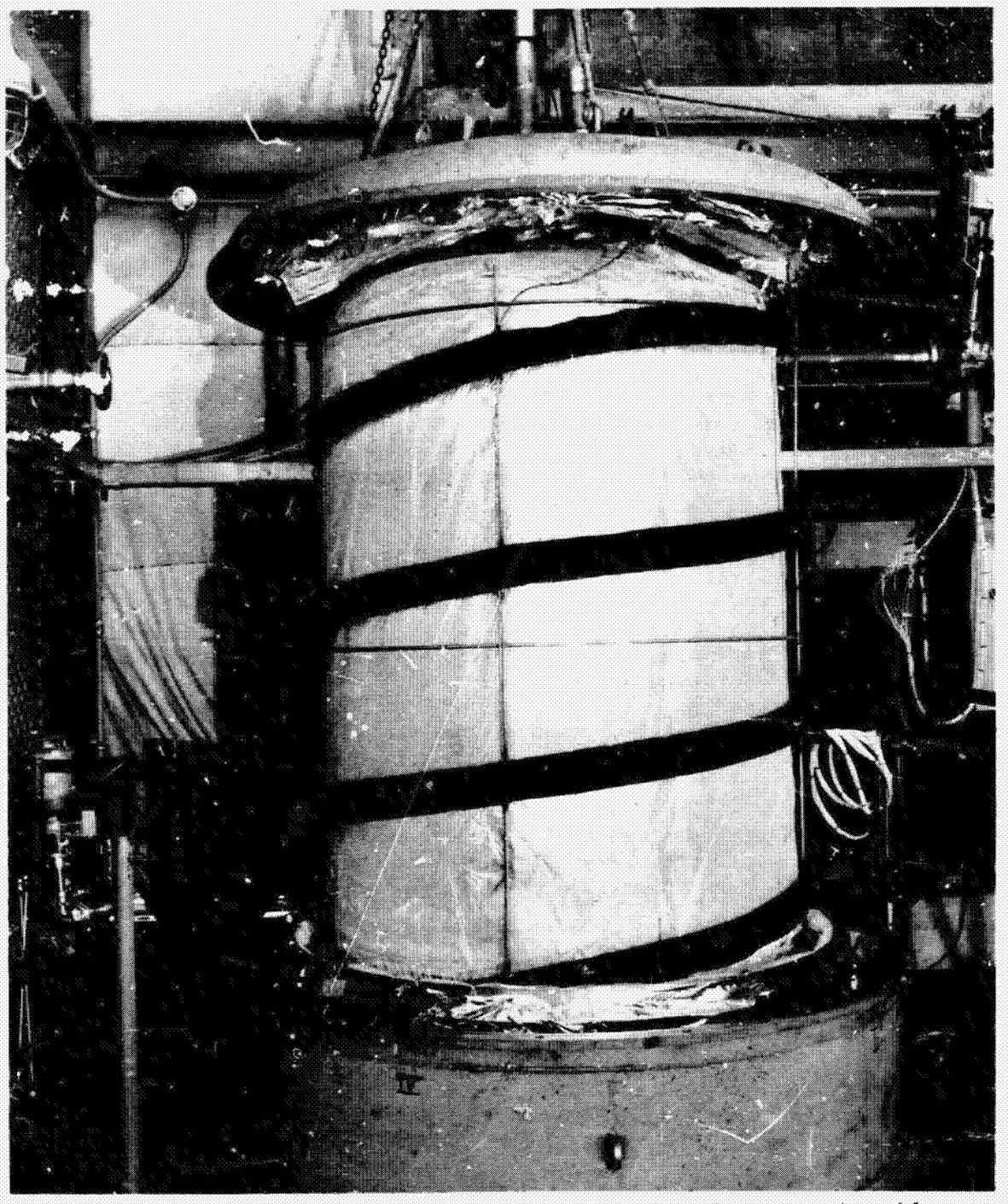

Figure IV-37 Integrated Insulation System Test Article During Assembly

4. Description of System Tests

Two steady-state boiloff tests were accomplished; one with the heat exchanger system activated, and one without it. After system and instrumentation checkout, purge and pumpdown operations, and filling of the tank with liquid hydrogen, test operations were begun on a three-shift per day basis.

The first test (I) was accomplished by allowing the system to reach steady-state conditions while maintaining a constant shroud temperature and a constant tank pressure by direct venting. The heat exchangers were inactivated by closing the manual throttling valves. The flow of GH_2 through the conventional vent line was regulated by means of a manual throttling valve to hold a constant tank pressure of 25 psia. The shroud temperature was manually regulated at 75°F by adjusting power supply voltage for the three shroud heaters.

Pertinent system variables were monitored and logged as a basis for determining when steady-state conditions had been reached. When these variables appeared to remain steady for an 8-hour period, recording of all variables on magnetic tape on an hourly basis was begun. Data was then recorded for about 8 hours while special attention was given to regulation of tank pressure and shroud temperatures. During this test, maximum variation of the tank pressure was +0.4 psi, -0.3 psi. However, these excursions were for relatively short periods, with an indicated deviation of less than 0.15 psi for a substantial part of the test period. Shroud temperatures as indicated at 8 measurement points, were maintained within 3 degrees of 75°F. The total time required from beginning of the tank fill operation to completion of the first test was approximately 62 hours.

The second test (II) was begun by topping the hydrogen tank. Valving was changed to initiate heat exchanger operation and the tank pressure was controlled by adjustment of the three manual valves. Shroud temperature control was maintained as in the first test. During the initial phase of the test, ratios of individual heat exchanger flow rates to the total vent flow were adjusted to determine their effect on system performance and to find the flow distribution resulting in minimum boiloff.

Again, after an 8-hour period of apparently steady operation, data recording was begun and continued for 8 hours. During this test phase, tank pressure was held to an indicated tolerance of 0.1 psi, which is near the readability of the gage. Shroud temperatures were maintained within ±5°F. The total elapsed time for the second test was approximately 46 hours.

5. Test Results

The results obtained from this test program are somewhat clouded by high extraneous heat leakage and a resulting high flow rate of cooling gas, thus masking the true effect of vent gas cooling. In the following paragraphs, the data obtained and the results of an analysis to interpret the data are presented. It is acknowledged that the accuracy of the conclusions drawn from the test data depends on the method of analysis and assumptions required to perform the analysis.

During Test I the average boiloff rate was 0.3218 lb_m/hr. For Test II, the average boiloff rate was 0.2803 lb_m/hr. Thus, on the basis of mass flow rate, an improvement of approximately 12.8% was realized. However, the liquid level was approximately 4 to 5 in. higher for the second phase of the test. This, plus the action of the heat exchangers, resulted in a difference in temperature of the ullage gas. Ullage temperature averaged 62.5°R and 51.5°R for the two test phases, respectively. Since the gas leaving the tank boundary is at approximately the ullage temperature, more heat is removed per lb for the higher temperature case. The heat removal rates, calculated on the basis of the ullage temperatures, are 80.0 Btu/hr and 61.5 Btu/hr for the two test phases, respectively. This represents a reduction in the heat removal rate of about 23%.

Pressure was manually controlled with reference to a Bourdon tube gage pressure indicator, with the control point continuously adjusted to account for barometric pressure. In order to control the pressure, periodic adjustment of flow rates was necessary. Thus, although near steady-state conditions were maintained for temperatures and pressures, the flow rates were cyclic. In Test I, the liquid bulk temperature also cycled between 39.98 and 40.05°R (as measured by the resistance thermometer). During the 8 hours over which flow rates were averaged, the temperature appears to have changed from the minimum temperature of 39.98°R to a final temperature of 40.04°R, or 0.06°R over the test period. For Test II, the temperature changed from 39.95° to 40.01°R in an almost straight line fashion during the last 6 hours of the test. Since the data appeared most stable during this period, the boiloff flow rates were averaged over the same 6-hour period. These temperature fluctuations were not apparent on inspection of the data readouts during the test.

Analysis of data from differential thermocouples in the liquid indicates that most of the bulk liquid followed the temperature as measured by the resistance thermometer near the bottom of the tank. If all of the liquid is assumed to have increased in temperature by 0.06°R over 8 hours in Test I, then the liquid absorbed heat at the approximate average rate of 5.25 Btu/hr. A temperature increase of 0.06°R over 6 hours in Test II results in a heat absorption rate of 7.2 Btu/hr. Adding these corrections to the heat removal rates given above, the average total heat inputs to the tank are found to be 85.25 and 68.7 Btu/hr for Tests I and II, respectively. On this basis, the heat exchanger operation resulted in an improvement of 19.4% over the uncooled case.

In the design of this test article, insulation blanket thicknesses were arbitrarily sized to achieve a significant improvement in boiloff due to operation of the heat exchanger system. Total heat input to the tank was predicted to be between 35 and 50 Btu/hr for the inactive heat exchanger case, depending on the actual performance of the insulation. A reduction of total boiloff of about 50% was predicted for the active heat exchanger case.

Although the reduction in total heat leak and boiloff rate was far less than expected, a reduction of heat flux through the tank-mounted insulation in excess of 50% was achieved. (The vent flow rate was about 3.5 times the rate that would be generated by the insulation heat flux.) This is indicated by the reduction in temperature of the outer surface, and consequently the temperature difference across the tank-mounted blanket. During the direct vent phase of the test, the average insulation surface temperature of the tank-mounted blanket was 441°R. This resulted in a temperature difference across the blanket of approximately 340° in the upper dome area and 400°R elsewhere. When the insulation heat exchanger was activated, these temperatures dropped to a range of 184 to 271°R, depending on position. This resulted in temperature differences across the blanket ranging from 144 to 191°R, with an average difference of 163°R. Because the thermal conductivity of multilayer insulation is expected to decrease with temperature, and the average temperature difference across the blanket during heat exchanger operation was about 47% of that measured without heat exchanger operation, the insulation heat flux was greatly reduced. The temperature of the inner surface of the shroud-mounted insulation ranged from 448 to 452°R for the Test I condition, with an average of 450.5°R, and from 215 to 293°R during Test II, with an average of 249.5°R.

The unimpressive overall performance gain appears to be due to an anomaly in the insulation system in the vicinity of the manhole cover. Design and fabrication of the test equipment was largely accomplished prior to the availability of the tank and vacuum chamber. Original 1960 shop drawings of the tank and

vacuum chamber were used to lay out the test assembly. When mating of the components was attempted, it was discovered that an error existed in the original drawings. Whereas the clearances in the manhole vicinity were expected to be small, an interference was found. Field changes were made to reduce the problem as much as possible. However, the final result was compression of the insulation in the manhole area, actual penetration of part of the insulation, and a small misalignment between the shroud barrel and top cone section. The effects of this problem were more severe than had been anticipated.

In order to evaluate the test data, a thermal network was set up for the system. The tank insulation, insulation heat exchanger, and shroud insulation were represented by 8 nodes each. Conductors were included to represent the insulation, radiative coupling between insulation blankets and between the heat exchanger and insulation blankets, heat transfer vertically along the insulation and through the annulus, radiation leakage through the shroud insulation, and the manhole heat leak. Coefficients for these categories of conductors were treated as input data. For each set of input data, the network was analyzed twice. First, the heat exchanger temperature was allowed to float to simulate the case of no cooling. For the second case, all conductors remained the same, but the heat exchanger temperatures were constrained to the values obtained during Test II to simulate heat exchanger operation.

The results of the program were then compared to the actual temperature and heat flux data for the two tests. This procedure was repeated, with the input data adjusted for each case, to improve the agreement between computed results and test data. Table IV-2 summarizes the results of this analysis.

Table IV-2 Test Data Correlation Summary

	Test I	Test II
Total Vent Flow Rate, lb_m/hr	0.3216	0.2803
Heat Content of Vent Gas, Btu/lb_m	248.8	219.4
Total Heat Removed, Btu/hr	80.0	61.5
Heat Absorbed in System, Btu/hr	5.25	7.2
Total Heat Entering System, Btu/hr	85.25	68.7
Insulation Heat Exchanger Flow Rate, lb_m/hr	0	0.1705
Vent Pipe Heat Exchanger Flow Rate, lb_m/hr	0	0.0365
Fill Pipe Heat Exchanger Flow Rate, lb_m/hr	0	0.0733
Heat Flux to Tank from Vent Pipe, Btu/hr	-2.5	0.88
Heat Flux to Tank from Fill Pipe, Btu/hr	1.31	0.31
Heat Flux through Tank-Mounted Insulation Blanket, Btu/hr	32.1*	10.6*
Heat Flux in Vicinity of Manhole, Btu/hr	54.5*	55.9*
Heat Flux into Annulus via Shroud Insulation, Btu/hr	11.6*	35.1*
Heat Flux into Annulus via Radiation through Gap in Shroud-Mounted Insulation, Btu/hr	20.9*	43.7*
Heat Removed by Insulation Heat Exchanger, Btu/hr	0	70.4 (68.1*)

*Computed values for best correlation of test data.

Analysis of the simulated system case that most closely correlates the data leads to the following observations and conclusions:

1) Based on calculations that most closely approximate the measured data, the heat flux through the damaged and compressed insulation in the vicinity of the manhole was the dominant source of heat flux to the tank, contributing approximately 54 to 56 Btu/hr;

2) A large heat flux to the annular region between the insulation blankets resulted from radiant heat transfer through a gap between the upper dome and barrel sections of the shroud-mounted insulation, and possibly through other butt joints in the shroud-mounted insulation. The assumed equivalent open area of these gaps that results in the best fit of the test data is 0.3 ft^2;

3) The average thermal conductivity of the tank-mounted insulation appeared to be approximately 7×10^{-5} Btu/hr ft °R for the Test I condition and 5.5×10^{-5} Btu/hr ft °R for the Test II condition at the operating temperatures. Similarly, the average thermal conductivity of the shroud-mounted insulation is estimated from the data analysis to be 9.5×10^{-5} Btu/hr ft °R for Test I conditions and 8.5×10^{-5} Btu/hr ft °R for Test II conditions. These values again are based on actual temperatures, and are consistent with the expected dependency of thermal conductivity on temperature. The large increase in heat flux through the shroud-mounted insulation and decrease in heat flux through the tank-mounted insulation on activation of the heat exchanger is not a result of a change in insulation characteristics, but is due to the great change in temperature difference across the respective insulation blankets, and is an expected characteristic of the cooled insulation system;

4) Heat flux through the tank-mounted insulation is estimated from the data reduction analysis to have decreased from 32.1 to 10.6 Btu/hr when the insulation heat exchanger was activated. This amounts to a 67% improvement. However, it must be noted that the hydrogen flow rate through the heat exchanger was approximately 3.5 times the boiloff generated by the insulation heat flux. This factor is partially compensated by the fact that the heat flux into the annulus is abnormally high;

5) The heat transfer between the heat exchanger fin and the insulation blanket can be approximately described by the following equation:

$$Q_{HX} = A_{HX} \mathcal{F}_{HX} \sigma \left(T_I^4 - T_{HX}^4 \right)$$

where A_{HX} = area of one side of the heat exchanger fin;

$\mathcal{F}_{H_X}$ is a gray body view factor with a value of 0.8.

T_{HX} and T_I are temperatures of the heat exchanger and insulation blanket surface, respectively;

6) The heat gained by the insulation heat exchanger was approximately 71 Btu/hr. The exit gas temperature was 200°R, which is within 93 degrees of the highest measured shroud temperature. In view of the abnormally high flow rate and heat load, this indicates that the heat exchanger was adequately sized;

7) Vertical radiation in the annulus appears to have resulted in vertical heat fluxes of 1 to 10 Btu/hr over the annulus cross-section. However, the data correlation was relatively insensitive to this parameter. Thermocouples mounted on the insulation surfaces facing the annulus midway between heat exchange convolutions varied as much as 24°R from thermocouples mounted on the insulation surface opposite the heat exchange fin. These results are also influenced by the high extraneous heat leaks and the abnormally high coolant gas flow rate.

D. STRUCTURAL TEST OF BORON STRUT

A concept for applying tension and compression loads to the structural fibers in a composite material tubular strut is presented in Chapter III. In order to verify the feasibility of this concept, two tubes were fabricated and tested to failure. Boron presents greater application difficulties than fiberglas because of its large fiber diameter and brittleness. Therefore, the boron epoxy tube concept was chosen for evaluation.

The specimens were constructed in accordance with the design shown in Figure III-9, but with modified end fittings to facilitate testing. Since the objective of the test was to evaluate the end fitting concept only, the tube lengths were reduced to approximately 6 in. S-glass, rather than graphite, was used to overwrap the ends of the boron fibers. One of each specimen was tested in tension and compression. Figure IV-38 shows a cross-section of the tensile specimen. The specimens were fabricated using "pre-preg" cloth consisting of boron fibers on either side of a glass scrim cloth. The scrim cloth used resulted in a spacing of approximately 0.005 in. and the wall thickness increased to approximately 0.040 in. accordingly. The volumetric percentage of boron fibers is approximately 36%. When subjected to approximately 800 lb tension, slippage occurred in one end fitting; in the other end fitting slippage occurred at approximately 1100 lb. No further slippage was noted to 6,000 lb. At this point, the specimen was removed from the fixture, and examined. Approximately 0.005 in. of slippage had occurred on each end. This protruding material was machined off the end fittings and the strut reassembled. It was then loaded in tension to failure at 8220 lb, with no further slippage noted.

Failure occurred at the beginning of the radius where the fibers deflect around the end fitting. This is expected because a preload is introduced in the boron fibers by the relatively high ratio of fiber diameter to a radius of curvature. If a degradation factor of approximately 16% is applied to account for preloading of the boron fibers caused by their formation around the 3-in. radius, a calculated average fiber strength of 272,000 psi is obtained.

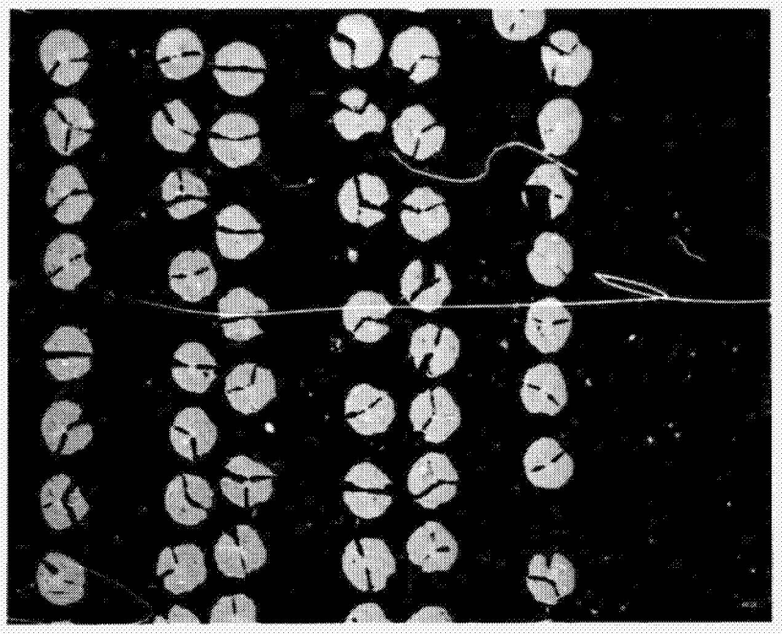

Figure IV-38 Cross Section of Boron Strut Tensile Test Specimen

Because this strut is tension-critical, the design was not optimized for compressive loading. The second specimen was loaded in compression to failure at 8720 lb. Failure occurred in the cylindrical portion of the tube. Some delamination of the fibers appeared to have occurred on the inside of the tube. The failed specimens are shown in Figure IV-39.

The end fitting design concept was judged to be adequate because compressive failure occurred in the cylinder section and tensile failure occurred at the expected weak point with reasonable ultimate strength. The small initial slippage of the composite on the end plug can probably be eliminated by a combination of improved curing process and greater tension in the overwrap fibers holding the boron in conformity with the plug contour. The use of graphite fibers for the overwrap should reduce slippage because of its higher elastic modulus. If the slippage cannot be totally eliminated, then the manufacturing process would include preloading the part to allow the slippage to occur before squaring the ends.

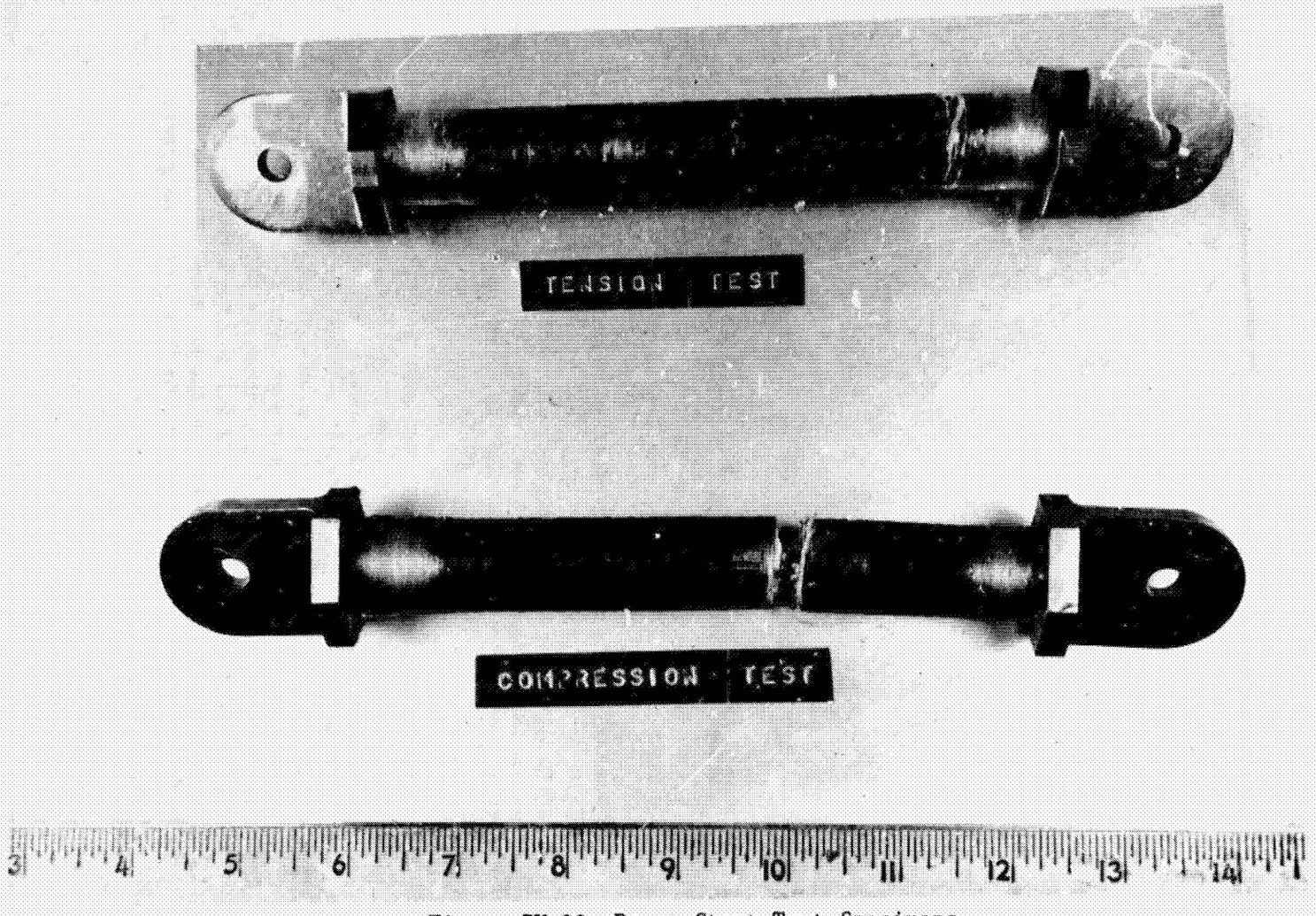

Figure IV-39 Boron Strut Test Specimens

V. CONCLUSIONS

Analytical studies indicate that for certain large-scale liquid-hydrogen space storage systems, a significant reduction of boiloff losses can be achieved by using the vent gas to intercept a part of the heat that would otherwise reach the hydrogen tank. This is accomplished primarily by intercepting heat within the tank insulation system, and secondarily by cooling the large pipes connected to the tank.

An attractive method for implementing the interception of heat within the insulation system is the installation of a heat exchanger between tank- and shroud-mounted insulation blankets. Analysis indicates that the heat exchanger will function properly if physically and thermally attached to the surface of either insulation blanket, or if supported between the insulation blankets with only radiative coupling to the insulation. Analytical predictions of the effectiveness of the radiatively coupled heat-exchanger concept were only partially verified by test.

On the basis of analytical calculations, heat entering a cryogen tank through the piping system can be reduced significantly (50% or more) by using the vent gas to intercept part of the heat flow. Because of the relatively low heat flux to the cryogen tank through its structural support system and the geometrical complexity of the support system, the use of vent gas to intercept a part of this heat flux is not warranted. The use of fiberglass epoxy and boron epoxy composite structural materials is calculated to reduce heat leakage through the tank support system by 60% or more. Graphite epoxy is not an attractive composite material for cryogenic tank supports because of its high measured thermal conductivity.

The feasibility of a concept for interposing a layer of hydrogen vapor between the tank wall and the liquid, using nonmetallic honeycomb core and a capillary partitioning barrier, was experimentally demonstrated. Calculations of predicted performance show little promise for this internal insulation concept for long-term space storage of hydrogen. For short-term missions, and applications specifically requiring an internal insulation system, the internal capillary insulation concept may be promising.

VI. REFERENCES

1. W. H. Sterbentz: "Interim Report, Liquid Propellant Thermal Conditioning System". Lockheed Missiles & Space Company, LMSC-A 839783, NASA CR-72113, Contract NAS3-7942. 20 April 1967.

2. R. P. Warren and J. W. Anderson: "A System for Venting a Propellant Tank in the Absence of Gravity". Advances in Cryogenic Engineering, Volume 12. 1967.

3. R. C. Mitchell, J. A. Stark and R. C. White: "Zero-g Hydrogen Tank Venting Systems". Advances in Cryogenic Engineering, Volume 12. 1967.

4. Dale W. Murphy, J. P. Gille and G. Robert Page: "Vent Free Fluorine Feed System". AFRPL-TR-67-323 (Volume I), MCR-67-416. March 1968. Confidential.

5. Hans M. Roder and Robert D. Goodwin: "Provisional Thermodynamic Functions for Para-Hydrogen". NBS-TN 130. December 1961.

6. "A Compendium of the Properties of Materials at Low Temperature (Phase I)". (Part II, Page 3.331, Curve H), WADD TR 60-56. October 1960.

7. Stephen H. Davis: "Convection in a Box: On the Dependence of Preferred Wave Number Upon the Rayleigh Number at Finite Amplitude." Journal of Fluid Mechanics, Volume 32, Part 3. 24 May 1968.

8. E. E. Morris and R. J. Alfering: "Cryogenic Boron-Filament-Wound Containment Vessels". Contract NAS3-10282 Final Report, NASA CR-72330. November 1967.

9. B. W. Cole and R. V. Cervelli: "Comparison of Composite and Non-Composite Structural Tubes". AIAA Paper No. 68-340. April 1968.

APPENDIX

MULTILAYER INSULATION THERMAL CONDUCTIVITY MODEL

Analysis of the effects of removing heat from the insulation region and of optimal insulation distributions for various heat exchanger configurations requires a mathematical description of the conductance of multilayer insulation as a function of temperature. For the purpose of arriving at such a description, the insulation will be treated as being comprised of flat radiation foils, each one isothermal and infinite in extent, separated by totally transparent spacers.

With these assumptions, then, the heat transfer per unit area from any foil at temperature T_1 to an adjacent foil at temperature T_2 will be

$$q_{1,2} = \frac{\sigma (T_1^4 - T_2^4)}{2/\epsilon - 1} + q_{\text{conduction}}$$

where σ is the Stefan-Boltzmann constant, ϵ is the emissivity of the two foil surfaces (assumed to have nearly the same emissivity), and $q_{\text{conduction}}$ is a term that accounts for conduction through the spacer material. If contact resistance and holes in the spacer material are all taken account of by an area factor α, then it can be expressed in terms of the thermal conductivity of the spacer material in solid form;

$$q_{\text{conduction}} = \frac{\alpha}{s} \int_{T_1}^{T_2} k\,(T)dT,$$

where s is the foil separation (distance between the two adjacent foils) and k (T) is the thermal conductivity of the spacer material as a function of temperature.

Consider now an insulation consisting of any number of foils, n, all equally spaced (s) and all with the same emissivity, ϵ. Then the considerations just discussed result in a system of (n-1) equations for the unknown heat flux, q (which in steady state does not vary across the insulation) and intermediate foil temperatures.

If the individual foil temperatures are T_1, T_2, ... T_n, we have

$$q = \sigma \frac{(T_1^4 - T_2^4)}{2/\epsilon - 1} + \frac{\alpha}{s} \int_{T_1}^{T_2} k(T)dT$$

$$q = \sigma \frac{(T_2^4 - T_3^4)}{2/\epsilon - 1} + \frac{\alpha}{s} \int_{T_2}^{T_1} k(T)dT$$

$$q = \sigma \frac{\left(T_{(n-1)}^4 - T_n^4\right)}{2/\epsilon - 1} + \frac{\alpha}{s} \int_{T_{n-1}}^{T_n} k(T)dT$$

Adding all the equations together gives q in terms of the outside foil temperatures, T_1 and T_n:

$$(n-1)\, q = \sigma \frac{\left(T_1^4 - T_n^4\right)}{2/\epsilon - 1} + \frac{\alpha}{s} \int_{T_1}^{T_n} k(T)dT$$

With the assumptions we have made, therefore, the multilayer insulation system can be treated for analysis purposes simply as two parallel insulators, one of them equivalent to the foil layers of the insulation taken as a single block of appropriate dimensions. This result is essentially due to two facts: since the spacer is assumed to be transparent, there is no coupling in any one element between radiation and conduction; and since ϵ and s were assumed to be the same for every foil, the equations could be written with constant coefficients; hence no coupling was introduced as a result of adding the elements in series. In reality, the heat fluxes through the two components correspond at only one point in the system to values obtained by considering them separately. Toward the hot end, the radiation heat flux generally becomes dominant whereas it may be insignificant at the cold side. Nevertheless, the total heat flux at any point is equal to the sum of the radiation and conduction heat fluxes obtained by computing them separately.

For real materials, the foil emissivity as well as the spacer conductivity should be expected to vary with temperature. This effect can be included in the model without introducing coupling between the terms (which would greatly complicate the result) if we restrict our attention to systems containing large numbers of foils, so that the temperature difference between any two adjacent foils can be treated as a small quantity. That is, if we define the temperature difference between any two foils "i" and "i + 1" as

$$T_i - T_{i+1} = \delta T_i$$

and if $\delta T_i \ll T_i$ for all $1 \leq i < n$, then $T_i^4 - T_{i+1}^4$ can always be approximated by the first term in its Taylor series expansion about T_i:

$$T_i^4 - T_{i+1}^4 \approx 4T_i^3 \, \delta T_i$$

Furthermore, the integrated spacer conductivity becomes approximately

$$\int_{T_i}^{T_{i+1}} k(T)dT \approx k(Ti) \, \delta T_i$$

With these approximations, the heat transfer between any two adjacent foils, one at temperature T_i and the other at $T_i - \delta T_i$, is

$$q = \left[\frac{4 \sigma T_i^3}{2/\epsilon \left(T_i\right) - 1} + \frac{\alpha}{s} k\left(T_i\right) \right] \delta T_i$$

or, writing $s = \frac{1}{N}$, where N is the number of foils per unit thickness,

$$\frac{q}{N} = \left[\frac{4 \sigma}{N} \frac{T_i^3}{2/\epsilon \left(T_i\right) - 1} + \alpha \, k\left(T_i\right) \right] \delta T_i \qquad [1]$$

As before, we obtain (m-1) such equations, if m is the actual total number of foils, by letting i assume integral values from 1 to (m-1). These (m-1) equations can be added, as in the constant coefficient case, provided that δT_i is small enough that the right hand side can be treated as a continuously varying function from equation to equation, allowing the laws of integral calculus to be used to perform the addition on the right side:

$$\frac{m-1}{N} q = \frac{4\sigma}{N} \int_{T_1}^{T_m} \frac{T^3}{\frac{2}{\epsilon(T)} - 1} dT + \alpha \int_{T_1}^{T_m} k(T)dT \qquad [2]$$

Notice that $\frac{m-1}{N}$ is the actual thickness of the insulation blanket.

Up to this point, we have been treating the case of a flat insulation blanket, infinite in extent. Now that integral representations have been introduced, it is a simple matter to extend the treatment to other configurations.

Consider, for example, an insulation blanket, total thickness t, applied to the outside of an infinitely long cylinder, radius R. If the number of foils is large enough, the view factor in the radiation term is essentially unity; hence, the right side of Equation [1] is unchanged. The left side becomes

$$\frac{q}{2 \pi r_i N}$$

where q is now heat transfer per unit length of the cylinder, and r_i is the radius of the foil at temperature T_i. Since 1/N is really always the change in radius associated with each δT_i, the change in temperature on the right side, the left hand sides of the array of equations can also be treated as a continuously varying function and integrated with 1/N = dr. Hence,

$$\frac{q}{2\pi} \log \left(1 + \frac{t}{R}\right) = \frac{4\sigma}{N} \int_{T_1}^{T_m} \frac{T_3}{\frac{2}{\epsilon(T)} - 1} dT + \alpha \int_{T_1}^{T_m} k(T)dT \qquad [3]$$

is the appropriate equation for heat transfer per unit length of an infinitely long circular cylinder.

Similarly, if we consider a sphere of radius R, covered by an insulation blanket of thickness t, then the total heat transfer into the sphere is given by

$$\frac{q}{4\pi R}\left(\frac{t}{R+t}\right) = \frac{4\sigma}{N}\int_{T_1}^{T_m}\frac{T^3}{\frac{2}{\epsilon(T)}-1}\,dT + \alpha\int_{T_1}^{T_m}k(T)dT \qquad [4]$$

The derivation can be carried a step farther by specifying the form of the temperature dependences of ϵ and k to some extent, in accordance with the measured properties of some of the most interesting materials.

Since our goal is to construct a mathematical model of the multilayer insulation, it is most convenient to work henceforth with an overall insulation effective conductivity, $k\ (T_2, T_1)$, defined by

$$q = \frac{T_2 - T_1}{L}\,k\ (T_2, T_1)$$

where q is the heat transfer per unit area from a surface at temperature T_2 to a surface a distance, L, away at temperature T_1.

Substituting this definition into Equation [2], with L for $\frac{m-1}{N}$ and T_2 for T_m, gives

$$k\ (T_2, T_1) = \frac{1}{T_2 - T_1}\int_{T_1}^{T_2}\left[\frac{4\sigma T^3}{\left(\frac{2}{\epsilon(T)}-1\right)N} + \alpha\,k(T)\right]dT \qquad [5]$$

The conductivity of the spacer material, k (T), is a well-defined and measurable property. In the case of nylon, for example, the conductivity is plotted as a function of temperature in the range T = 20 to 500 degrees*. This curve is rather closely approximated by the function

*Final Report, Volume II, Contract NAS8-20353, Lockheed Missiles and Space Company, A84 882, June 25, 1967, pp 4.2-7.

$$k\ (T) = 0.2\left[1 - e^{-0.015T}\right]\frac{Btu}{ft\text{-}hr\text{-}^{\circ}R} \qquad [6]$$

The emissivity of the radiation shield, ϵ (T), is less well known than the spacer conductivity. Although the emissivity of a laboratory sample of the shield material can be pinned down very closely, the emissivity as applied to a space vehicle is not expected to be as good because of damage to the aluminized coating, flaws, penetrations, contamination, etc., which reduce the reflectivity of the shield surface. Curves (presented on pp 2-51 and 4.2-17*) for the emissivity of 0.25-mil aluminum foil are fairly well approximated, for temperature below 400°R, by the function

$$\epsilon\ (T) = 0.0025 + 0.005\left(\frac{T}{100}\right)$$

If the degradation of the reflector caused during application is considered to be microscopic black areas, a constant value should be added to this function. On the basis of an "as-applied" emissivity of about 0.04 for T = 400°R, the following emissivity function would be indicated:

$$\epsilon\ (T) = 0.02 + 0.005\left(\frac{T}{100}\right) \qquad [7]$$

For our purposes at present, though, we merely wish to specify the form of these temperature dependencies; hence, it is sufficient to take

$$k\ (T) = \eta\left(1-e^{-\delta T}\right), \text{ say,} \qquad [8]$$

$$\epsilon\ (T) = \rho + \gamma T. \qquad [9]$$

The quantity $\left(\frac{2}{\epsilon(T)} - 1\right)^{-1}$ can now be expanded in a Maclaurin series in terms of the small quantity $\frac{\epsilon(T)}{2}$:

$$\left(\frac{2}{\epsilon(T)} - 1\right)^{-1} = \frac{\epsilon(T)}{2}\left(1 + \frac{\epsilon(T)}{2} + \frac{\epsilon^2(T)}{4} + \ldots.\right)$$

*Final Report, Volume II, Contract NAS8-20353, Lockheed Missiles and Space Company, A84 882, June 25, 196 , pp 4.2-7.

or, with $\epsilon(T)$ given by Equation [9] and taking the series as far as the second order term in β and the first order term in γT:

$$\left(\frac{2}{\epsilon(T)} - 1\right)^{-1} \approx \frac{1}{2}\left(\beta + \gamma T + \frac{\beta^2}{2} + \beta\gamma T\right). \qquad [10]$$

Substituting Equations [8] and [10] into Equation [5] and integrating gives

$$k\ (T_2, T_1) = \frac{1}{T_2 - T_1}\left[\frac{\sigma}{N}\left\{\left(\frac{\beta}{2} + \frac{\beta^2}{4}\right)\left(T_2^4 - T_1^4\right) + \frac{2\gamma}{5}\ (1+\beta)\left(T_2^5 - T_1^5\right)\right\} + \alpha\eta\left(T_2 - T_1 - \frac{e^{-\delta T_1} - e^{-\delta T_2}}{\delta}\right)\right]. \qquad [11]$$

For example, taking $\beta = 2\text{x}10^{-2}$, $\gamma = 5\text{x}10^{-5}$, $\delta = 1.5\text{x}10^{-2}\,^{\circ}R^{-1}$, $\eta = 0.2\ \frac{Btu}{ft\text{-}hr\text{-}^{\circ}R}$, and $N = 500\ ft^{-1}$, the curves shown in Figure A-1 are generated for the various indicated values of α.

This model has been compared to unpublished test data for a nylon-spacer insulation specimen and appears to correlate with the data within 10% by proper adjustments of N and α.

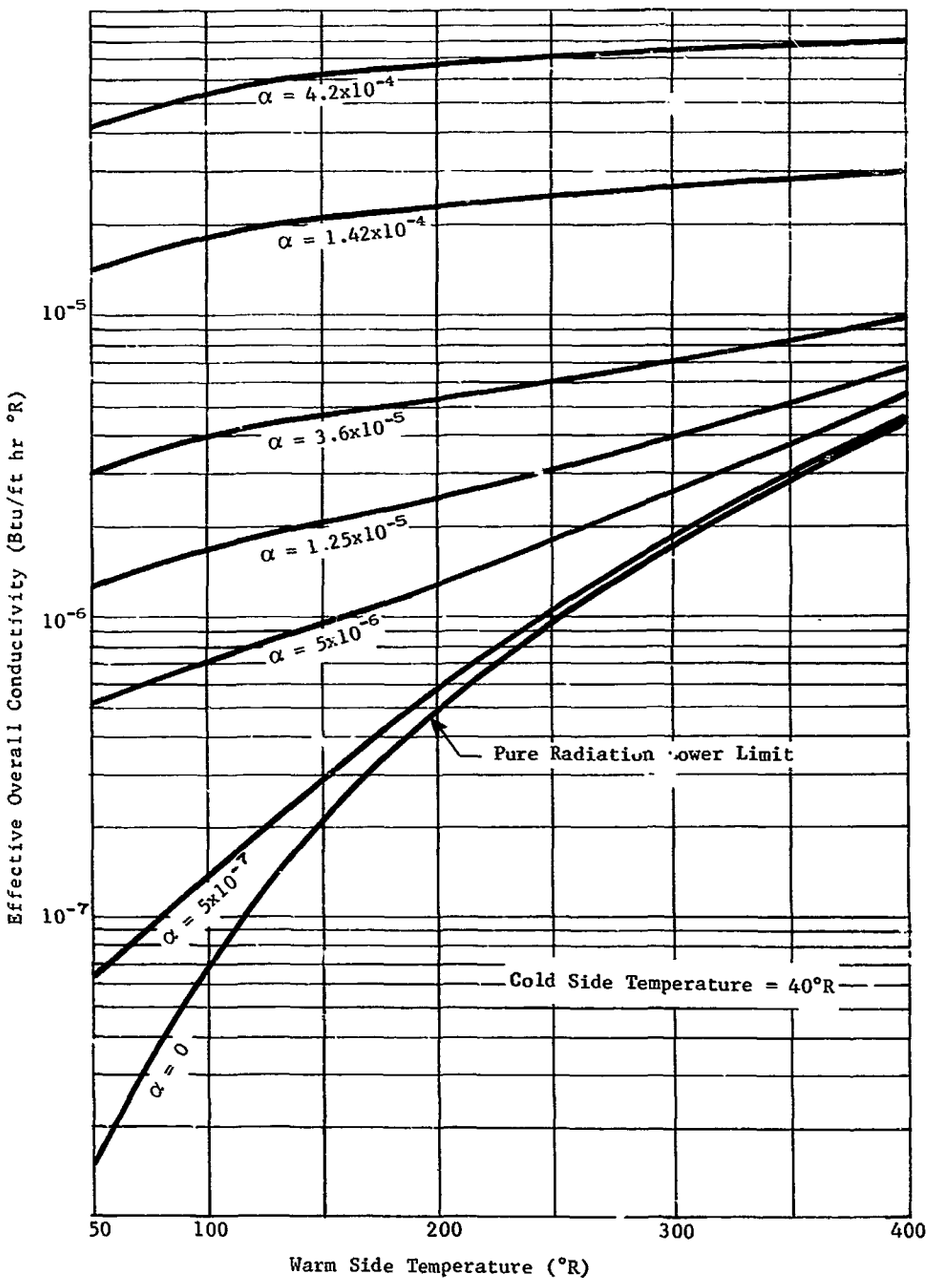

Figure A-1 Insulation Thermal Conductivity Model for Several Values of α